

INDIRECT NUMERICAL INTEGRATION, DIFFERENCE APPROXIMATION,
AND CIRCUIT SIMULATION OF TRANSMISSION LINES

BY

DMITRI BORIS KUZNETSOV

Dipl., Moscow Electrotechnical Institute of Telecommunication, 1988
M.S., University of Illinois, 1993

THESIS

Submitted in partial fulfillment of the requirements
for the degree of Doctor of Philosophy in Electrical Engineering
in the Graduate College of the
University of Illinois at Urbana-Champaign, 1996

Urbana, Illinois

© Copyright by Dmitri Boris Kuznetsov, 1996

INDIRECT NUMERICAL INTEGRATION, DIFFERENCE APPROXIMATION, AND CIRCUIT SIMULATION OF TRANSMISSION LINES

Dmitri Boris Kuznetsov, Ph.D.
Department of Electrical and Computer Engineering
University of Illinois at Urbana-Champaign, 1996
Jose E. Schutt-Ainé, Advisor

This dissertation includes three topics in the transient analysis of linear systems: *indirect numerical integration*, *difference approximation*, and *circuit simulation of transmission lines*.

Indirect numerical integration is a new class of numerical integration methods with ideal accuracy, convergence and stability properties. The methods are based on a novel time-response invariant discrete synthesis. The foundations and general principles of indirect numerical integration are discussed in detail. The dissertation includes the complete set of indirect numerical integration formulas in the three canonic forms of state-variable representation.

Difference approximation is a general method for applying numerical integration to systems characterized by discrete samples of their responses. General principles of the method are analyzed, the set of indirect numerical integration formulas for the difference approximation is given, and novel interpolation-based approximation methods are presented.

The above two techniques are applied to *the transient simulation of transmission lines*. The author attempts to formulate a high-level description of the transmission line simulation method that has maximum efficiency, accuracy and applicability to the transient simulation of high-speed digital circuits. To formulate the approach, most significant aspects of the problem are identified, and alternative approaches in each of the aspects are analyzed and compared to find the combination which results in maximum efficiency, accuracy and applicability for the transient analysis of high-speed digital circuits.

The step-by-step implementation of the approach for uniform and nonuniform multiconductor lossy frequency-dependent lines characterized by samples of their responses is presented. The resulting transmission line model can be directly incorporated into a circuit simulator. The implementation includes ac, dc and transient analyses. The method has been adopted in several industrial and commercial circuit simulators, and in numerous real-life simulation exercises proved to be reliable and accurate. It is shown on an extensive set of runtime data that, based on this approach, the accurate line modeling in a circuit simulator is as efficient as the simple replacement of interconnects with lumped resistors.

ACKNOWLEDGMENTS

The author wishes to thank his advisor, Professor Jose Schutt-Ainé, for enduring guidance and support. The author is grateful to Professor Raj Mittra for guidance and many hours of fruitful discussions leading to the development of the internal-reflection nonuniform transmission line model, and for finding industrial applications for the results of the author's research.

Thanks are due to Dr. Wiren Dale Becker, Mr. Wendemagegnehu Beyene and Dr. Kyung Suk Oh for providing numerical data for the examples in Chapter 2. The author is thankful to Mr. Hem Satsangi for installing the author's transmission line model in Spice, Dr. C. Kumar for implementing the model in Cadence's DFSSignoise, and Dr. Rui Wang for adopting the model in Intel's circuit simulator.

TABLE OF CONTENTS

1. INTRODUCTION	1
2. INDIRECT NUMERICAL INTEGRATION	4
2.1. Introduction	4
2.1.1. Numerical integration	4
2.1.2. Convergence, accuracy and stability	5
2.1.3. Linearization methods	5
2.2. Indirect Numerical Integration	6
2.2.1. Time-response invariant discrete synthesis	6
2.2.2. Stability	9
2.2.3. Local interpolation error	9
2.2.4. Convergence	10
2.2.5. Canonic state-variable representations	11
2.2.6. Indirect numerical integration formulas in Appendix A	12
2.3. Applications	15
2.4. Conclusions	20
3. DIFFERENCE APPROXIMATION	22
3.1. Introduction	22
3.2. General Principles of Difference Approximation	23
3.2.1. Fundamental issues	23
3.2.2. Canonic forms	24
3.2.3. Complex-to-real mapping, magnitude, real- and imaginary-part approximations	25
3.2.4. Difference approximation of multiport systems	27
3.2.5. Matrix delay separation	27

3.3. Approximation Methods	28
3.3.1. Comparison of approximation methods	28
3.3.2. Relaxation interpolation method	30
3.3.3. Direct interpolation-based method for frequency-domain difference approximation	34
3.4. Difference Approximation and Asymptotic Waveform Evaluation	40
3.5. Conclusions	43
4. CIRCUIT SIMULATION OF TRANSMISSION LINES	45
4.1. Introduction	45
4.2. System Model for Transmission Lines	46
4.3. Formulation of Optimal Approach	48
4.3.1. Formulation	50
4.3.2. Line characterization	50
4.3.3. Line model	52
4.3.4. Transient simulation method	52
4.3.5. Approximation methods	54
4.3.6. Summary of the optimal approach	55
4.4. Simulation of Uniform Lines	55
4.4.1. Frequency-domain line model for transient analysis	55
4.4.2. Difference approximation	57
4.4.2.1. Matrix delay separation	58
4.4.2.2. Matrix complex rational approximation method for the frequency-domain difference approximation	59
4.4.2.3. Indirect numerical integration	60
4.4.3. Companion model	61
4.4.4. Line model for ac and dc analyses	63
4.4.5. Initial conditions for transient analysis	64
4.4.6. Optimal line simulation algorithm	64
4.4.7. Numerical results	65
4.5. Simulation of Nonuniform Lines	68
4.5.1. Open-loop model	68
4.5.2. Open-loop internal-reflection model	71
4.5.3. Numerical results	75
4.6. Conclusions	79

5. CONCLUSIONS.....	80
APPENDIX A. INDIRECT NUMERICAL INTEGRATION FORMULAS	83
A.1. Canonic and Parallel Canonic Forms	83
A.2. Cascade Canonic Form	85
APPENDIX B. OPEN-LOOP TRANSMISSION-LINE TRANSFER FUNCTIONS	86
APPENDIX C. FUNDAMENTAL TIME-DOMAIN OPEN-LOOP RESPONSES OF TWO-CONDUCTOR LINES	88
APPENDIX D. OPEN-LOOP TRANSFER FUNCTIONS OF PARABOLICALLY TAPERED LINES	90
APPENDIX E. EXPRESSIONS FOR OPEN-LOOP INTERNAL- REFLECTION FUNCTIONS IN TERMS OF OPEN-LOOP FUNCTIONS	92
LIST OF REFERENCES	94
VITA	98

1. INTRODUCTION

This dissertation is a continuation of the work described in [2]. It includes three topics in the area of transient simulation of linear systems, namely: *indirect numerical integration*, *difference approximation*, and *circuit simulation of transmission lines*.

Numerical integration is a general method for numerical solution of differential equations which has numerous applications. In this dissertation, we consider numerical integration in its application to the transient simulation of dynamic systems, and use the corresponding notation and terminology.

Numerical integration represents one of the three classes of transient simulation methods (the other two are numerical transformation and convolution). Numerical integration is the most efficient and practically applicable of the three. In contrast to the numerical convolution and transformation techniques, numerical integration has linear computational complexity, can directly (without relaxation) handle nonlinear and time-varying systems, does not introduce time- or frequency-response truncation errors, supports variable time stepping, and is directly compatible with recursive time-domain solvers employed by circuit simulators.

Numerical integration is based on the discretization of the system differential equations resulting in discrete-time algebraic equations. The latter are used to perform the transient simulation recursively in the time domain.

In the case of direct numerical integration methods, the differential equations are discretized using a discrete approximation for integral/differential operators based on an approximation for the system response. The discrete approximation is applied to the derivatives in the differential equations to transform the latter into discrete-time algebraic equations. Direct numerical integration includes such conventional methods as Runge-Kutta, linear multistep formulas, forward and backward Euler formulas, trapezoidal rule, and Gear's formulas.

Indirect numerical integration is a new class of numerical integration methods with ideal accuracy, convergence and stability properties. Indirect numerical integration is based on the analytical relationship between the discrete samples of the excitation and response. To obtain the

relationship, the system differential equations are discretized by means of the novel time-response invariant discrete synthesis. The resulting discrete-time difference equations differ from those obtained via the conventional numerical integration methods only in the values of the coefficients, and can replace the latter to efficiently perform transient simulation of dynamic circuits and systems in exactly the same manner.

The foundations of indirect numerical integration and its general principles are discussed in Chapter 2. The complete set of the indirect numerical integration formulas is presented in Appendix A.

While being the only transient simulation method with linear computational complexity, numerical integration is based on discretization of the system differential equations, and can not be directly applied to systems characterized by measured or simulated samples of their responses, which are often encountered in practice. A general systematic solution to this problem is to approximate any frequency or time response of the system with the corresponding response of a system whose differential equations are known. Then numerical integration can be applied and the difference equations can be readily obtained.

This procedure is called *the difference approximation*. Its applications include efficient transient simulation of systems characterized by discrete data samples, transcendental transfer functions, and higher-order systems (the order-reduction problems). In recent years, the difference approximation has been used by an increasing number of time-domain simulation methods such as Asymptotic Waveform Evaluation (AWE) techniques, techniques used with the Finite-Difference Time-Domain method to model frequency-dependent materials and implement surface-impedance boundary conditions, and numerous transmission line simulation methods. The theory behind the difference approximation, however, has not been studied adequately.

Chapter 3 of this dissertation attempts to fill the gap and to analyze the general principles and foundations of the difference approximation, common for all of its applications. In addition, it presents novel interpolation-based approximation methods, and discusses AWE as an important special case of the difference approximation.

The problem of *transmission line simulation* gained special importance with the development of high-speed digital electronics. As transient times become faster, the transmission line behavior of electronic interconnects starts to significantly affect transient waveforms, and accurate modeling of on-board and even on-chip interconnects becomes an essential part of the design process. The complexity of contemporary digital circuits necessitates the simultaneous simulation of thousands of lossy coupled frequency-dependent lines surrounded by thousands of nonlinear active devices. Lines to be simulated may be characterized by measured or electromagnetically simulated samples of their responses.

The problem of line simulation involves several areas of science, such as electromagnetics, computational mathematics, and circuit and system theories. The solution of the problem is straightforward in the sense that all of the components involved are well known and need only to be combined together. The integration of areas, however, is a difficulty that keeps the problem open and accounts for the diversity of developed methods.

This thesis presents an original attempt to identify the components of the problem and to formulate a high-level description of a method which provides maximum efficiency, accuracy and applicability for the transient analysis of digital circuits. Such an approach allows one to more accurately assess and compare the performance of numerous and diverse methods.

Chapter 4 presents the formulation of the optimal approach, and discusses many of the existing line simulation methods. It also describes step-by-step implementation of the optimal method for uniform and nonuniform multiconductor lossy coupled frequency dependent lines, and presents numerical verification of the method's accuracy and efficiency.

2. INDIRECT NUMERICAL INTEGRATION

2.1. Introduction

2.1.1. Numerical integration

Numerical integration is a general method for numerical solution of differential equations which has numerous applications. In this dissertation, we consider numerical integration in its application to the transient simulation of dynamic systems and use the corresponding notation and terminology.

Numerical integration represents one of the three classes of transient simulation methods (the other two are numerical transformation and convolution). Numerical integration is the most efficient and practically applicable of the three. In contrast to the numerical convolution and transformation techniques, numerical integration has linear computational complexity, can directly (without relaxation) handle nonlinear and time-varying systems, does not introduce time- or frequency-response truncation errors supports variable time stepping, and is directly compatible with recursive time-domain solvers employed by circuit simulators.

Numerical integration is based on the discretization of system differential equations¹, resulting in discrete-time algebraic equations. The latter are used to perform the transient simulation recursively in the time domain.

In the case of direct numerical integration methods, the differential equations are discretized using a discrete approximation for integral/differential operators based on an approximation for the system response. The discrete approximation is applied to the derivatives in the differential equations to transform the latter into discrete-time algebraic equations. Direct

¹Numerical integration can be applied to systems whose differential equations are not available (e.g., systems characterized with discrete samples of their frequency- or time-domain responses) via the difference approximation technique described in the next chapter and [1], [2].

numerical integration includes such conventional methods as Runge-Kutta, linear multistep formulas, forward and backward Euler formulas, trapezoidal rule, and Gear's formulas [5], [6].

Typically, the system response is approximated with a polynomial of order p . In this case, p is called *the order* of the method. If the discrete approximation for integral/differential operators contains the present-time derivative of the response, the method is called *implicit*; otherwise, it is called *explicit*.

An important feature of numerical integration is that the discrete-time equations obtained via different numerical integration methods, including indirect numerical integration presented in Section 2.2, differ only in the values of the coefficients, but have very different properties which depend greatly on the way in which the original continuous-time equations were discretized.

2.1.2. Convergence, accuracy and stability

Important characteristics of a numerical integration method are *convergence*, *accuracy* and *stability*. Accuracy for direct numerical integration methods is characterized by the local truncation error (LTE), which represents the error introduced at the current time iteration by truncation of the higher-order terms in the polynomial approximation of the continuous signal used to obtain the discrete-time approximation for derivatives. Consequently, the order of the LTE is $p + 1$. For conventional numerical integration methods, LTE provides an effective way of estimating error introduced at each time iteration at its source, and is commonly used for step control.

Stability properties of a numerical integration method are estimated with respect to a first-order linear homogeneous test equation

$$\dot{y}(t) = \lambda y(t). \quad (2.1)$$

Ideally, stability properties of the numerical solution should match those of the exact solution. Implicit and explicit methods have radically different stability properties. Finally, convergence indicates whether the numerical solution converges to the exact solution as the time step goes to zero.

2.1.3. Linearization methods

For the transient simulation of nonlinear dynamic systems, numerical integration is applied in conjunction with linearization methods. There are three groups of linearization methods [3],

namely, separation of linear and nonlinear parts, harmonic linearization (used for narrow-bandwidth systems), and iterative linearization.

The separation of linear and nonlinear parts has limited but important applications such as circuit simulation based on the modified nodal approach (MNA) [5] in which linear and nonlinear circuit elements and subcircuits are modeled and represented independently in the circuit matrix by their stamps. Transmission line models described in Chapter 4 and [14], [15] may serve as an example of such separation.

The iterative linearization methods, such as Katzenelson and Newton-Raphson [4], [5], are the most general. The Katzenelson method approximates a nonlinear function by a piecewise linear one, whereas the Newton-Raphson method solves nonlinear equations in a relaxation iterative fashion based on the first-order Taylor expansion of the nonlinear function. As a result, the Katzenelson method is more efficient, while the Newton-Raphson method is more accurate but prone to convergence problems.

Numerical integration is especially well-suited for use with iterative linearization methods, because it performs the transient analysis iteratively in small increments, and linearization can be performed locally and accurately. With the transformation and convolution techniques, the linearization can be applied only globally, leading to relaxation methods which additionally degrade efficiency and accuracy of the transient simulation.

2.2. Indirect Numerical Integration

2.2.1. Time-response invariant discrete synthesis

In [2], a new class of numerical integration methods—*indirect numerical integration*—was introduced. Indirect numerical integration is based on the analytical relationship between the discrete samples of the excitation and response. To obtain the relationship, the system differential equations are discretized by means of the novel *time-response invariant discrete synthesis*. It proceeds in the following three steps.

1. Assume the excitation to be piecewise² of a certain form (e.g., staircase, piecewise-linear or quadratic). This will be the form of the invariance.
2. Find the general solution of the system differential equations for the assumed form of the excitation.

²On the intervals between the discrete time points.

3. Express unknown constants of the general solution in terms of the discrete samples of the excitation and response by using the samples as boundary conditions.

The result is a discrete-time model of the continuous system, which, for linear stationary systems, has the form of difference equations, and, for this reason, is called *the system difference model*. The difference model is used for the transient simulation in exactly the same manner as the discrete equations obtained via direct numerical integration methods, and, as for direct methods, the computational complexity is linear.

Example. To illustrate the derivation of indirect numerical integration formulas, let us apply the ramp-response invariant discrete synthesis to the following first-order linear scalar differential equation

$$\dot{y}(t) = \lambda y(t) + x(t), \quad (2.2)$$

where $x(t)$ is the excitation, $y(t)$ is the response, and $\dot{y}(t) = dy(t)/dt$.

1. For the ramp invariance, the excitation is assumed to be piecewise linear

$$x(t) = at + b, \quad t_{n-1} \leq t \leq t_n. \quad (2.3)$$

2. Then, the general solution of the differential equation (2.2) is

$$y(t) = -\frac{a+b\lambda}{\lambda^2} - \frac{a}{\lambda}t + ce^{\lambda t}, \quad t_{n-1} \leq t \leq t_n, \quad (2.4)$$

where c is an arbitrary constant.

3. Finally, by applying the boundary conditions

$$x(t_n) = x_n,$$

$$x(t_{n-1}) = x_{n-1},$$

$$y(t_n) = y_n,$$

$$y(t_{n-1}) = y_{n-1},$$

to the invariance function (2.3) and general solution (2.4), the general solution can be expressed as

$$y_n = \frac{e^{\lambda T_n} - \lambda T_n - 1}{\lambda^2 T_n} x_n + \frac{1 + (\lambda T_n - 1)e^{\lambda T_n}}{\lambda^2 T_n} x_{n-1} + e^{\lambda T_n} y_{n-1}, \quad (2.5)$$

where $T_n = t_n - t_{n-1}$ is the time step.

The formula (2.5) is the ramp-invariant difference model of a continuous system described by the differential equation (2.2). ■

The total number of samples of the excitation and response in a difference model equals the total number of the unknown constants in the invariance function and general solution (a , b , and c in the above example) plus one. For linear two-port systems, the derivation can be reduced to table lookups and purely algebraic operations by using Laplace and Z -transforms to solve differential equations and express the general solution in terms of discrete samples [2].

The invariance has to be of zero order (the step invariance) or higher. The impulse invariance can not be used for indirect numerical integration, because the system response to a δ -sampled excitation has to be additionally integrated to converge to the exact response as the time step goes to zero [3], [7]. The invariance function does not necessarily have to be a polynomial.

Theorem 2.1. During the transient simulation, *the difference model interpolates the discrete samples of the excitation with the invariance function and provides the exact solution of the system differential equations for the interpolated excitation.*

Proof: Follows directly from the definition of the time-response invariant discrete synthesis, according to which the difference model *is* the exact analytical solution of the system differential equations expressed in terms of the discrete samples of the excitation and response, and for the excitation interpolated by the invariance function. ■

In effect, Theorem 2.1 simply rephrases the definition of the time-response invariant discrete synthesis.

Corollary 2.1. For excitations which are piecewise of the same form as the form of the invariance, the difference model provides the exact solution.

Proof: The invariance function will exactly match the excitations which are piecewise of the same form as the form of the invariance. Thus, according to Theorem 2.1, the difference model will provide the exact solution in this case. ■

For instance, a ramp-invariant difference model provides the exact system response to a piecewise linear excitation, such as a pulse with linear rise and fall. Notice that Corollary 2.1 imposes no limitations on the value of the time step.

Corollary 2.2. Any difference model provides the exact solution of the homogeneous test equation (2.1).

Proof: Any invariance function will match the zero excitation exactly. Thus, according to Theorem 2.1, the difference model will provide the exact solution in this case. ■

Notice that Corollary 2.2 imposes no limitations on the value of the time step or the form of the invariance.

2.2.2. Stability

The stability properties of a numerical integration formula are evaluated with respect to the homogeneous test equation (2.1).

Theorem 2.2. Any difference model of the homogeneous test equation (2.1) matches exactly its stability properties.

Proof: According to Corollary 2.2, any difference model provides the exact solution of the homogeneous test equation. Thus, it also matches exactly the stability properties of that equation. ■

Theorem 2.2 imposes no limitations on the form of the invariance or the value of the time step. The separation into explicit and implicit is not applicable to indirect numerical integration methods because they use no approximation for derivatives.

2.2.3. Local interpolation error

The accuracy of conventional numerical integration methods is characterized by the local truncation error. LTE represents the error introduced at the current time iteration by truncation of the higher-order terms in the power series expansion of the signals to which the discrete approximation for derivatives is applied. Thus, for conventional numerical integration methods, LTE provides an effective way to estimate the local error at its source. In the case of indirect numerical integration, no approximation for the derivatives is made, and LTE is no longer effective in estimating the local error. For indirect numerical integration, the only error arises from the interpolation of the excitation with the invariance function. The expressions for the local interpolation errors are given in Table 2.1. The expressions were obtained with respect to a one-order-higher interpolation. They can be used to control the time stepping during the transient simulation.

Similarly to the LTE for the direct methods, the local interpolation error provides an efficient way to estimate the local numerical integration error at its source, which, for indirect

TABLE 2.1
LOCAL INTERPOLATION ERRORS

Local Interpolation Error	Step Invariance $\tilde{x}(t) = x_{n-1},$ $t_{n-1} \leq t \leq t_n$	Ramp Invariance $\tilde{x}(t) = x_{n-1} + \frac{x_n - x_{n-1}}{T_n} t, \quad t_{n-1} \leq t \leq t_n$
Maximum Absolute Error $\epsilon_a = \max_{t_{n-1} \leq t \leq t_n} x(t) - \tilde{x}(t) $	$ x_n - x_{n-1} + O(T_n^2)$	$\frac{T_n T_n(x_{n-1} - x_{n-2}) - T_{n-1}(x_n - x_{n-1}) }{4T_{n-1}(T_n + T_{n-1})} + O(T_n^3)$
Mean-Square Error $\epsilon_m = \sqrt{\frac{1}{T_n} \int_{t_{n-1}}^{t_n} (x(t) - \tilde{x}(t))^2 dt}$	$\frac{ x_n - x_{n-1} }{\sqrt{3}} + O(T_n^2)$	$\frac{T_n T_n(x_{n-1} - x_{n-2}) - T_{n-1}(x_n - x_{n-1}) }{\sqrt{30} T_{n-1}(T_n + T_{n-1})} + O(T_n^3)$

Note: $x(t)$ is the excitation, $\tilde{x}(t)$ is the interpolating function (the invariance function), and $T_n = t_n - t_{n-1}$ is the time step.

numerical integration, is always in the excitation, in contrast to the direct numerical integration methods which introduce an error in every derivative present in the original continuous-time equation and result in the LTE being always present either in the response or in both the response and excitation. Transforming the local interpolation error to the response is not practical because this operation depends not only on the order of the invariance but also on the specific form of the difference model, and results in complicated expressions which are computationally more expensive than numerical integration itself.

2.2.4. Convergence

As mentioned in Section 2.1.2, convergence characterizes whether the discrete solution converges to the exact solution as the time step goes to zero.

Theorem 2.3. An indirect numerical integration method is convergent iff the interpolation with the invariance function converges to the input waveform as the time step goes to zero.

Proof: Follows directly from the fact that the only error in the indirect numerical integration comes from the interpolation of the excitation with the invariance function. ■

Corollary 2.3. Indirect numerical integration methods with polynomial forms of invariance are convergent.

Proof: Polynomial interpolation of zero order and higher converges to the original function as the interpolation step goes to zero. Thus, according to Theorem 2.3, an indirect numerical integration method with the polynomial form of invariance is convergent. ■

Notice that Corollary 2.3 does not require the excitation to be continuous.

Corollary 2.4. The impulse-invariant indirect numerical integration method is not convergent.

Proof: The δ -impulse interpolation does not converge to the original function as the interpolation step goes to zero. Thus, according to Theorem 2.3, an impulse-invariant indirect numerical integration method is not convergent. ■

However, if the δ -impulse interpolation is integrated, it converges. Therefore, an impulse-invariant difference model can be made convergent by an additional integration.

Corollary 2.5. The difference model of any form of invariance is convergent for a homogeneous test equation (2.1).

Proof: Any invariance function interpolates the zero excitation exactly. Thus, according to Theorem 2.3, the statement of this corollary is true. ■

2.2.5. Canonic state-variable representations

When a difference model goes more than one step back in time, its accuracy is reduced because of the overlap between the local domains of invariance. Then, the exact result is obtained only for the excitations which are *globally* of the same form as the form of the invariance. To preserve the *piecewise* exactness, a difference model has to go back only one time step. This is achieved by means of state variable formulations, which transform higher-order differential equations into a system of first-order equations. There are three conventional ways of introducing state variables which correspond to the three canonic forms of system representation: *canonic*, *parallel canonic* and *cascade* (or *series*) *canonic forms* [3], [7].

The canonic form corresponds to the standard state variable formulation. It represents higher-order differential equations as first-order matrix differential equations [3]. The canonic form is the most general of the three, and can be used for multiport systems with nondistinct poles.

The parallel canonic form represents a higher-order system as a set of first-order systems connected in parallel. The transfer function has then the form of a sum of first-order rational

polynomial functions, and fundamental time-domain responses have the form of an exponential series. The parallel canonic form is not general, and can only be used for systems with distinct poles.

In the cascade canonic form, a higher-order system is represented as a set of first-order systems connected in cascade. The cascade canonic form does not preserve the invariance of difference models for higher-order systems. This form is not suitable for representation of multiport systems, and has no general closed-form expressions for the fundamental time-domain responses.

The complete set of step- and ramp-invariant indirect numerical integration formulas in the three canonic forms for arbitrary-order multiport linear stationary systems is given in Appendix A.

2.2.6. Indirect numerical integration formulas in Appendix A

To obtain a difference model of a system using Appendix A, one has to represent either the system differential equations, the transfer function, or a fundamental time-domain response in one of the three canonic forms. The corresponding difference models are then readily given in Appendix A directly in terms of the parameters of the canonic representations.

The following example illustrates the application of the time-response invariant discrete synthesis to multiport systems (in matrix form) on the derivation of the step-invariant canonic difference model from Appendix A.

Example. The canonic state equation is

$$\dot{\mathbf{z}}(t) = \mathbf{\Omega}\mathbf{z}(t) + \mathbf{C}\mathbf{x}(t), \quad (2.6)$$

where $\mathbf{x}(t)$ is the $l \times 1$ excitation vector, $\mathbf{z}(t)$ is the $m \times 1$ system state vector, $\mathbf{\Omega}$ is the $m \times m$ system matrix, and \mathbf{C} is the $m \times l$ control matrix [3].³

1. For the step invariance, the excitation is assumed to be staircase (piecewise constant)

$$\mathbf{x}(t) = \mathbf{a}, \quad t_{n-1} \leq t \leq t_n. \quad (2.7)$$

2. Then, the general analytic solution of the differential equation (2.6) is

$$\mathbf{z}(t) = \mathbf{\Omega}^{-1}(\mathbf{F}(t) - \mathbf{I})\mathbf{C}\mathbf{a} + \mathbf{F}(t)\mathbf{b}, \quad (2.8)$$

where \mathbf{I} is the $m \times m$ identity matrix, \mathbf{b} is an arbitrary $m \times 1$ constant vector, and

³Throughout the dissertation, capital boldface, small boldface and normal italic symbols denote matrices, vectors and scalars, respectively.

$$\mathbf{F}(t) = \mathbf{e}^{\Omega t}$$

is the fundamental matrix [3]. The boldface $\mathbf{e}^{\Omega t}$ denotes matrix exponential.⁴

3. Finally, by applying the boundary conditions

$$\mathbf{x}(t_{n-1}) = \mathbf{x}_{n-1},$$

$$\mathbf{z}(t_n) = \mathbf{z}_n,$$

$$\mathbf{z}(t_{n-1}) = \mathbf{z}_{n-1},$$

to the invariance function (2.7) and general solution (2.8), the general solution can be expressed as

$$\mathbf{z}_n = \mathbf{F}(T_n)\mathbf{z}_{n-1} + \Omega^{-1}(\mathbf{F}(T_n) - \mathbf{I})\mathbf{C}\mathbf{x}_{n-1}. \quad (2.9)$$

The formula (2.9) is the step-invariant difference model of a multiport continuous system described by the matrix canonic state equation (2.6). Notice that the derivation used no assumptions on the Ω and \mathbf{C} matrices other than Ω being invertible. ■

Compared to the step-invariant models, the ramp-invariant models increase the simulation accuracy with no increase in the computational complexity. The step-invariant models, however, do not contain the present-time sample of the excitation, which is important for applications such as circuit simulation discussed in Chapter 4. The ramp-invariant formulas are given in two forms: with equalized present- and past-time coefficients, and with zero present-time coefficient. The latter form, however, is somewhat more computationally involved and requires storing an old value of one of the coefficients. These forms were derived by transforming the state variables in the discrete domain so as to equalize the coefficients or to null one of them, with the purpose of reducing the number of multiplications.

Increasing the order of the invariance beyond the ramp invariance increases the computational complexity without a substantial increase in accuracy. It also results in multistep difference models for first-order differential equations, and a state-variable representation has to be applied once again in the discrete domain to preserve the invariance of the formulas.

The difference models obtained via indirect and conventional numerical integration methods which employ an approximation for derivatives of the same order as the order of the invariance differ only in the values of the coefficients. Consequently, the storage requirements and number of arithmetic operations per time step for indirect and conventional numerical

⁴The bold-face functions are used throughout the dissertation to denote matrix functions such as the matrix exponential and matrix power.

integration methods are the same, provided that all the matrices are full and the difference models are already available. However, different numerical integration and linearization methods may have different effects on sparsity of sparse systems, which is also application-specific.

To nonlinear time-varying systems, the formulas are applied in conjunction with staircase approximation for the time variance and linearization techniques described in the preceding section. Alternatively, the time-response invariant discrete synthesis can be applied directly to nonlinear time-varying systems. The first approach is more universal, whereas the second is more accurate but application-specific and limited to nonlinear differential equations which have analytical solutions.

Analytical efforts involved in the derivation of indirect numerical integration formulas can be greater than those for conventional methods. In addition, formulation of the state equations in the canonic forms is a difficult and application-specific problem, and can be computationally more expensive than subsequent numerical integration. There are, however, numerous and important applications, such as asymptotic waveform evaluation (AWE) [12], [13], difference approximation described in Chapter 3, and examples from the next section, in which the system is already represented in a canonic form.

Evaluation of exponential functions in the coefficients of difference models is computationally inexpensive, because the functions contain the time step (which is always small) as an argument. Furthermore, the coefficients have to be recomputed only when the value of the time step changes.

Figure 2.1 shows a comparison of transient responses of a third-order system simulated with the ramp-invariant indirect numerical integration method and trapezoidal rule (both applied to the canonic state equations). As one can observe, the indirect numerical integration provides the exact results, whereas, for the same time step, the trapezoidal rule introduces a significant error (although the local interpolation error for the ramp invariance is even one order lower than the LTE for the trapezoidal rule). The simulation runtime for the indirect numerical integration (including evaluation of the coefficients) was only half of the runtime for the trapezoidal rule for the same time step. For a comparable accuracy, the simulation runtime for the trapezoidal rule is in excess of 25 times that for the indirect numerical integration.

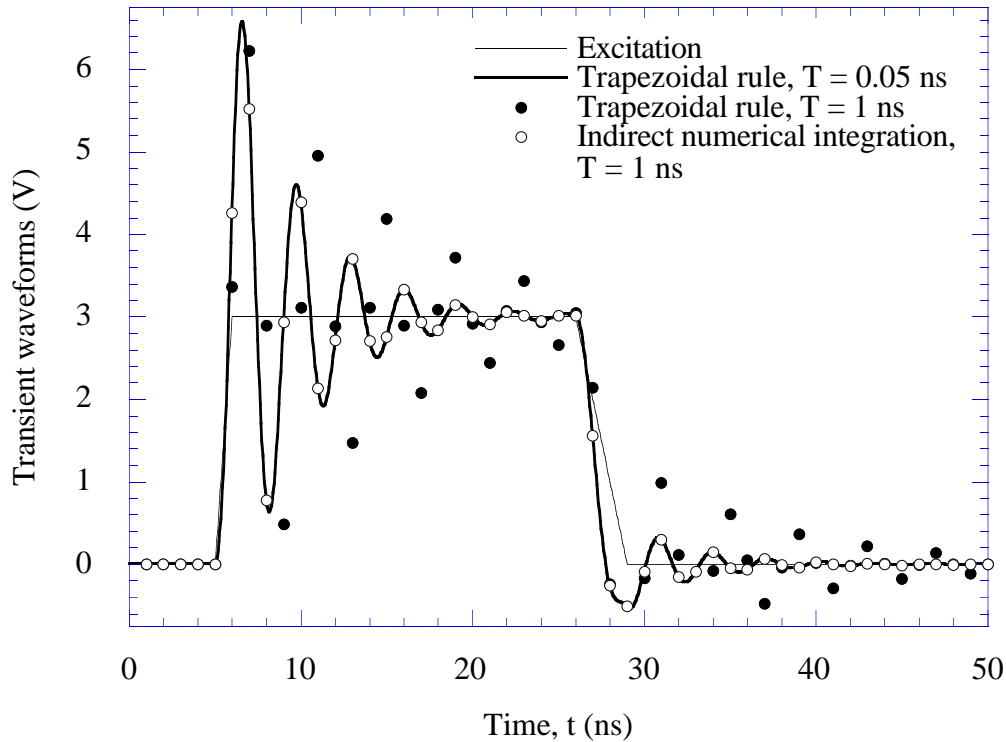


Fig. 2.1. Comparison of the ramp-invariant indirect numerical integration method and trapezoidal rule.

2.3. Applications

While offering the improved accuracy, convergence and stability properties, the discrete-time difference equations obtained via indirect numerical integration differ from those obtained via the conventional methods only in the values of the coefficients, and, in many cases, can replace the latter to efficiently perform transient simulation of circuits and systems in exactly the same manner.

Indirect numerical integration covers, as special cases, many important techniques which have been used extensively for a number of years, such as recursive convolution [8]-[11], the step-invariance method of infinite impulse response digital filter design [3], [7], approximation of the response of a linear network to an arbitrary piecewise linear input waveform used with the AWE methods [12], [13], and even the trapezoidal rule, which is a ramp-invariant difference

model for a simple integrator but acts as a direct numerical integration method for more complex systems.

The introduction of the novel time-response invariant discrete synthesis and indirect numerical integration as a new class of numerical integration methods generalizes and provides a deeper systematic insight into some of these techniques and their properties. For instance, it explains why the convolution integral can be taken recursively for some kernels by showing that these cases are equivalent to numerical integration of finite-order ordinary differential equations. It also extends the digital filter design techniques, previously limited to scalar constant-time-step systems by the use of the Z-transformation, to multiport variable-time-step discrete-time systems. Indirect numerical integration has also found a number of new applications, some of which are illustrated below.

Indirect numerical integration was applied to transient simulation of transmission lines as described in Chapter 4. Figure 2.2 shows a comparison of transient waveforms for a circuit consisting of lossy transmission lines, nonlinear elements (MOSFETs) and lumped linear elements, simulated in Spice using the built-in convolution-based model for lossy transmission lines [16] and an otherwise similar indirect numerical integration based model. Figure 2.2 shows

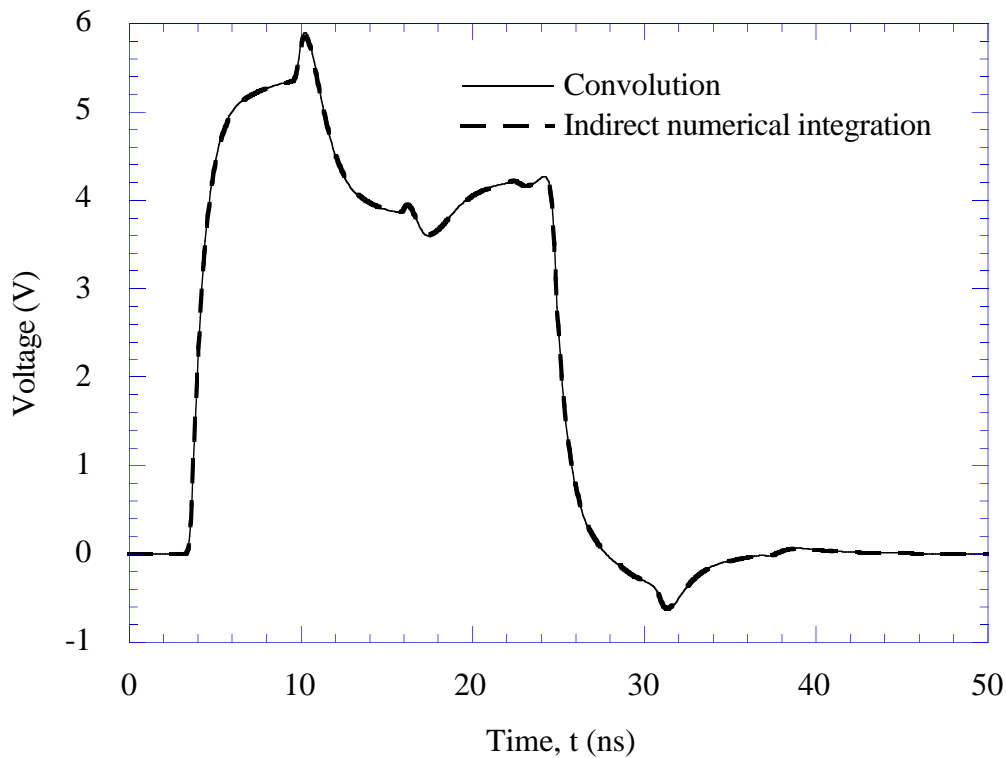


Fig. 2.2. Comparison of transient waveforms simulated in Spice using the built-in convolution-based model for lossy transmission lines and an indirect numerical integration based model.

that the waveforms are indistinguishable, although the total simulation runtime was reduced by two orders of magnitude.

In Oh and Schutt-Ainé [10], ramp-invariant indirect numerical integration is used to implement the surface impedance boundary conditions for the finite-difference time domain (FDTD) method. Figure 2.3 shows the simulated electric field distribution for a two-dimensional scattering from a square cylinder. The total order of indirect numerical integration carried out to model the surface of the scatterer was 1280. As shown in [10], the results are in a good agreement with those for conventional FDTD, and the size of the problem is significantly reduced.

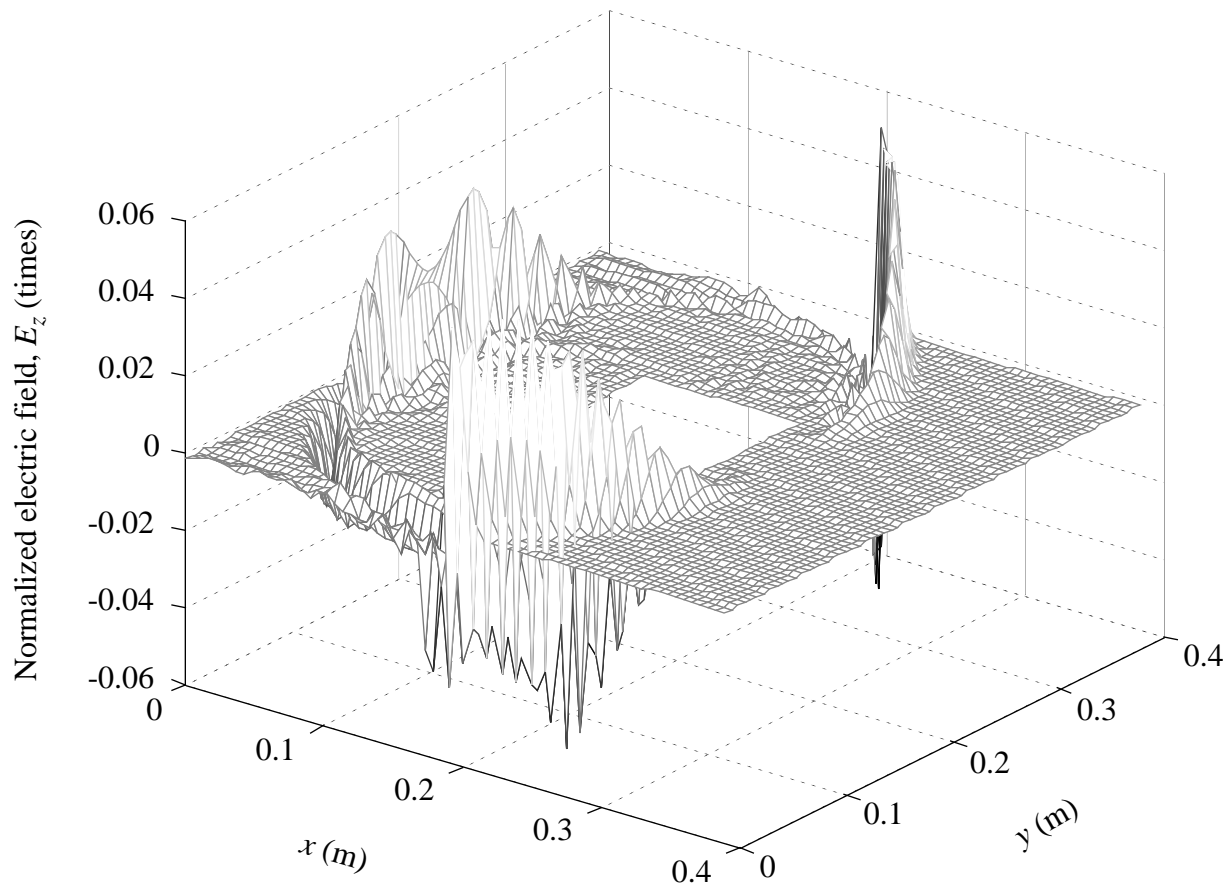


Fig. 2.3. Electric field distribution simulated using FDTD with surface impedance boundary conditions based on indirect numerical integration.

Indirect numerical integration in conjunction with AWE is used to simulate transient behavior of semiconductor devices, Beyene and Schutt-Ainé [17]. Using moment-matching AWE techniques, the partial diffusion equation is approximated by ordinary differential equations which are then solved using indirect numerical integration. Figure 2.4 shows the distribution of excess minority carrier concentration in the n -type region of a p^+n junction simulated using step-invariant indirect numerical integration.

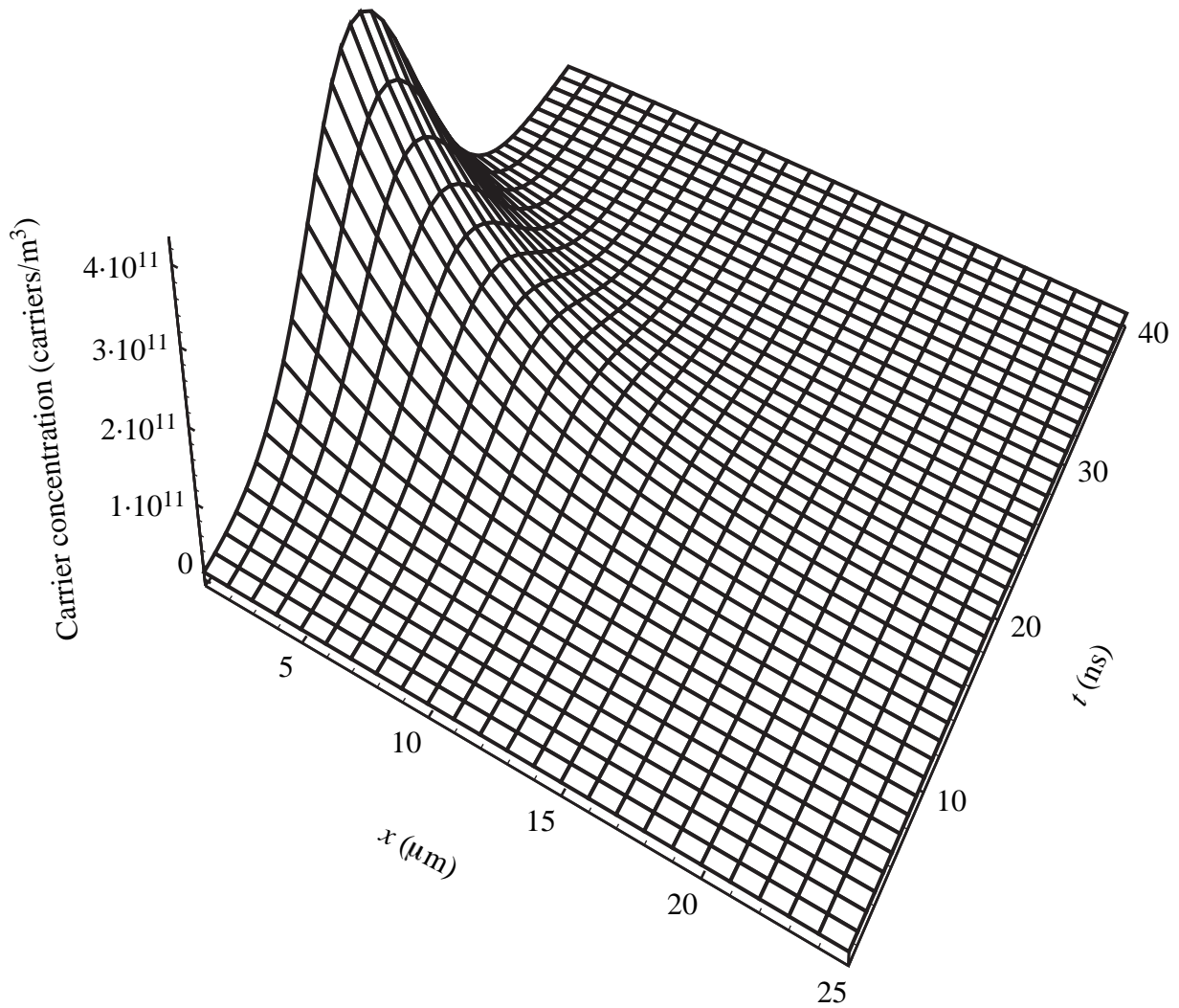
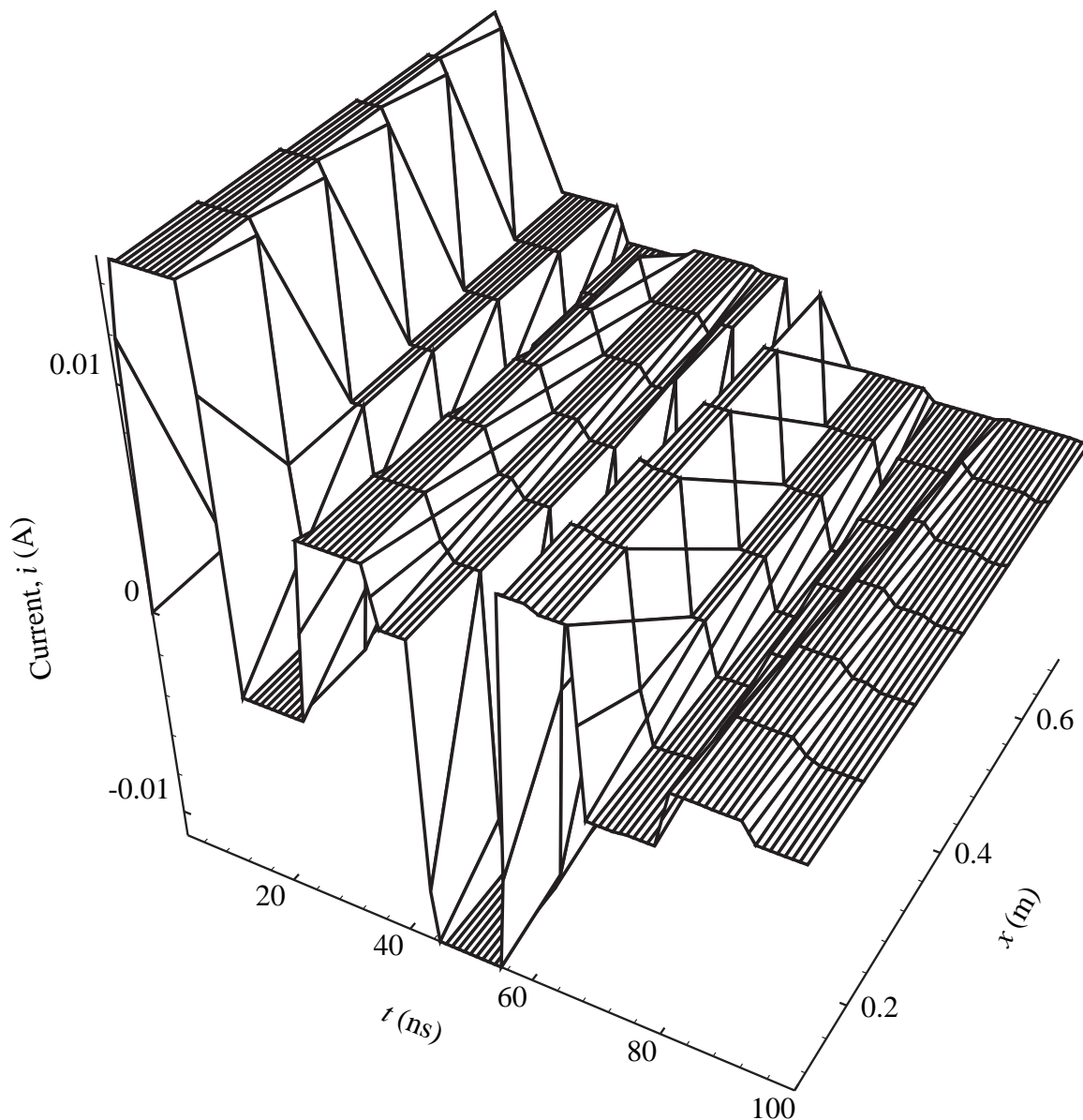


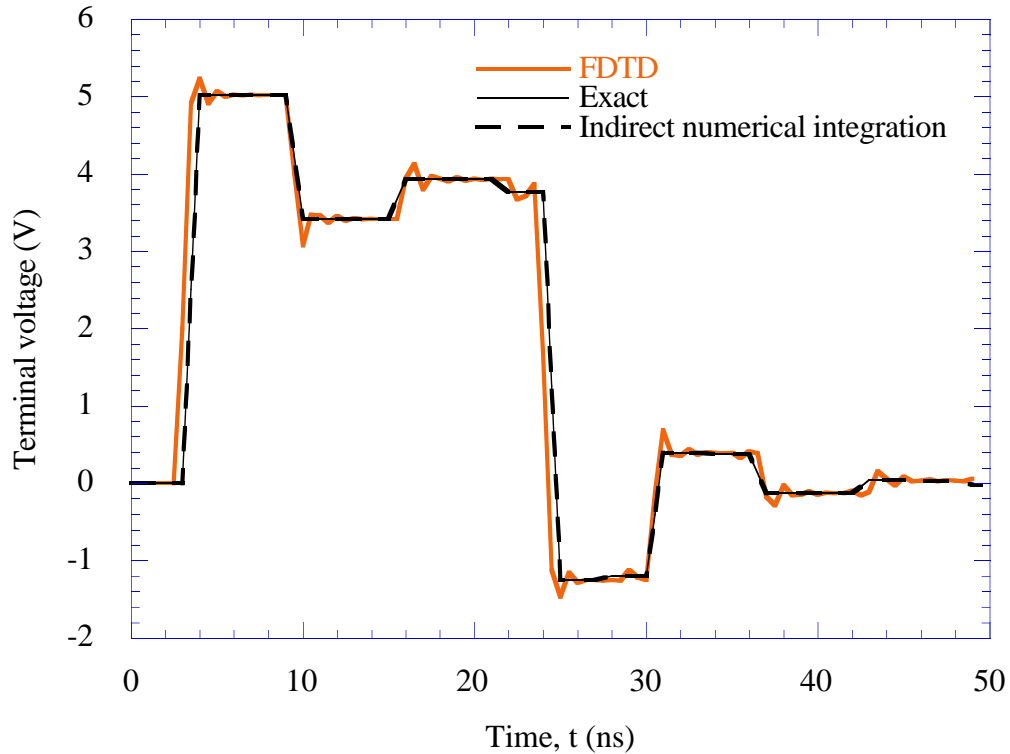
Fig. 2.4. Distribution of carrier density simulated using indirect numerical integration applied in conjunction with AWE to solve the diffusion equation.

In the following example, indirect numerical integration is used to directly solve the partial Telegrapher's equations [2]. Ramp-invariant indirect numerical integration was applied to separately discretize the time and spatial sides of the partial differential equations while treating the other side as an excitation. Figure 2.5 shows the simulated current distribution along a transmission line and comparison of the transient waveforms with those simulated using the



(a)

Fig. 2.5. (a) Current distribution along a transmission line simulated using indirect numerical integration applied to solve Telegrapher's equations. (b) Comparison of transient waveforms at the transmission line terminal.



(b)

Fig. 2.5 continued.

FDTD method based on the central-difference (direct) numerical integration scheme. Figure 2.5 shows that indirect numerical integration provides the exact results, whereas FDTD introduces a substantial error.

2.4. Conclusions

This chapter presented indirect numerical integration [21], a new class of numerical integration methods based on the novel time-response invariant discrete synthesis. While offering improved accuracy, convergence and stability properties, the discrete-time difference equations obtained via indirect numerical integration differ from those obtained via the conventional numerical integration methods only in the values of the coefficients, and, in many cases, can replace the latter to efficiently perform transient simulation of dynamic circuits and systems in exactly the same manner.

The foundations of indirect numerical integration and its general principles were discussed in detail in the Section 2.2. Finally, the complete set of the step- and ramp-invariant indirect numerical integration formulas is presented in Appendix A.

3. DIFFERENCE APPROXIMATION

3.1. Introduction

Numerical integration is the most efficient transient simulation method (the only method with linear computational complexity). It is based on discretization of the system differential equations resulting in discrete-time difference equations which are used to perform the transient simulation of the system recursively in the time domain. In practice, systems are often characterized by measured or simulated samples of their responses, and the differential equations are not available. A general systematic solution to this problem is *to approximate any frequency or time response of the system with the corresponding response of a system whose differential equations are known*. Then numerical integration can be applied and the difference equations can be readily obtained.

This procedure is called *the difference approximation*. Its applications include efficient transient simulation of systems characterized by discrete data samples, transcendental transfer functions, and higher-order systems (the order-reduction problems). In recent years, the difference approximation has been used by an increasing number of time-domain simulation methods such as Asymptotic Waveform Evaluation (AWE) techniques [12], [13], techniques used with the Finite-Difference Time-Domain method to model frequency-dependent materials [18] and implement surface-impedance boundary conditions [10], [18], and numerous transmission line simulation methods [8], [19], [20]. The theory behind the difference approximation, however, has not been studied adequately.

This chapter attempts to fill the gap and to analyze the general principles and foundations of the difference approximation, common for all of its applications. In addition, Section 3.3 presents novel interpolation-based approximation methods, and Section 3.4 discusses AWE as an important special case of the difference approximation.

3.2. General Principles of Difference Approximation

3.2.1. Fundamental issues

The fact that the difference approximation is based on an approximation does not mean that it is less accurate than numerical convolution and transformation techniques which can be applied directly to the samples of system responses. The latter methods employ a discrete approximation of the samples, which is potentially less accurate than the functional approximation employed by the difference approximation.

The approximating system for the difference approximation should be of a type to which numerical integration is easily applied. From this standpoint, systems described by stationary ordinary linear differential equations with constant (frequency-independent) coefficients are the most suitable, and their use will be implied throughout the chapter. We will also limit the discussion to linear systems. To nonlinear systems, the same techniques are applied in conjunction with linearization methods [3]-[5].

The foremost issue to address is the fundamental possibility of such an approximation, or, in other words, whether the exact representation is possible when the approximation order approaches infinity. Unfortunately, even for linear stationary systems the answer is, in general, no. The difference approximation with the above approximating systems is fundamentally possible only for systems with constant parameters. Systems with frequency-dependent parameters (which includes all real electromagnetic systems such as transmission lines) can not, in general, be described exactly by the ordinary differential equations of even infinite order.⁵ In practice, it means that for systems with frequency-dependent parameters the approximation accuracy can not be improved by increasing the order of the approximation beyond some point. For most of the practical cases, however, a satisfactory (within a few percent) accuracy can be achieved. For systems with constant parameters, any desired degree of accuracy can be achieved by increasing the approximation order.

Although any system response can be used for the difference approximation, to attain maximum accuracy one should approximate a response which is as close as possible to the

⁵This fact can be easily understood if one considers the power-series expansions of the original and approximating transfer functions. The exact representation implies that the coefficients of the power-series expansions coincide. Transfer functions of the approximating systems considered in the paper have the form of rational polynomial functions with real coefficients (consequently, the coefficients of the power series are real as well). For the systems with frequency-dependent parameters, the coefficients are, in general, complex, and, therefore, can not be matched.

response to be simulated. At the same time, it should be a simple fundamental response. In the time domain such a response is the transient characteristic (unit-step response). Approximation of the transient characteristic results in the closest correlation between the approximation and simulation errors. If the impulse characteristic (δ -impulse response) is approximated, the approximation error is integrated during the transient simulation. In the case of the ramp-response approximation, the approximation error is differentiated. In the frequency domain, it is best to approximate the transfer function, because higher-order frequency-domain responses are singular at the zero frequency.

3.2.2. Canonic forms

For the approximating systems considered, the frequency-domain responses have the form of rational polynomial functions, and the time-domain responses are composed of the exponential and damped harmonic functions. The expressions for the transfer functions, impulse, step and ramp responses, the corresponding differential equations, and indirect numerical integration formulas in the three canonic forms [3] of state-variable representation for arbitrary-order multiport systems are given in Appendix A.

The canonic form (the standard state-variable formulation) starts with the common-fraction representation of the rational polynomial transfer function

$$\mathbf{H}(j\omega) = \frac{\mathbf{Q}(j\omega)}{p(j\omega)} = \frac{\mathbf{C}_0 + j\omega\mathbf{C}_1 + (j\omega)^2\mathbf{C}_2 + \dots + (j\omega)^M\mathbf{C}_M}{1 + j\omega\beta_1 + (j\omega)^2\beta_2 + \dots + (j\omega)^M\beta_M}. \quad (3.1)$$

In the parallel canonic form, a higher-order system is represented as a set of first-order systems connected in parallel, and the transfer function is in the form of a sum of first-order rational polynomial functions

$$\mathbf{H}(j\omega) = \mathbf{H}_\infty + \sum_{m=1}^M \frac{\mathbf{A}_m}{1 + j\omega / \omega_{cm}}. \quad (3.2)$$

According to the residue theorem [23], the partial expansion coefficients, \mathbf{A}_m , are related to the common fraction form as follows [22]:

$$\mathbf{A}_m = -\frac{\mathbf{Q}(-\omega_{cm})}{\sum_{k=1}^M k\beta_k (-\omega_{cm})^k},$$

and the final value

$$\mathbf{H}_\infty = \frac{1}{\beta_M} \mathbf{C}_M.$$

Because the coefficients \mathbf{C}_m and β_m of the common fraction (3.1) are real, the system poles, $-\omega_{cm}$, (the roots of the denominator of Equation (3.1)) and the partial expansion coefficients, \mathbf{A}_m , are either real or form complex-conjugate pairs. Complex poles should be used only for the difference approximation of systems with oscillating time-domain responses. Aperiodic systems should be approximated with only real poles.

The parallel canonic form can be used only for systems with distinct poles. It is, also, the most suitable form for the time-domain approximation, because, in this case, the dynamic parts of the fundamental time-domain responses have the form of a simple exponential series

$$\mathbf{F}(t) = \sum_{m=1}^M \mathbf{D}_m e^{-\omega_{cm} t}. \quad (3.3)$$

In the cascade canonic form, a higher-order system is represented as a set of first-order systems connected in cascade, and the transfer function has the form of a product of the first-order rational polynomial functions:

$$H(j\omega) = H_0 \prod_{m=1}^M \frac{1 + j\omega / \omega_{pm}}{1 + j\omega / \omega_{cm}}. \quad (3.4)$$

The cascade canonic form is not suitable for approximation of multiport systems (in matrix form) nor for the time-domain difference approximation.

The difference approximation procedure consists of one step: *Approximate a system response in the time or frequency domain with the corresponding response from Appendix A. The system difference model is readily given in Appendix A, directly in terms of the approximation parameters.* The frequency-domain difference approximation is more general because it can be performed in all of the three canonic forms, and system responses are usually measured in the frequency domain.

3.2.3. Complex-to-real mapping, magnitude, real- and imaginary-part approximations

Although transfer functions are complex, the fact that the coefficients of the approximating rational polynomial function are real prohibits performing the frequency-domain difference approximation directly in the complex form. For systems with constant parameters, transfer functions can be mapped into the real domain by scaling the frequency with the factor of $-j$. The

approximation is then performed with the correspondingly scaled rational polynomial functions in the real domain. This implies, however, that the original transfer functions are given in the functional form with frequency-independent parameters.

In the general case of frequency-dependent systems characterized by discrete samples of their responses, one can exploit the fact that for any analytic complex function the real and imaginary parts are uniquely (to an additive constant) related by the Riemann-Cauchy equations and are harmonic conjugates of each other [22], [23]. In practice, this means that one can approximate only the real part, imaginary part or magnitude of the original function (which are real) with the corresponding part of the approximating function, and the rest will match automatically.

The magnitude, real- and imaginary-part approximations can be performed via an approximation with a rational polynomial function of the squared frequency. To retrieve the approximation parameters, the result of the real-part approximation has to be put in the form

$$\mathbf{Re}(\mathbf{H}(j\omega)) = \mathbf{H}_\infty + \sum_{m=1}^M \frac{\mathbf{A}_m}{1 + \omega^2 / \omega_{cm}^2}, \quad (3.5)$$

and the normalized imaginary-part approximation in the form

$$\frac{1}{\omega} \mathbf{Im}(\mathbf{H}(j\omega)) = \sum_{m=1}^M \frac{-(1 / \omega_{cm}) \mathbf{A}_m}{1 + \omega^2 / \omega_{cm}^2}. \quad (3.6)$$

Then ω_{cm} and \mathbf{A}_m in the expressions (3.5) and (3.6) will correspond to those in (3.2).

Similarly, after the rational polynomial approximation of the squared magnitude is represented in the following form:

$$|H(j\omega)|^2 = H_0^2 \frac{(1 + \omega^2 / \omega_{p1}^2)(1 + \omega^2 / \omega_{p2}^2) \dots (1 + \omega^2 / \omega_{pM}^2)}{(1 + \omega^2 / \omega_{c1}^2)(1 + \omega^2 / \omega_{c2}^2) \dots (1 + \omega^2 / \omega_{cM}^2)}, \quad (3.7)$$

ω_{cm} and ω_{pm} in (3.7) will correspond to those in (3.4). The magnitude approximation is insensitive to the delay component of the original function.

The relationships (3.5)-(3.7) hold not only for real but also for complex-conjugate poles and zeros (except for purely imaginary poles and zeros).

The systems to be simulated are usually known to be stable, and the approximating poles should be located in the left half of the complex plane. Because the real-part and magnitude approximations are performed in terms of the squared poles, they can not generate unwanted right-half-plane poles.

3.2.4. Difference approximation of multiport systems

There are two ways of applying the difference approximation to a multiport system. First, the system can be treated as a single multiport system, and the difference approximation is performed in the matrix form. Second, a multiport system can be treated as a set of two-port systems connected in the order of the matrix multiplication, and the scalar difference approximation is applied individually to each element of the matrix transfer function or transient characteristic. The computational complexity of the transient simulation is the same for both approaches (the computational complexity of numerical integration is linearly proportional to the order of difference approximation). The number of the state variables, however, is linearly proportional to the number of the system ports for the first approach and quadratically for the second.

For symmetric $n \times n$ matrix transfer functions, such as admittance matrices, the number of scalar transient simulations to be performed can be reduced from n^2 to $n(n+1)/2$ by converting the matrices into the self/mutual-parameter form [19].

3.2.5. Matrix delay separation

A two-port (scalar) dynamic linear system is said to contain a *delay* τ , if its one-sided time-domain response $h(t)$ can be written as

$$h(t) = \hat{h}(t - \tau)1(t - \tau),$$

where $1(t)$ is the unit step function. In other words, the delay is merely a time shift. Then, the phase of the frequency-domain response $H(\omega)$ will contain a linear component $-\omega\tau$:

$$H(\omega) = \hat{H}(\omega)e^{-j\omega\tau}.$$

We will call $\hat{h}(t)$ and $\hat{H}(\omega)$ the *delayless responses*. For most of the practical delayless transfer functions, such as open-loop delayless transfer functions of transmission lines discussed in Chapter 4, the phase is limited at infinity. In this case, the delay also corresponds to the infinite-frequency slope of the phase of the transfer function. Using this property, one can estimate the delay component in a system characterized by measured frequency-domain data by the high-frequency asymptote of the phase.

To increase the accuracy, the delay component should be separated from the original function before the approximation. For multiport systems, the conventional *modal*

transformation approach to the frequency-domain delay separation consists of the diagonalization of the square matrix transfer function $\mathbf{H}(\omega)$,

$$\mathbf{H}(\omega) = \mathbf{M}(\omega) \mathbf{H}_m(\omega) \mathbf{M}^{-1}(\omega),$$

and extraction of the scalar delays from the elements of the diagonal transfer function matrix, $\mathbf{H}_m(\omega)$, [8], [19]. The eigenvector matrix, $\mathbf{M}(\omega)$, is, in general, a nonminimum-phase function⁶ with unstable time-domain responses, which limits the applicability of the technique to few special cases in which the eigenvectors of $\mathbf{H}(\omega)$ are constant.

In a general case, the delay can be separated by the novel *matrix delay separation technique*, which represents the matrix transfer function as follows:

$$\mathbf{H}(\omega) = \hat{\mathbf{H}}(\omega) \mathbf{M} e^{-j\omega \mathbf{T}_m} \mathbf{M}^{-1},$$

where

$$\hat{\mathbf{H}}(\omega) = \mathbf{H}(\omega) \mathbf{e}^{+j\omega \mathbf{T}}$$

is the delayless matrix transfer function. The technique uses a novel notion of the *matrix delay*, \mathbf{T} , which generalizes the scalar delay to multiport systems. Analogously to the scalar systems, the matrix delay is the infinite-frequency slope of the argument of the matrix exponential representation of $\mathbf{H}(\omega)$, which is the matrix equivalent of phase. However, in the time domain, the matrix delay not only shifts the responses, but also creates coupling between them. The diagonal modal-delay matrix, \mathbf{T}_m , is the eigenvalue matrix of \mathbf{T} , and \mathbf{M} is the constant eigenvector matrix of \mathbf{T} . The elements of \mathbf{T}_m are the same as the modal delays obtained with the modal transformation technique. The difference approximation is applied to $\hat{\mathbf{H}}(\omega)$. Specific examples of the matrix delay separation can be found in Chapter 4.

3.3. Approximation Methods

3.3.1. Comparison of approximation methods

As shown in the preceding section, the difference approximation can be performed via the scalar exponential series approximation in the time domain, or rational polynomial approximation in the frequency domain. The choice of the approximation method affects overall efficiency and

⁶A transfer function whose poles are not restricted to the left half of the complex plane.

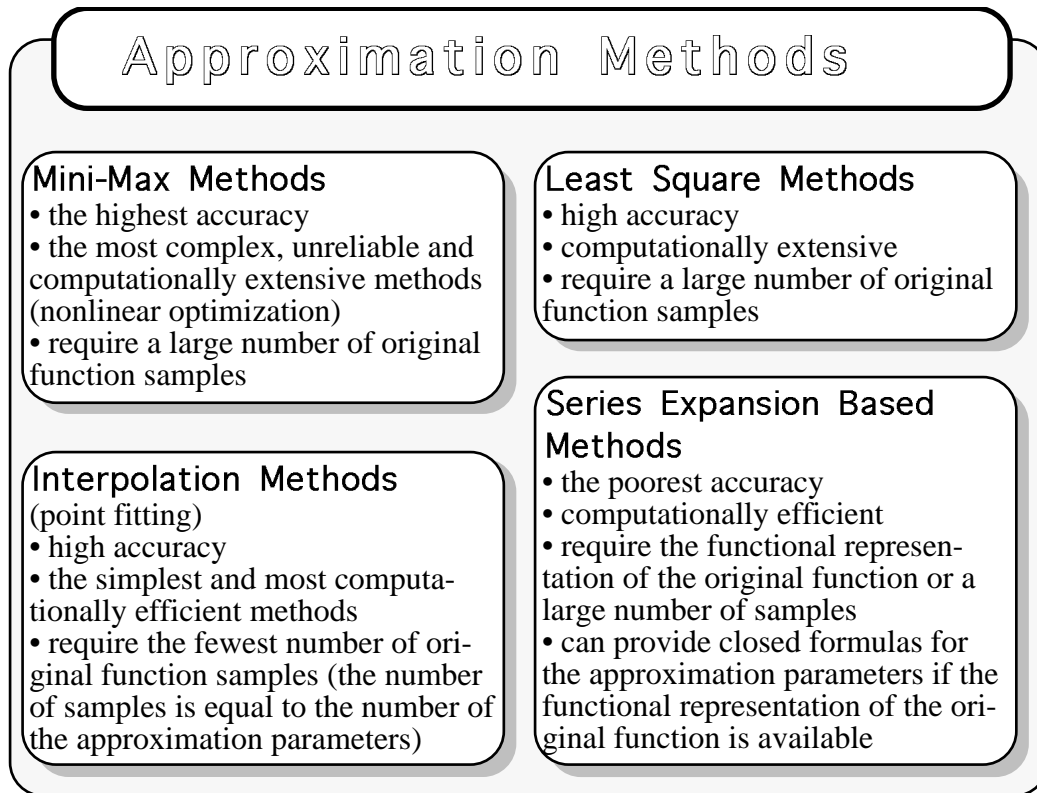


Fig. 3.1. Approximation methods.

accuracy of the difference approximation. Based on approximation criteria, approximation methods can be categorized into four major groups: minimum maximum error based (mini-max) methods, least square methods, interpolation methods and series expansion based methods (see Fig. 3.1). Mini-max methods provide the highest accuracy, but result in the most inefficient and unreliable algorithms [24], [25]. Least square methods provide high accuracy, but are still computationally extensive for nonlinear problems. Prony’s method [26] and its modifications, such as pencil-of-function method [27], reduce the exponential approximation to a linear least-square problem, which can be solved efficiently, but extract the poles by minimizing the linear prediction error instead of the approximation error and are restricted to uniform sampling. Another efficient least-square based method—Laguerre expansion—is limited to approximations with a single repeated pole [20]. Series expansion based methods (such as Padé synthesis used for AWE [24], [25], [28]) are computationally efficient, but provide the poorest accuracy.

Interpolation (point-fitting) agrees exactly with the original function on a given set of samples. Interpolation provides high accuracy, and is the most efficient among the approximation methods. It is reducible to a linear problem for both exponential (Prony’s

TABLE 3.1
COMPARISON OF APPROXIMATION METHODS

Approximation Method	Maximum Relative Error	Relative run time
Mini-max approximation	0.0004%	200
Least squares approximation	0.002%	50
Interpolation	0.003%	1.0
Economized rational approximation	0.004%	2.0
Padé synthesis at zero	0.06%	1.3
Padé synthesis at infinity	0.3%	1.5

interpolation [26]) and rational polynomial [24], [25] approximations. It also requires the minimal number of samples, which is important when the original responses are obtained from electromagnetic simulations.

Table 3.1 presents typical values of maximum relative error and computational efficiency for various approximation methods as applied to the frequency-domain rational polynomial approximation of open-loop transmission-line functions introduced in Chapter 4. Economized rational approximation starts with Padé synthesis, which is not accurate away from the expansion point, and then perturbs it to reduce the leading coefficient of error in the given approximation interval [24], [25]. As one can observe, interpolation provides accuracy comparable with that of least square approximation, and is 200 times more efficient than mini-max approximation. Interpolation is also up to two orders of magnitude more accurate and 30-50% more efficient than Padé synthesis used by the AWE. As shown in Section 3.4, for more complicated functions, the accuracy of AWE approximation is much worse than that listed in Table 3.1.

3.3.2. Relaxation interpolation method

This method is applicable to interpolation of limited aperiodic functions with a sum or product of limited monotonous functions. It can be used for low-order real-pole time- and frequency-domain difference approximation of aperiodic systems, such as open-loop transmission line functions. The method reduces the solution of complicated nonlinear equations for the

interpolation with a sum or product of simpler basis functions to a recursive solution of equations involving only one basis function at a time, which can often be solved analytically.

The method is based on the assumption that the basis functions are approaching the limiting value at different rates. Consequently, the first basis function dominates at the first interpolation interval, and its parameters can be estimated separately. This basis function is then removed from the original function, which makes the second basis function dominant. The process is repeated until it passes through all of the basis functions. The subsequent passes are made using the approximation parameters estimated previously to iteratively improve the accuracy. Because the method takes advantage of the specific properties of the original and approximating functions, it has much better convergence than the more general Newton-Raphson method.

Let us first consider the interpolation with a sum of basis functions:

$$\tilde{f}(x) = F_\infty + \sum_{m=1}^M \varphi_m(x).$$

If all of the basis functions, $\varphi_m(x)$, have the final value of zero (which can always be achieved by lumping nonzero final values in F_∞), the relaxation interpolation algorithm proceeds as follows.

1. Single interpolation pass:

1.1. The final value, F_∞ , may be either given or determined iteratively along with other unknown parameters. If F_∞ is not given, compute

$$F_\infty = f(x_0) - \sum_{m=1}^M \varphi_m(x_0),$$

where $f(x)$ is the original function, and x_0 is the largest abscissa among the interpolation points.

1.2. For each basis function $\varphi_m(x)$ determine (if possible, analytically) the unknown approximation parameters $\alpha_{m1}, \dots, \alpha_{mL_m}$ from the system of equations

$$\begin{cases} \varphi_m(\alpha_{m1}, \dots, \alpha_{mL_m}, x_{m1}) = \theta_m(x_{m1}) \\ \vdots \\ \varphi_m(\alpha_{m1}, \dots, \alpha_{mL_m}, x_{mL_m}) = \theta_m(x_{mL_m}), \end{cases} \quad (3.8)$$

where

$$\theta_m(x) = f(x) - F_\infty - \sum_{\substack{k=1, \\ k \neq m}}^M \varphi_k(x). \quad (3.9)$$

The systems of equations are solved recursively starting with $m = 1$ and finishing with $m = M$, where x_{11} is the largest abscissa (or the second to largest if F_∞ is not given) and x_{ML_M} is the smallest abscissa. The order of computation is important.

2. Repeat step 1 until convergence.

For the interpolation with a product of basis functions

$$\tilde{f}(x) = F_0 \prod_{m=1}^M \varphi_m(x),$$

we will assume that all of the basis functions have the initial value of unity (which can always be achieved by factoring nonunit initial values in F_0). Then the relaxation interpolation algorithm takes the following form.

1. Single interpolation pass:

- 1.1. The initial value F_0 may be either given or determined iteratively along with the other unknown parameters. If F_0 is not given, compute

$$F_0 = \frac{f(x_0)}{\prod_{m=1}^M \varphi_m(x_0)},$$

where x_0 is the smallest abscissa among the interpolation points.

- 1.2. For each basis function $\varphi_m(x)$ determine (if possible, analytically) the unknown approximation parameters $\alpha_{m1}, \dots, \alpha_{mL_m}$ from the system of equations (3.8) where

$$\theta_m(x) = \frac{f(x)}{F_0 \prod_{\substack{k=1, \\ k \neq m}}^M \varphi_k(x)}. \quad (3.10)$$

The systems of equations are solved recursively starting with $m = 1$ and finishing with $m = M$, where x_{11} is the smallest abscissa (or the second to smallest if F_0 is not given) and x_{ML_M} is the largest abscissa. (Note that the order is the reverse of that for the series form.)

2. Repeat step 1 until convergence.

The number L_m of the interpolation points x_{m1}, \dots, x_{mL_m} used in the system of equations (3.8) for the m th basis function equals the number of unknown parameters $\alpha_{m1}, \dots, \alpha_{mL_m}$ to be determined for the basis function. The total number of the interpolation points equals the total number of the approximation parameters, i.e., $\sum_{m=1}^M L_m$ if F_∞ (or F_0) is given and $1 + \sum_{m=1}^M L_m$ if F_∞ (or F_0) is determined iteratively.

The relaxation nature of the method permits easy imposition of constraints on the approximation parameters, e.g., to eliminate imaginary and nondominant poles (poles with small partial expansion coefficients). Constraints are imposed at step 1.2 by skipping the basis functions $\phi_k(x)$ in the right-hand side of the expressions (3.9) and (3.10) for which the approximation parameters determined during the current pass do not satisfy the constraints. (As a result, the final order of the approximation may be smaller than that originally specified.) Similarly, the basis functions with $k > m$ are skipped at the first pass because their parameters have not yet been evaluated.

For the time- and frequency-domain difference approximation, the system of equations (3.8) can be solved analytically. The corresponding formulas are given in Table 3.2. The total number of interpolation points is $2M$ if the limiting values are given and $2M + 1$ if they are determined iteratively. The interpolation points should be chosen so that the variation of the original function from point to point would be about the same. The end of the interpolation interval should be chosen so that approximately 95-99% of the total sweep of the original function would fall within the interpolation interval.

The convergence of the method depends on how rapidly the basis functions are approaching the limiting value compared to the original function, and on the number of the basis functions. The exponential interpolation converges especially rapidly, because the exponential basis functions are very quickly decreasing. Figure 3.2 shows the results of a single-pass fifth-order relaxation exponential interpolation of transient characteristics of transmission-line propagation functions.

Figure 3.3 presents an example of the third-order real-part relaxation interpolation of the characteristic admittance of a multiconductor nonuniform transmission line. As can be seen, although only the real part was approximated, the magnitude and phase are well-matched.

The relaxation interpolation method is used for transmission line simulation [2] and with the method of moments for capacitance computations in a multilayered dielectric medium [31]. In numerous simulation exercises, the relaxation interpolation method demonstrated much better convergence than exponential approximation based on the Newton-Raphson method [8], and efficiency superior to that of the Prony's method [26].

TABLE 3.2

RELAXATION INTERPOLATION FORMULAS FOR THE DIFFERENCE APPROXIMATION

Type of Approximation	Basis Functions, ϕ_m	Analytical Solution of (3.8) for the Approximation Parameters
Frequency-domain real-part approximation in the parallel form (3.5)	$\frac{a_m}{1 + (\omega / \omega_{cm})^2}$	$\omega_{cm} = \sqrt{\frac{\omega_{m2}^2 \theta_m(\omega_{m2}) - \omega_{m1}^2 \theta_m(\omega_{m1})}{\theta_m(\omega_{m1}) - \theta_m(\omega_{m2})}},$ $a_m = \theta_m(\omega_{m2}) (1 + (\omega_{m2} / \omega_{cm})^2)$
Frequency-domain magnitude approximation in the cascade form (3.7)	$\frac{1}{1 + (\omega / \omega_{cm})^2}, \text{ if } \theta_m(\omega_{m1}) < 1;$ $1 + (\omega / \omega_{pm})^2, \text{ if } \theta_m(\omega_{m1}) > 1$	$\omega_{cm} = \omega_{m1} / \sqrt{1/\theta_m(\omega_{m1}) - 1},$ $\omega_{pm} = \omega_{m1} / \sqrt{\theta_m(\omega_{m1}) - 1}$
Time-domain approximation in the parallel form (3.3)	$d_m e^{-\omega_{cm} t}$	$\omega_{cm} = \frac{\ln(\theta_m(t_{m2})/\theta_m(t_{m1}))}{t_{m1} - t_{m2}},$ $d_m = \theta_m(t_{m2}) e^{\omega_{cm} t_{m2}}$

3.3.3. Direct interpolation-based method for frequency-domain difference approximation

Rational polynomial interpolation in the common-fraction form

$$\tilde{f}(x) = \frac{c_0 + c_1 x + c_2 x^2 + \dots + c_L x^L}{1 + \beta_1 x + \beta_2 x^2 + \dots + \beta_M x^M} \quad (3.11)$$

can be performed directly by matching (3.11) with the original function at a set of points and premultiplying both sides of each equation with the denominator. This results in the following linear system of equations [24], [25]:

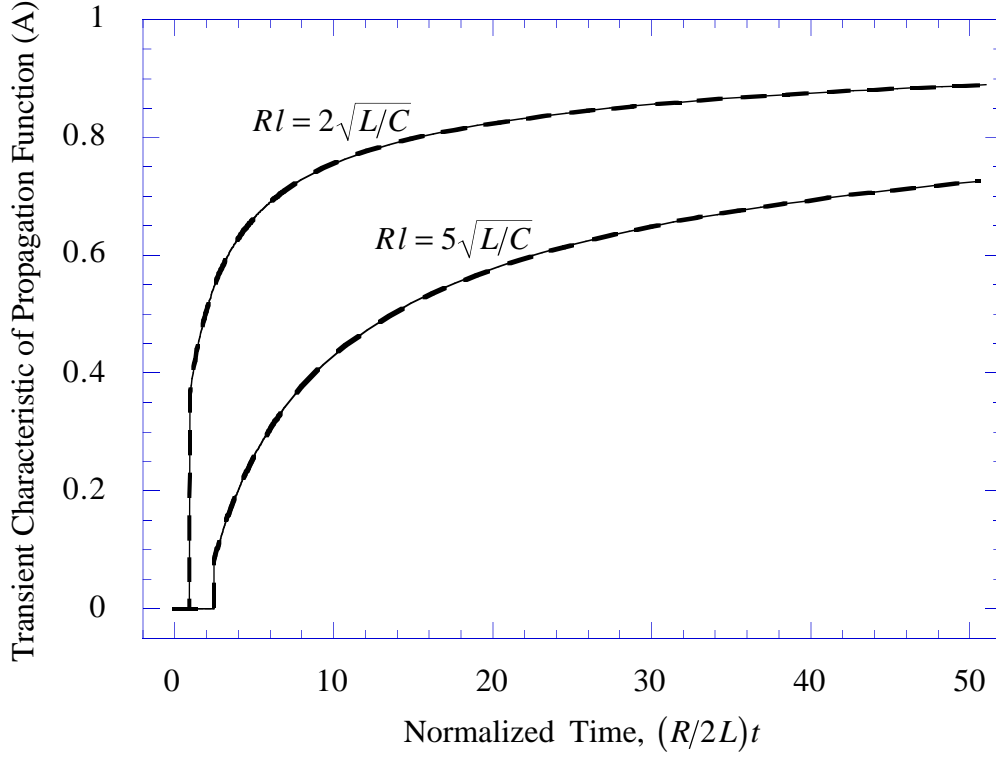
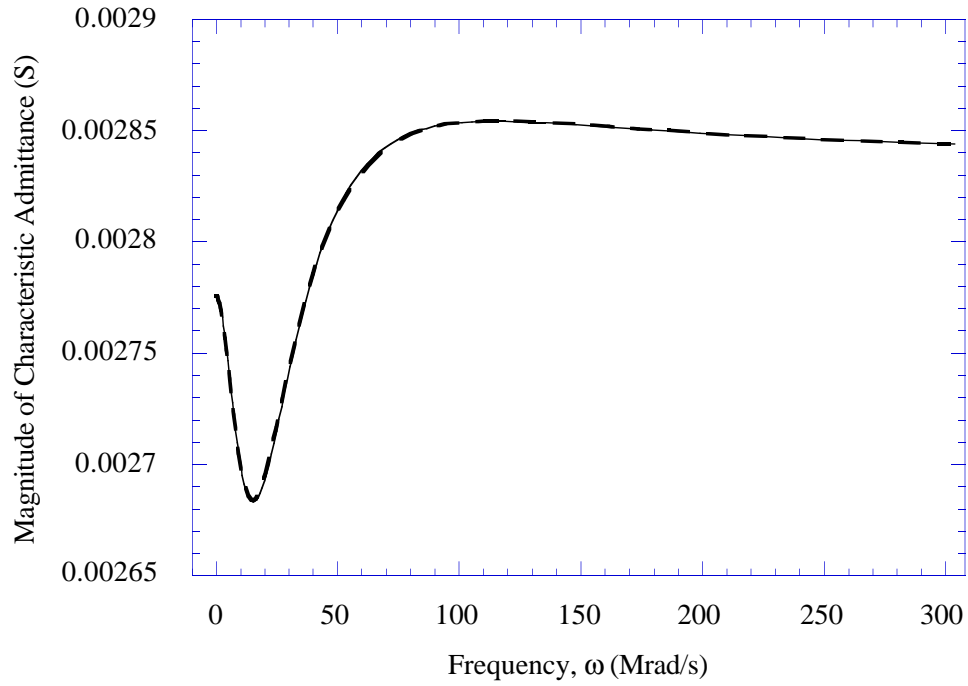


Fig. 3.2. An example of the relaxation exponential interpolation. Thin continuous curves correspond to the original functions and thick dashed curves to the interpolating functions.

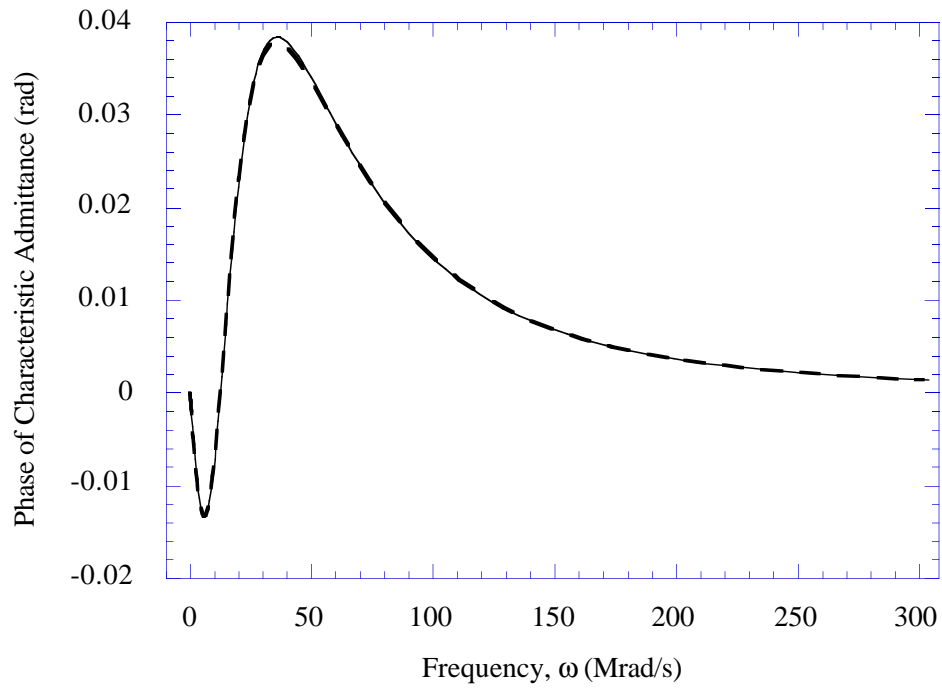
$$\begin{bmatrix} 1 & x_1 & x_1^2 & \dots & x_1^L & -x_1 f(x_1) & -x_1^2 f(x_1) & \dots & -x_1^M f(x_1) \\ 1 & x_2 & x_2^2 & \dots & x_2^L & -x_2 f(x_2) & -x_2^2 f(x_2) & \dots & -x_2^M f(x_2) \\ \vdots & \vdots & \vdots & \dots & \vdots & \vdots & \vdots & \dots & \vdots \\ 1 & x_K & x_K^2 & \dots & x_K^L & -x_K f(x_K) & -x_K^2 f(x_K) & \dots & -x_K^M f(x_K) \end{bmatrix} \begin{bmatrix} c_0 \\ \vdots \\ c_L \\ \beta_1 \\ \vdots \\ \beta_M \end{bmatrix} = \begin{bmatrix} f(x_1) \\ f(x_2) \\ \vdots \\ f(x_K) \end{bmatrix}, \quad (3.12)$$

where $f(x)$ is a complex-to-real mapping, squared magnitude, real part, or normalized imaginary part of the original transfer function as discussed in Section 3.2. Correspondingly, x stands for either s or ω^2 . Because the system (3.12) involves powers of x , the approximation interval, x_K , should be normalized to unity to make the system better conditioned.

The number of samples required for interpolation is $K = L + M + 1$ (it is, also, the order of the linear system of equations to be solved). Then, solving (3.12) produces a rational polynomial function which coincides with $f(x)$ at all of the interpolation points.



(a)



(b)

Fig. 3.3. (a) Magnitude and (b) phase of the original function (thin continuous curves) and real-part relaxation interpolation (thick dashed curves).

For a set of samples larger than $L + M + 1$, the least square solution of the system (3.12) can be obtained. However, it minimizes the approximation error premultiplied by the denominator, which can lead to an inaccurate approximation. Better results are obtained with the method of averages, which partitions the larger number of equations into $L + M + 1$ subsets in order of the increasing argument [22]. The equations within each subset are added up, which makes the system consistent. The method is effective in averaging out the noise in measured data.

The denominator of the common-fraction approximation is then factored to extract the system poles, $-\omega_{cm}$. (Recall that magnitude and real-part approximations yield squared poles, and, consequently, can not produce unstable right half plane poles.) Unwanted poles (e.g., purely imaginary poles), if any, are removed, and the remaining poles are used to formulate equations for the partial expansion coefficients, a_m , of the parallel canonic form

$$\tilde{H}(j\omega) = H_\infty + \sum_{m=0}^M \frac{a_m}{1 + j\omega / \omega_{cm}}. \quad (3.13)$$

Consequently, the order M of (3.13) is less than or equal to that of (3.11).

The equations can be formulated for the real mapping, real (3.5) or imaginary (3.6) part of (3.13), or for any combination of these at once. For instance, matching the real and imaginary parts of the original transfer function $H(\omega)$ with the corresponding parts of (3.13) at a set of frequencies $\{0, \omega_1, \omega_2, \dots, \omega_K\}$ leads to the following linear system of equations

$$\left(\begin{array}{c} \left[\begin{array}{ccc} 1 & \frac{1}{1 + \omega_1^2 / \omega_{c1}^2} & \dots & \frac{1}{1 + \omega_1^2 / \omega_{cM}^2} \\ 1 & \frac{1}{1 + \omega_1^2 / \omega_{c1}^2} & \dots & \frac{1}{1 + \omega_1^2 / \omega_{cM}^2} \\ & \vdots & & \vdots \\ 1 & \frac{1}{1 + \omega_K^2 / \omega_{c1}^2} & \dots & \frac{1}{1 + \omega_K^2 / \omega_{cM}^2} \\ \hline 0 & \frac{-\omega_1 / \omega_{c1}}{1 + \omega_1^2 / \omega_{c1}^2} & \dots & \frac{-\omega_1 / \omega_{cM}}{1 + \omega_1^2 / \omega_{cM}^2} \\ & \vdots & & \vdots \\ 0 & \frac{-\omega_K / \omega_{c1}}{1 + \omega_K^2 / \omega_{c1}^2} & \dots & \frac{-\omega_K / \omega_{cM}}{1 + \omega_K^2 / \omega_{c1}^2} \end{array} \right] \end{array} \right) \mathbf{x} = \mathbf{b} = \begin{bmatrix} H_0 \\ Re(H(\omega_1)) \\ \vdots \\ Re(H(\omega_K)) \\ \hline Im(H(\omega_1)) \\ \vdots \\ Im(H(\omega_K)) \end{bmatrix}. \quad (3.14)$$

For interpolation $M = 2K$, and both real and imaginary parts of the original transfer function are matched exactly at all of the K frequency points and dc.

For an arbitrarily larger number of points, the least square solution of (3.14) is obtained from

$$\mathbf{A}^T \mathbf{A} \mathbf{x} = \mathbf{A}^T \mathbf{b},$$

or using the pseudo-inverse (singular value decomposition) [32]. To match the dc value $H_0 = H_\infty + \sum_{m=1}^M a_m$ exactly, (3.14) is rewritten as

$$\tilde{\mathbf{A}} \mathbf{D} = \begin{pmatrix} \begin{bmatrix} 1 & 0 & \dots & 0 \\ 0 & 1 & \dots & 0 \\ & & \ddots & \\ 0 & 0 & \dots & 1 \\ -1 & -1 & -1 & -1 \end{bmatrix}_{M+1 \times M} \end{pmatrix} \begin{pmatrix} \hat{\mathbf{x}} = \begin{bmatrix} H_\infty \\ a_1 \\ a_2 \\ \vdots \\ a_{M-1} \end{bmatrix} \end{pmatrix} = \hat{\mathbf{b}} = \tilde{\mathbf{b}} - H_0 \tilde{\mathbf{a}}_M, \quad (3.15)$$

where $\tilde{\mathbf{A}}$, $\tilde{\mathbf{a}}_M$, and $\tilde{\mathbf{b}}$ denote \mathbf{A} , the last column of \mathbf{A} , and \mathbf{b} with the first row removed. After the least square solution of (3.15) is obtained, a_M is computed as

$$a_M = H_0 - H_\infty - \sum_{m=1}^{M-1} a_m. \quad (3.16)$$

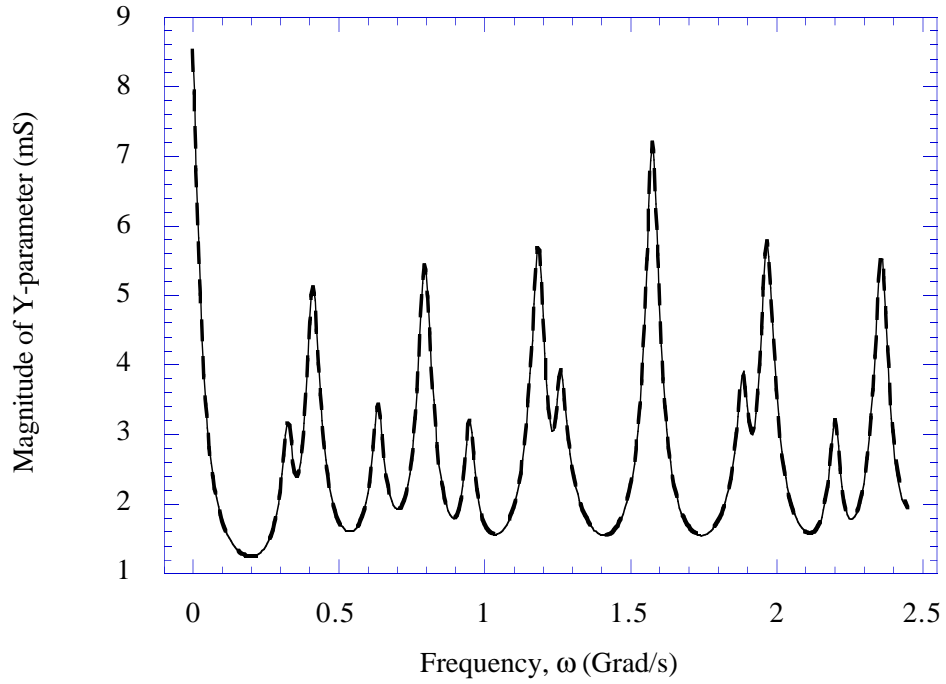
To match a given final value H_∞ exactly, it is subtracted from the original transfer function and removed from Equations (3.14) and (3.15) by removing the first column of \mathbf{A} and $\tilde{\mathbf{A}}$, the first row of \mathbf{x} , $\hat{\mathbf{x}}$, \mathbf{b} and $\hat{\mathbf{b}}$, and the first row and column of \mathbf{D} .

To summarize, the direct approximation method proceeds as follows.

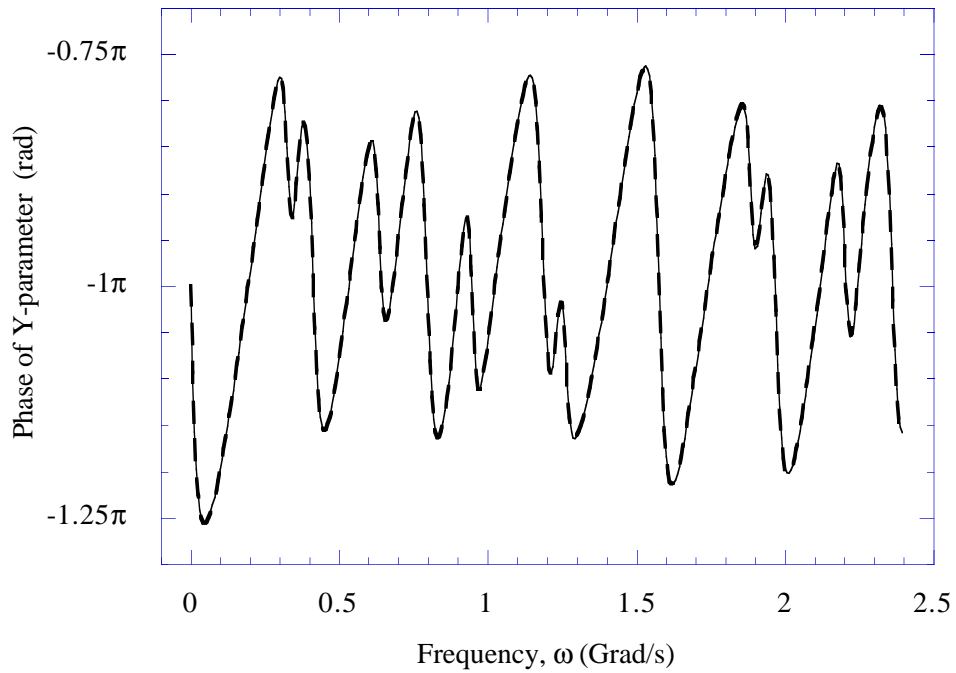
1. Fit the complex-to-real mapping, squared magnitude, real part, or normalized imaginary part of the original transfer function with the common fraction (3.11)-(3.12). This step requires solving a linear real system of equations of the order $L + M + 1$.
2. Extract the poles by finding roots of the denominator of the common fraction, and remove unwanted poles, if any. The order of the polynomial to be factored is M .
3. Adjust the partial expansion coefficients of the parallel canonic form to compensate for the removed poles by fitting complex-to-real mapping, real or imaginary part, or any combination of these at once (3.13)-(3.16). This requires solution of an $M + 1$ -order system of linear equations. The elements of the system matrix \mathbf{A} (3.14) either are real or form complex conjugate pairs.

The most accurate approximation results from fitting the real part at step 1 and both real and imaginary parts at once at step 3.

The direct approximation method is used for the transient simulation of transmission lines, and, in numerous simulation exercises, proved to be reliable, accurate and efficient. Figure 3.4 shows an example of the 54th-order approximation of a Y -parameter macromodel for the subcircuit of three coupled parabolically tapered lines from [20].



(a)



(b)

Fig. 3.4. Approximation of a Y -parameter macromodel for a subcircuit of three coupled parabolically tapered transmission lines. (a) Magnitude and (b) phase of the original function (thin continuous curves) and approximating function (thick dashed curves).

Both magnitude and phase of the original and approximating functions are in an excellent match. Note also that the delay has been completely removed by the matrix delay separation technique.

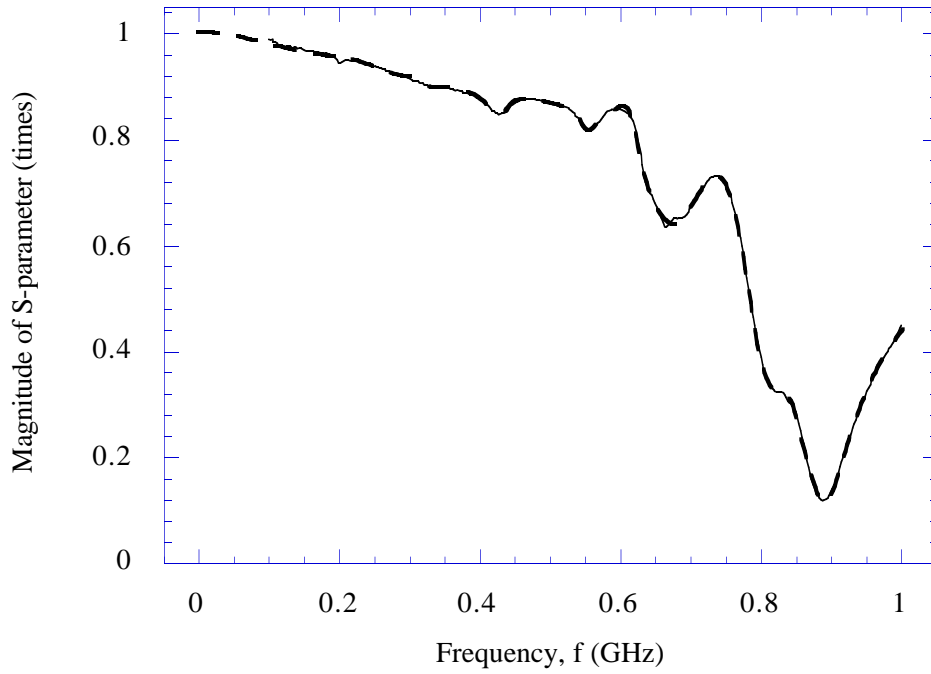
Figure 3.5 shows the 24th-order approximation of measured S -parameter data for a 256-pin surface-mounted IC package with complicated internal interconnects and delay left in. In both examples, the poles were extracted from the real-part approximation. An empirical rule for determining the order of the approximation is to multiply the number of bending points of the original function by a factor of 1.5-3.5.

3.4. Difference Approximation and Asymptotic Waveform Evaluation

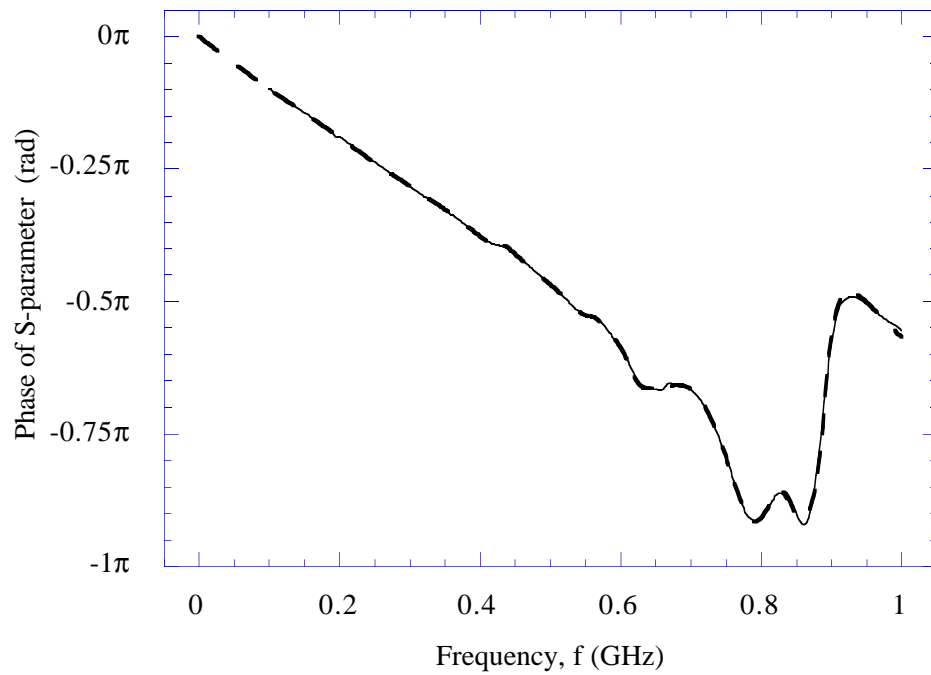
As mentioned earlier in this chapter, the difference approximation covers some AWE methods as a special case. Because of the wide popularity of the AWE, its analysis based on the general principles of the difference approximation discussed in this chapter may be of interest.

AWE applies Padé synthesis to construct an approximate rational polynomial transfer function of a system. Padé synthesis matches the coefficients of the Taylor series expansions of the original and approximating functions. Because coefficients of the power series in the frequency domain correspond to the moments of the time-domain waveforms, Padé synthesis provides a very accurate estimate of such important waveform characteristics as attenuation, delay and overshoot with a low-order approximation. It is, also, computationally efficient.

The main applications of AWE include estimation of signal degradation and transient simulation of digital circuits. Originally, AWE methods were used with the state-variable formulation of circuit equations and were applied to the analysis of completely linearized MOSFET circuits with lumped RLC representation of interconnects [28]. The state-variable formulation allows for very efficient transient and ac analyses of linear circuits (without solving circuit equations at each time or frequency iteration). The computational complexity is primarily influenced by the order of the differential state equations, not by the size (number of nodes) of the circuit. Consequently, for huge RLC circuits the order reduction by the AWE method provided tremendous (several orders of magnitude) speedup.



(a)



(b)

Fig. 3.5. Approximation of measured S-parameter data for a 256-pin surface-mounted IC package. (a) Magnitude and (b) phase of the original function (thin continuous curves) and approximating function (thick dashed curves).

An accurate simulation, however, requires nonlinear models for active elements. For nonlinear systems, the state-variable formulation requires matrix inversion at each linearization point and loses its superior efficiency. For this reason, transient simulation of nonlinear circuits is usually performed using the Modified Nodal Approach (MNA) [5], which (for transient analysis of nonlinear circuits) provides about the same efficiency as the state-variable formulation, but allows for much easier formulation of the circuit equations (directly from the netlist by inspection).

The AWE is combined with the MNA by creating linear (usually Y -parameter) macromodels for linear subnetworks and applying the AWE to the Y -parameters to reduce their order [12], [13]. When the linear subnetworks contain distributed lines, AWE methods based on the Y -parameter macromodels suffer from all of the drawbacks of the closed-loop distributed-line characterization as discussed in Chapter 4. An extension of the AWE with the method of characteristics [13], [33] uses open-loop distributed-line characterization and models each line individually, while creating macromodels only for the lumped subcircuits. This AWE method is closest to the optimal line simulation method formulated in Chapter 4.

For the MNA-based transient simulation, the computational complexity is primarily affected by the size of the circuit equations, and the reduction of the order of the numerical integration by applying the AWE does not produce a noticeable speedup. The macromodels, on the other hand, may significantly increase the efficiency of the simulation by eliminating internal nodes of linear subnetworks, because the computational complexity of the MNA is cubically proportional to the number of nodes. Realistic digital circuits, however, do not normally contain large linear subcircuits.

As applied to a transient simulation, the AWE is a special case of the frequency-domain difference approximation, which uses Padé synthesis and complex-to-real mapping. As a result, it inherits all of the drawbacks of the complex-to-real mapping and series expansion based difference approximation methods (see Fig. 3.1 and Table 3.1). It provides the poorest accuracy and produces spurious positive poles. The poor accuracy of AWE is due to the fact that it does not fit the original transfer function directly, but matches the coefficients of the power series expansions of the original and approximating functions. As a result, it also requires a functional representation of the original function, and is not, in general, applicable to systems with frequency-dependent parameters. Modifications of AWE in a direction away from the single-point Padé synthesis (such as economized rational approximation and complex frequency hopping [29], [30]) improve the accuracy, but reduce the efficiency.

As shown in Table 3.1, the AWE approximation based on a single-point Padé synthesis is up to two orders of magnitude less accurate and 30-50% less efficient than simple interpolation. For more complicated functions, the accuracy of AWE is worse than that listed in Table 3.1.

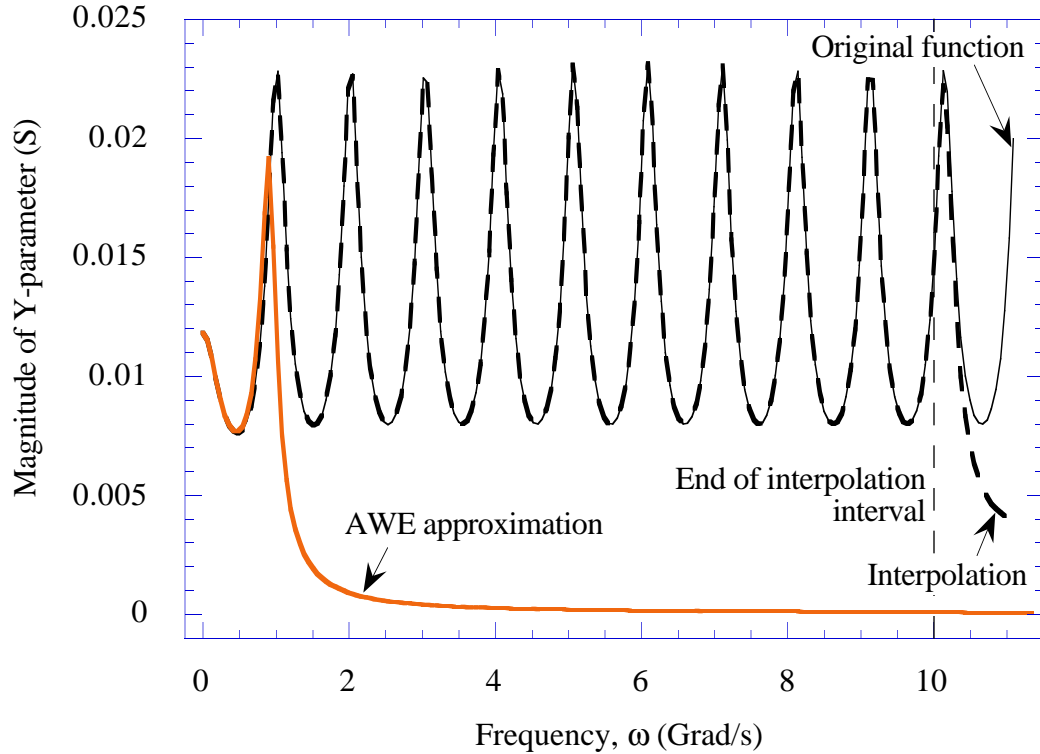


Fig. 3.6. Comparison of the AWE and interpolation.

Figure 3.6 shows a comparison of the 30th-order AWE approximation (Padé synthesis at 0) and magnitude interpolation of a Y -parameter macromodel for a transmission line. Figure 3.6 shows that the AWE approximation is only accurate in a small interval around the expansion point, whereas the same-order rational interpolation provides accurate results in the entire interpolation interval from 0 to 10 Grad/s.

In its other application, for an efficient and accurate estimation of signal degradation (such as attenuation, delay and overshoot estimation) the AWE, as a moment-matching method, provides excellent results and is indispensable for such applications as performance-driven placement and routing.

3.5. Conclusions

In this chapter, the difference approximation, a general method for applying numerical integration to systems whose differential equations are not known, was discussed. The general principles of the time- and frequency-domain difference approximation were analyzed, including

the fundamental possibility of the approximation, three canonic forms of the state-variable representation, complex-to-real mapping, magnitude, real- and imaginary-part approximations, and approximation of multiport systems. The novel matrix delay separation technique was introduced, which avoids the use of frequency-dependent eigenvector matrices. The complete set of indirect numerical integration formulas for time- and frequency-domain difference approximations in matrix form for multiport systems with arbitrary numbers of inputs and outputs, and in the three canonic forms of the state variable representation, is given in Appendix A.

Various approximation methods were compared, and novel interpolation-based methods were introduced. The relaxation interpolation method is applicable to low-order time- and frequency-domain real-pole approximations of aperiodic systems. The direct interpolation-based method performs frequency-domain complex-pole approximation of arbitrary numbers of arbitrarily spaced complex samples. This method averages out the noise in measured data, and fits both real and imaginary parts of the original function at once. The method proceeds in two steps. First, the poles of the system are extracted with the method of averages, and then the partial expansion coefficients are adjusted via least-square approximation. The complexity of this method is that of two linear solutions and one polynomial factoring. The orders of the linear systems and polynomial depend only on the order of the approximation and not on the number of samples. Both approximation methods can fit the initial and final values of the original response exactly, can impose constraints on the poles, and, in numerous real-life simulation exercises, proved to be reliable, accurate and efficient.

4. CIRCUIT SIMULATION OF TRANSMISSION LINES

4.1. Introduction

The problem of transmission line simulation gained special importance with the development of high-speed digital electronics. As transient times become faster, the transmission line behavior of electronic interconnects starts to significantly affect transient waveforms, and accurate modeling of on-board and even on-chip interconnects becomes an essential part of the design process. The complexity of contemporary digital circuits necessitates the simultaneous simulation of thousands of lossy coupled frequency-dependent lines surrounded by thousands of nonlinear active devices. Lines to be simulated may be characterized by measured or electromagnetically simulated samples of their responses.

There are two approaches to interconnect simulation. The first approach creates a macromodel for a linear subcircuit which may contain many transmission lines and other linear elements [13], [35]. This thesis discusses the second approach, in which each multiconductor line is treated as an individual circuit element.

The problem of line simulation involves several areas of science, such as electromagnetics, computational mathematics, and circuit and system theories. The solution of the problem is straightforward in the sense that all of the components involved are well-known and have only to be combined together. The integration of areas, however, is a difficulty that keeps the problem open and accounts for the diversity of developed methods.

This chapter presents an original attempt to identify the components of the problem and to formulate a high-level description of a method which provides maximum efficiency, accuracy and applicability for the transient analysis of digital circuits. Such an approach allows one to more accurately assess and compare the performance of numerous and diverse methods.

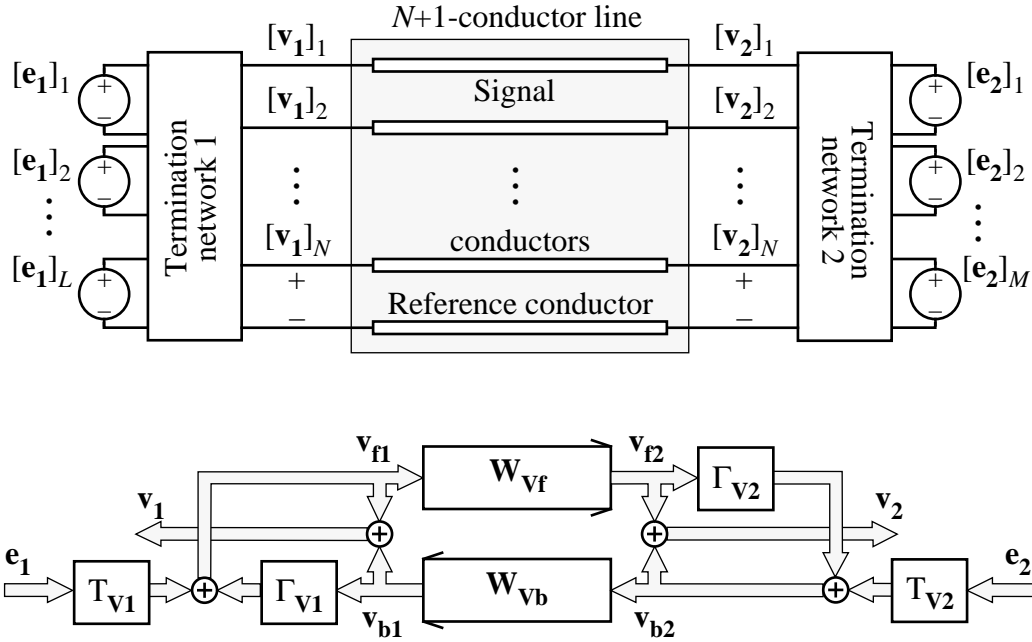


Fig. 4.1. System model for transmission lines.

The next section introduces the system model for transmission lines and briefly reviews the transmission line physics. Section 4.3 presents the formulation of the optimal approach and discusses many of the existing line simulation methods. Section 4.4 describes step-by-step implementation of the optimal method for uniform lines and presents numerical verification of the method's accuracy and efficiency. It also summarizes the indirect numerical integration and difference approximation techniques and extends the direct interpolation-based method introduced in Chapter 3 to the approximation of multiport systems in matrix form. Finally, Section 4.5 describes application of the method to nonuniform lines.

4.2. System Model for Transmission Lines

Before attempting to formulate the optimal approach, we will briefly review the transmission line physics. The system diagram representation of a line with terminations is shown in Fig. 4.1. W_{vf} and W_{vb} represent the forward and backward matrix propagation functions for voltage waves; T_1 , T_2 and Γ_1 , Γ_2 stand for the near- and far-end matrix transmission and reflection

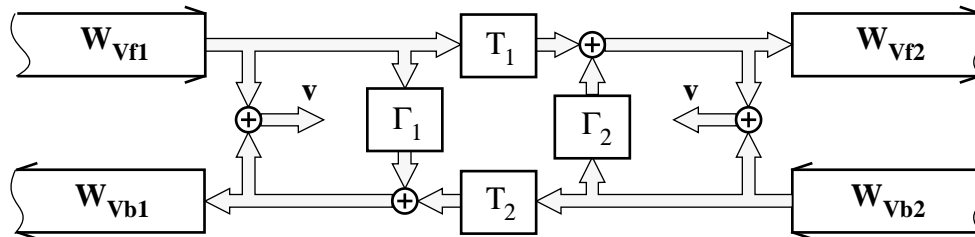
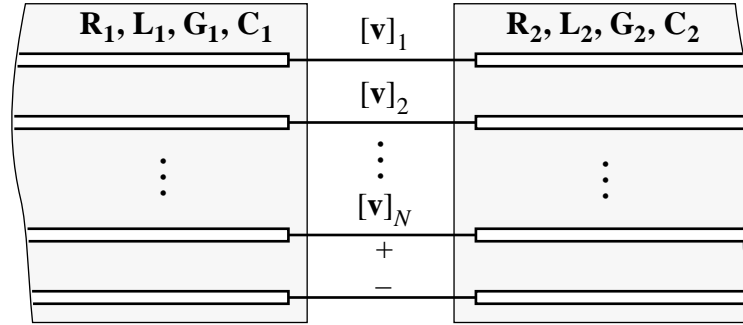


Fig. 4.2. System model for a line-to-line junction.

coefficients.⁷ The model reproduces the general relationship between the physical phenomena of wave propagation, transmission, reflection and coupling in a distributed system. It can represent arbitrarily distributed systems such as transmission lines, waveguides and plane-wave propagation. The model is very useful for system analysis of distributed systems, and allows one to write the macrosolution for a distributed system without complicated mathematical derivations. The mathematical justification of the model can be found in [2].

An important special case occurs when the line terminates in another line. The system diagram representation of a line-to-line junction is shown in Fig. 4.2. It can be used for the solution of multilayered plane-wave propagation problems, for the analysis of many common waveguide structures, and for the derivation of generalized transmission and reflection coefficient formulas and scattering parameter formulas. The system model for a transmission line tree was also developed [2].

As one can observe from Fig. 4.1, the processes taking place in a transmission line are very simple. Signals from the excitation sources attenuate in the termination networks and propagate along the line. As the forward wave reaches the far-end termination, it reflects, propagates backward, reflects from the near-end termination, propagates forward again, and so on in a loop. The voltage at any point along the line, including terminals, is a superposition of

⁷Since only multiconductor lines will be considered, the modifier “matrix” will be omitted in the future for brevity.

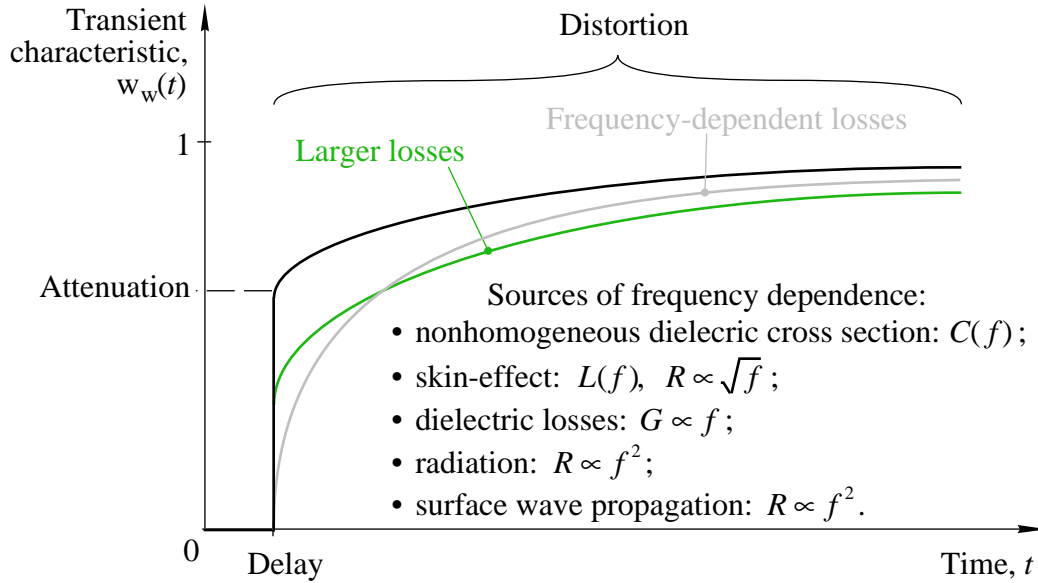


Fig. 4.3. Transient characteristic (the unit-step response) of a propagation function.

the forward and backward propagating waves. Coupling between the conductors of a multiconductor line is represented by the off-diagonal terms of the propagation functions.

The propagation functions, \mathbf{W}_{vf} and \mathbf{W}_{vb} , describe how a wave is affected by its propagation from one termination to another, and are equal for the forward and backward directions: $\mathbf{W}_{vf} = \mathbf{W}_{vb}$. As a wave propagates along the line, it experiences delay, attenuation and distortion (see Fig. 4.3). Lines with frequency-dependent parameters, and, therefore, all real lines, do not contain the attenuation component. A transient simulation technique is necessary only to simulate the distortion which corresponds to the dynamic part of the propagation function. Attenuation is simply a multiplication by a constant, and delay is merely a time shift. Consequently, for distortionless lines (which include lossless lines and some special cases of lossy lines [2], [34]) no transient simulation method is required, and time-domain recursive formulas relating the terminal and excitation waveforms can be written directly from Fig. 4.1 [2].

4.3. Formulation of Optimal Approach

To formulate the optimal approach to the transient simulation of transmission lines, major aspects of the problem will be analyzed, viz., *the formulation, the line characterization, the line model, and the transient simulation method* (see Fig. 4.4). Alternative approaches in each of the

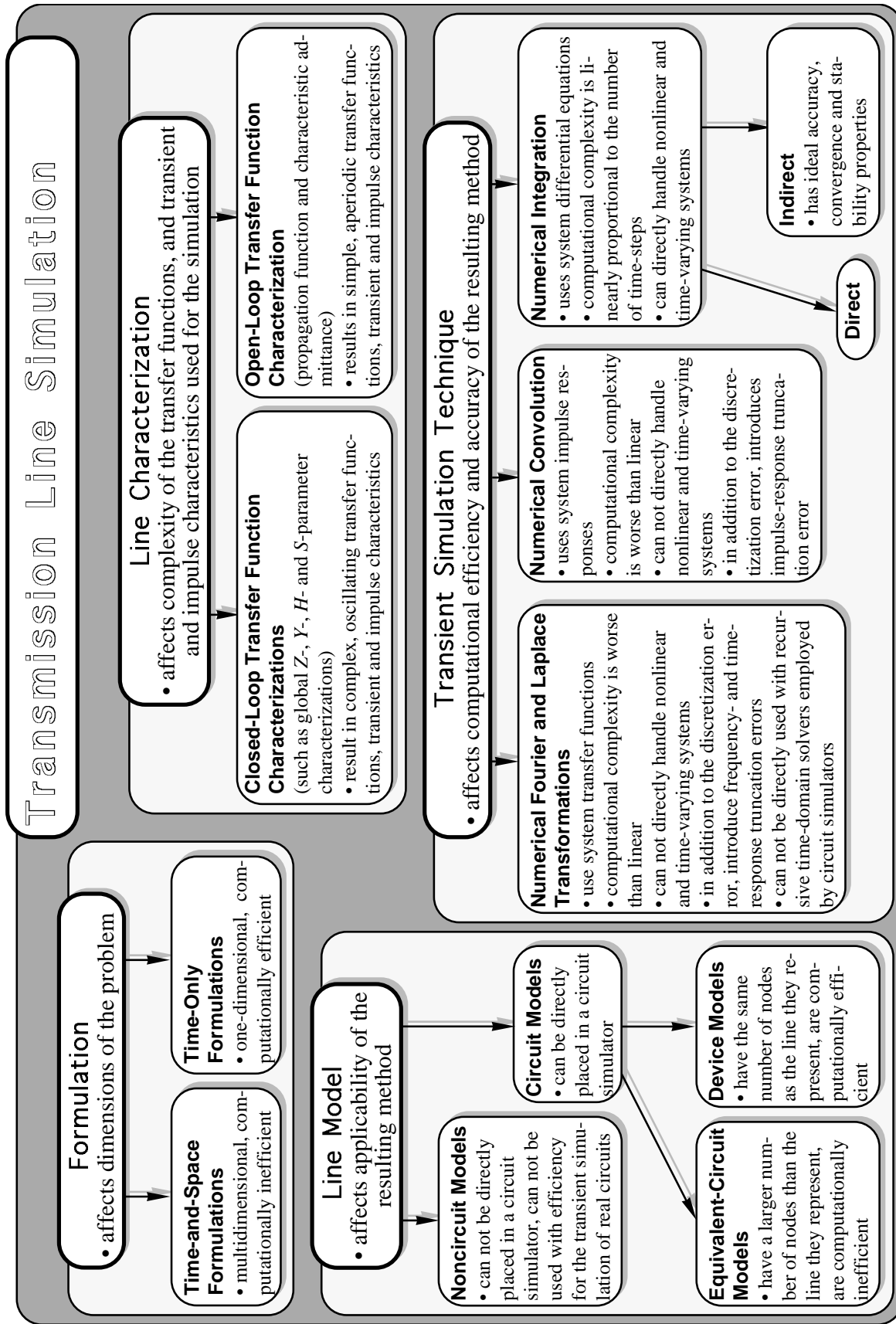


Fig. 4.4. Aspects of transmission line simulation.

aspects will be compared to find the optimal combination, which results in *maximum efficiency*, *accuracy* and *practical applicability*.

4.3.1. Formulation

The formulation affects dimensions of the problem. One can distinguish between *time-and-space formulations* and *time-only formulations*.

Time-and-space formulations (such as segmentation models [36], [37]) are based on the voltage and current distribution inside the line. These formulations are multidimensional and computationally extensive.

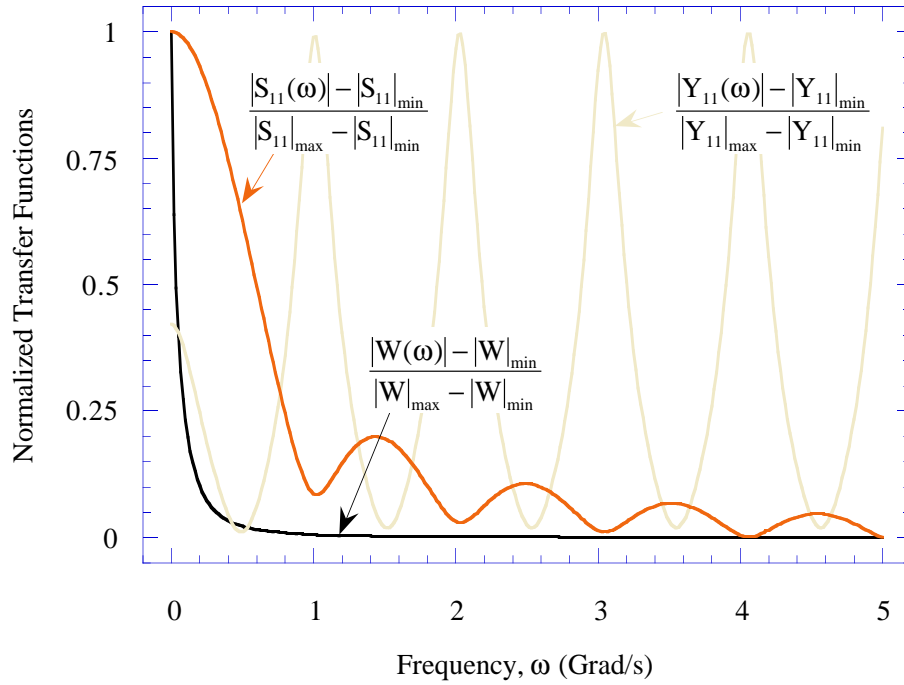
Time-only formulations deal exclusively with the voltages and currents at the line terminals. These formulations are one-dimensional and more efficient. Consequently, to achieve maximum efficiency, the line simulation should be based on a time-only formulation.

4.3.2. Line characterization

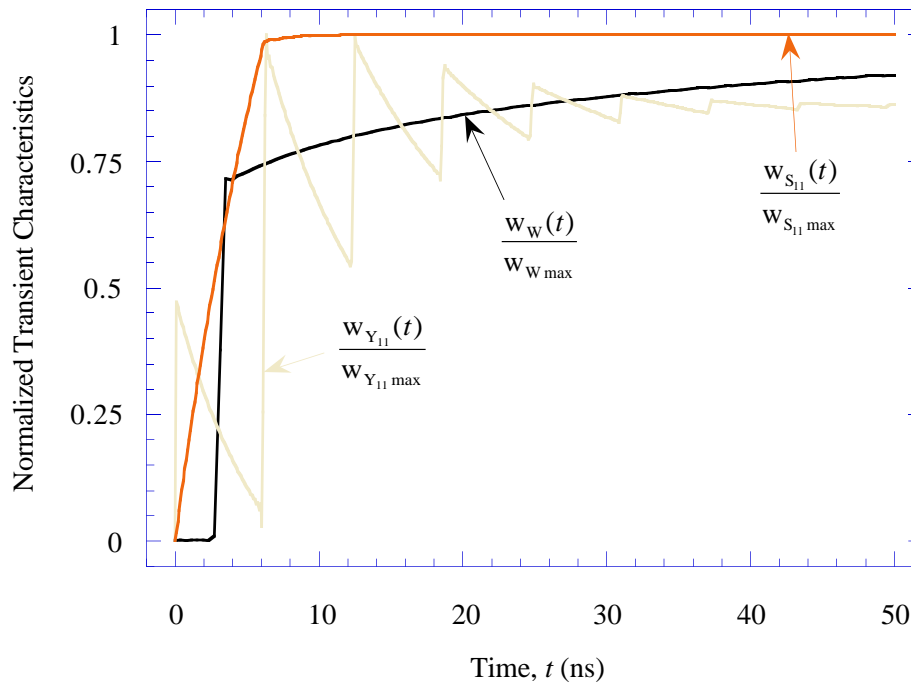
The system diagram [2] in Fig. 4.1 shows that a line with terminations forms a feedback system. Therefore, one can distinguish between *closed-* and *open-loop characterizations*.

Closed-loop characterizations (such as *Z-*, *Y-*, *H-* and *S-*parameter characterizations [38], [39]) include reflections from the terminations, and lead to complicated oscillating transfer functions and transient characteristics (unit-step responses).

The open-loop characterization (direct characterization in terms of the propagation functions) separates forward and backward waves and results in the simplest transfer functions and transient characteristics (see Fig 4.5). Complexity of the transfer functions and transient characteristics is an important factor affecting accuracy and efficiency of the transient simulation. Consequently, to attain maximum efficiency and accuracy, the line simulation should be based on the open-loop characterization. The complete set of expressions for the open-loop functions for uniform lines is given in Appendix B.



(a)



(b)

Fig 4.5. (a) Examples of open- and closed-loop transfer functions and (b) transient characteristics. The scattering parameters correspond to the matched lossless reference system.

4.3.3. Line model

Line models can be divided into two large groups: *circuit* and *noncircuit*.

Noncircuit models can not be directly integrated into a circuit simulator. As a result, these models can not be efficiently applied to the transient analysis of real circuits containing thousands of nonlinear active devices. Examples of noncircuit models are the scattering-parameter model [38] and system model shown in Fig. 4.1.

Circuit models can be directly incorporated into a circuit simulator and are of prime practical interest. They relate voltages and currents at the line terminals and do not depend on the terminations. Circuit models can, in turn, be subdivided into *equivalent-circuit* and *device models*.

Equivalent-circuit models have a larger number of nodes than the line they represent. Examples of equivalent-circuit models are lumped and pseudo-lumped segmentation models [36], modal decomposition models for multiconductor lines [16], [36], [40] and equivalent-circuit modeling of the propagation function and characteristic impedance based on Padé synthesis [41].

Device models have the same number of nodes as the line they represent. A well-known example of device models is the method of characteristics [19], [20], [33], [42], [43]. The circuit simulation time is cubically proportional to the number of nodes and to the number of voltage and current variables. Consequently, to achieve maximum efficiency and practical applicability, the line simulation should be based on a device model that does not require the introduction of current variables.

4.3.4. Transient simulation method

The transient simulation method is the prime factor affecting efficiency of the line simulation. The selection of the transient simulation methods is confined to *the numerical Fourier and Laplace transformations, numerical convolution* and *numerical integration*.

For *the transformation and convolution methods*, the computational complexity is higher than linear. These methods can not directly handle nonlinear and time-varying systems, and, along with the discretization error, introduce time- and/or frequency-response truncation error. In addition, the transformation methods can not be directly used with recursive time-domain solvers employed by circuit simulators, which leads to relaxation techniques which additionally degrade the overall efficiency and accuracy [43]. Examples of the convolution-based techniques are the Spice model for lossy lines [16] and the scattering-parameter approach [38].

Numerical integration has linear computational complexity; it can directly handle nonlinear and time-varying systems, does not introduce truncation error, supports variable time-stepping, and is compatible with recursive time-domain solvers. Numerical integration methods can be subdivided into *direct* and *indirect*.

Direct numerical integration is based on approximations for integrals or derivatives and includes such conventional methods as linear multistep formulas, Euler, Euler-Cauchy and Runge-Kutta techniques.

Indirect numerical integration discussed in Chapter 2 is based on the time-response invariant discrete synthesis, and has ideal accuracy, convergence and stability properties. Consequently, to achieve maximum efficiency, accuracy and practical applicability, the line simulation should be based on indirect numerical integration. Indirect numerical integration covers as special cases such techniques as recursive convolution [8], [20] and approximation of the response of a linear network to an arbitrary piecewise linear input waveform used by some of the asymptotic waveform evaluation (AWE) methods [12].

To systems characterized by samples of their responses, numerical integration is applied via *the difference approximation method* described in Chapter 3. The method is based on the approximation of the system response with the corresponding response of a system for which numerical integration formulas are already available. The complexity of the difference approximation method is only that of the approximation itself. As soon as a system response has been approximated, the numerical integration formulas are readily available directly in terms of the approximation parameters.

To attain maximum efficiency and accuracy, the difference approximation should be applied in the domain of system characterization. For transmission lines it usually is the frequency domain. The time-domain approximation should be used only when time-domain responses are available. The complete set of analytical expressions for the fundamental time-domain open-loop responses of two-conductor uniform constant-parameter lines is given in Appendix C. It also includes a new simple and accurate asymptotic approximation for the responses of propagation functions.

To improve accuracy, the delay should be separated from the propagation functions before the difference approximation is applied. The conventional frequency-domain method of delay separation for multiconductor lines is based on diagonalization with the frequency-dependent *modal transformation* matrices [8], [19], [33]. These matrices are nonminimum-phase functions of frequency with unstable time-domain responses, which limits the applicability of the modal transformation to special cases in which the matrices are constant [16], [44]

A novel *matrix delay separation method* [1] avoids the use of the frequency-dependent modal transformation matrices and is applicable for a general case of matrix transfer functions

containing delay. For uniform lines, the formulas for the matrix delay separation from the propagation functions are included in Appendix B, and, for the parabolically tapered lines, in Appendix D.

4.3.5. Approximation methods

The choice of the approximation method for the difference approximation affects the overall efficiency, accuracy and reliability of the line simulation. Based on approximation criteria, approximation methods can be categorized into four major groups: *minimum maximum error based methods*, *least square based methods*, *interpolation methods*, and *series expansion based methods* (see Fig. 3.1).

Mini-max methods provide the highest accuracy, but result in the most inefficient and unreliable algorithms (nonlinear optimization).

Least square methods provide high accuracy, but are still computationally extensive. The examples of least squares based methods for the time-domain difference approximation are Prony's method [26] and pencil-of-function method [27].

Series expansion based methods (such as Padé synthesis used for the AWE [24], [25], [28]) are computationally efficient, but provide the poorest accuracy.

Interpolation (point-fitting) agrees exactly with the original function on a given set of samples. It provides high accuracy for simple functions, such as open-loop transmission-line responses, and is the most efficient among the approximation methods. It also requires the fewest original function samples, which is important when the samples are obtained from electromagnetic simulations. Consequently, to achieve maximum efficiency, the line simulation should be based on interpolation.

Table 3.1 presents the typical values of maximum relative error in the full frequency range from zero to infinity and relative runtimes for various approximation methods as applied to the third-order frequency-domain difference approximation of open-loop transmission-line functions.

Interpolation provides accuracy comparable with that of the least square approximation, and is 200 times more efficient than mini-max approximation. Interpolation is also up to two orders of magnitude more accurate and 30-50% more efficient than Padé synthesis. Notice also that, because of the simplicity of the open-loop characterization, a very high accuracy is achieved with as low as third-order approximation and as few as seven samples of the original function used for the interpolation.

4.3.6. Summary of the optimal approach

To summarize, the analysis of the problem showed that to achieve maximum efficiency, accuracy and practical applicability, the line simulation should be based on:

- time-only formulation;
- open-loop characterization;
- device model which does not require the introduction of current variables;
- indirect numerical integration;
- frequency-domain difference approximation based on the interpolation and matrix delay separation.

A method close to the optimal, but based on the time-domain difference approximation, was first proposed by Semlyen and Dabuleanu [8], and was further developed by Gruodis and Chang [19] to accommodate the frequency-domain approximation. The advantages of the approach were recognized only in recent years, and an increasing number of techniques close to optimal is being published [33], [20], including techniques based on the AWE, recursive convolution and method of characteristics. The applicability of the methods, however, had been limited by the lack of accurate, reliable and efficient frequency-domain approximation and delay separation techniques such as interpolation-based approximation methods and matrix delay separation, and by the lack of open-loop models for nonuniform lines.

The author's implementation of the optimal method for uniform lines is outlined in the next section. The implementation of the method for nonuniform lines is described in Section 4.4.

4.4. Simulation of Uniform Lines

4.4.1. Frequency-domain line model for transient analysis

The frequency-domain element characteristic (for transient analysis) that does not require the introduction of current variables and is suitable for the line modeling is given by

$$\begin{cases} \mathbf{i}_1(\omega) = \mathbf{Y}_1(\omega) \mathbf{v}_1(\omega) - \mathbf{j}_1(\omega) \\ \mathbf{i}_2(\omega) = \mathbf{Y}_2(\omega) \mathbf{v}_2(\omega) - \mathbf{j}_2(\omega). \end{cases} \quad (4.1)$$

The conventions for the terminal voltages and currents are shown in Fig. 4.6. The expressions relating the matrix admittances \mathbf{Y}_1 and \mathbf{Y}_2 and vector current sources \mathbf{j}_1 and \mathbf{j}_2 to the transmission line characteristics are derived directly from the continuity conditions for the

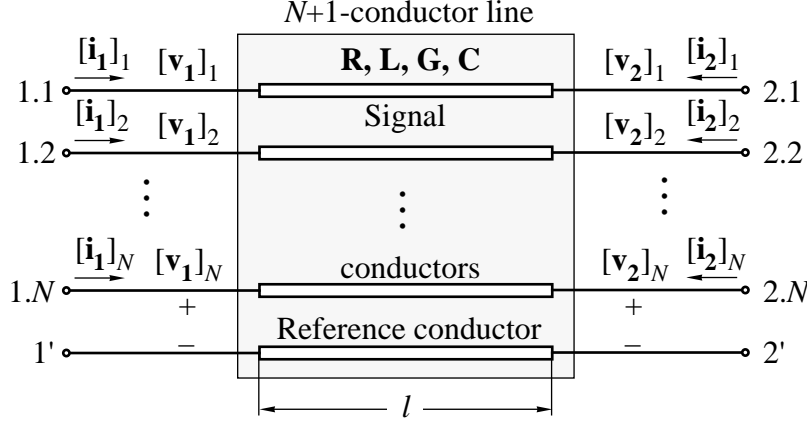


Fig. 4.6. Conventions for the voltages and currents at the line terminals.

voltages and currents at the line terminals. To separate forward and backward waves and open the feedback loop, the current source \mathbf{j}_1 must depend only on the backward wave, and \mathbf{j}_2 only on the forward wave. This condition uniquely defines $\mathbf{Y}_1, \mathbf{Y}_2$ and $\mathbf{j}_1, \mathbf{j}_2$ as follows:

$$\mathbf{Y}_1(\omega) = \mathbf{Y}_2(\omega) = \mathbf{Y}_c(\omega) \quad (4.2)$$

and

$$\begin{cases} \mathbf{j}_1(\omega) = 2\mathbf{i}_{b1}(\omega) \\ \mathbf{j}_2(\omega) = 2\mathbf{i}_{f2}(\omega), \end{cases} \quad (4.3)$$

where \mathbf{Y}_c stands for the characteristic admittance, and the forward and backward current waves, $\mathbf{i}_{f1}, \mathbf{i}_{f2}$ and $\mathbf{i}_{b1}, \mathbf{i}_{b2}$, are related as follows:

$$\begin{cases} \mathbf{i}_{b1}(\omega) = \mathbf{W}_{\text{fb}}(\omega) [\mathbf{i}_{b2}(\omega) = \mathbf{i}_2(\omega) + \mathbf{i}_{f2}(\omega)] \\ \mathbf{i}_{f2}(\omega) = \mathbf{W}_{\text{fr}}(\omega) [\mathbf{i}_{f1}(\omega) = \mathbf{i}_1(\omega) + \mathbf{i}_{b1}(\omega)]. \end{cases} \quad (4.4)$$

The propagation functions for the forward and backward current waves are equal, $\mathbf{W}_{\text{fr}} = \mathbf{W}_{\text{fb}} = \mathbf{W}_{\text{I}}$. The open-loop device model (4.1)-(4.4) is equivalent to the generalized method of characteristics [19], [20], [43].

The propagation function and characteristic admittance can be computed from the insertion loss data [19], scattering parameters [45], or distributed $RLGC$ parameters:

$$\mathbf{W}_{\text{I}}(\omega) = \mathbf{e}^{-\mathbf{K}_{\text{I}}(\omega)l},$$

$$\mathbf{Y}_c(\omega) = \mathbf{K}_{\text{I}}(\omega) \mathbf{Z}^{-1}(\omega),$$

where l is the length of the line,

$$\mathbf{K}_l(\omega) = [\mathbf{Y}(\omega) \mathbf{Z}(\omega)]^{\frac{1}{2}}$$

is the propagation constant for current waves,

$$\mathbf{Y}(\omega) = \mathbf{G}(\omega) + j\omega \mathbf{C}(\omega),$$

$$\mathbf{Z}(\omega) = \mathbf{R}(\omega) + j\omega \mathbf{L}(\omega)$$

are the admittance and impedance per unit length, and \mathbf{R} , \mathbf{L} , \mathbf{G} and \mathbf{C} are the resistance, inductance, conductance and capacitance per unit length. Boldface $(\cdot)^{\frac{1}{2}}$ and $\mathbf{e}^{(\cdot)}$ denote matrix square root and matrix exponential, respectively.

4.4.2. Difference approximation

To perform the transient analysis, indirect numerical integration is applied to the propagation functions and characteristic admittances in the frequency-domain line model (4.1)-(4.4) by using the difference approximation method.

For the difference approximation in the parallel canonic form, samples of the frequency-domain transfer function are approximated with the rational polynomial function

$$\tilde{\mathbf{H}}(j\omega) = \tilde{\mathbf{H}}_{\infty} + \sum_{m=0}^M \frac{1}{1 + j\omega / \omega_{cm}} \mathbf{A}_m, \quad (4.5)$$

or samples of the time-domain unit-step response are approximated with the exponential series

$$\tilde{\mathbf{h}}(t) = \tilde{\mathbf{H}}_0 - \sum_{m=1}^M e^{-\omega_{cm} t} \mathbf{A}_m,$$

where $\tilde{\mathbf{H}}_0$ and $\tilde{\mathbf{H}}_{\infty}$ denote the initial and final values of the approximating transfer function $\tilde{\mathbf{H}}(j\omega)$.

Because the open-loop functions are aperiodic, they have to be approximated with only real poles, $-\omega_{cm}$. In addition, the poles have to be negative to assure stability.

To represent the original functions accurately with the minimum number of samples, the variation of the original function from sample to sample should be about the same. The following empirical formula for the sampling frequencies was found to provide good results

$$\omega_k = \omega_K \left(1 - \cos \frac{\pi k}{2K} \right), \quad k = 0, 1, \dots, K.$$

The end of the approximation interval, ω_k , should be chosen so that the original function would closely approach its final value. This assures that the resulting indirect numerical integration formulas will be accurate in the full frequency and time ranges from zero to infinity. Because of their simplicity, the open-loop functions can be accurately fit with the 3rd-9th-order approximation, and represented by 7-19 samples.

4.4.2.1. Matrix delay separation

To increase the accuracy, the delay is separated from the matrix propagation function before the approximation. The conventional (modal-transformation) approach [8], [19], [33] is based on the diagonalization of the matrix propagation function

$$\mathbf{W}_I(\omega) = \mathbf{M}_I(\omega) \mathbf{W}_{\text{Im}}(\omega) \mathbf{M}_I^{-1}(\omega).$$

The scalar delays are then extracted from the elements of the diagonal eigenvalue (modal propagation function) matrix, $\mathbf{W}_{\text{Im}}(\omega)$. This technique produces two full and one diagonal transfer-function matrix in place of one. In addition, the eigenvector (modal-transformation) matrix, $\mathbf{M}_I(\omega)$, is, in general, a nonminimum-phase function of frequency with unstable time-domain responses, which limits the applicability of this technique to a few special cases [16], [44] in which the eigenvectors are constant.

The absence of general methods for the delay separation from the matrix propagation function was a substantial limitation for the applicability of the approximation-based multiconductor transmission line simulation techniques. The problem is resolved by a novel matrix delay separation method which avoids the use of the frequency-dependent eigenvector matrices. It represents the matrix propagation function in the following form:

$$\mathbf{W}_I(\omega) = \hat{\mathbf{W}}_I(\omega) \hat{\mathbf{M}}_I \mathbf{e}^{-j\omega T_{\text{Im}}} \hat{\mathbf{M}}_I^{-1},$$

where T_{Im} and $\hat{\mathbf{M}}_I$ are the constant eigenvalue and eigenvector matrices of the propagation delay matrix

$$T_I = (\mathbf{C}(\infty) \mathbf{L}(\infty))^{-\frac{1}{2}} l = \mathbf{K}_I(\infty) l.$$

Difference approximation is applied to the delayless propagation function

$$\hat{\mathbf{W}}_I(\omega) = \mathbf{W}_I(\omega) \mathbf{e}^{j\omega T_I}.$$

The delays in the diagonal modal-delay matrix T_{Im} are simulated using a low-order spline of the simulated time points.

4.4.2.2. Matrix complex rational approximation method for the frequency-domain difference approximation

The frequency-domain difference approximation is performed by a novel matrix complex rational approximation method. The method fits samples of an $N \times N$ complex matrix transfer function $\mathbf{H}(\omega)$ with the rational polynomial function (4.5) at the set of arbitrarily spaced frequencies $\{0, \omega_1, \omega_2, \dots, \omega_K\}$. The method proceeds in three steps.

First, the real part of the sum of the elements of the original matrix function,

$$H_{\Sigma}(\omega) = \sum_{i=1}^N \sum_{j=1}^N [\mathbf{H}(\omega)]_{ij},$$

is fit with the real part of the complex rational polynomial function, which is a real rational polynomial function of squared frequency

$$Re(\tilde{H}_{\Sigma}(j\omega)) = \frac{c_0 + c_1 \omega^2 + c_2 (\omega^2)^2 + \dots + c_M (\omega^2)^M}{1 + \beta_1 \omega^2 + \beta_2 (\omega^2)^2 + \dots + \beta_M (\omega^2)^M}. \quad (4.6)$$

The following linear system of equations results from matching the real part of the original function with (4.6) at the set of frequencies and premultiplying both sides of each equation with the denominator

$$\begin{bmatrix} 1 & 0 & \dots & 0 & | & 0 & \dots & 0 \\ 1 & \omega_1^2 & \dots & \omega_1^{2M} & | & -\omega_1^2 Re(H_{\Sigma}(\omega_1)) & \dots & -\omega_1^{2M} Re(H_{\Sigma}(\omega_1)) \\ & & & \vdots & & & & \vdots \\ 1 & \omega_K^2 & \dots & \omega_K^{2M} & | & -\omega_K^2 Re(H_{\Sigma}(\omega_K)) & \dots & -\omega_K^{2M} Re(H_{\Sigma}(\omega_K)) \end{bmatrix} \begin{bmatrix} c_0 \\ \vdots \\ c_M \\ \beta_1 \\ \vdots \\ \beta_M \end{bmatrix} = \begin{bmatrix} Re(H_{\Sigma}(0)) \\ Re(H_{\Sigma}(\omega_1)) \\ \vdots \\ Re(H_{\Sigma}(\omega_K)) \end{bmatrix}. \quad (4.7)$$

For interpolation, $K = 2M$ and solving (4.7) produces a rational polynomial function which coincides with the real part of the original function at all of the sampling points. For a set of samples larger than $2M + 1$, the least square solution of the system (4.7) can be obtained. However, it minimizes the approximation error premultiplied with the denominator, which can lead to inaccurate approximation. Better results are achieved with the method of averages [22], which partitions the larger number of equations into $2M + 1$ subsets in order of the increasing of ω . The equations within each subset are added up, which makes the system consistent. The method is effective in averaging out the noise in measured data.

After the real part has been approximated, the denominator of (4.6) is factored yielding the squared poles, $-\omega_{cm}^2$. Consequently, no unstable right-half-plane poles can be produced. However, there still can be spurious complex conjugate and purely imaginary poles, which are

removed. The remaining real negative poles are used to formulate the equations for the partial expansion coefficients, \mathbf{A}_m , of (4.5). As a result, the order M of (4.5) is less than or equal to that of (4.6).

Matching the real and imaginary parts of each element of the original matrix transfer function $\mathbf{H}(\omega)$ with the corresponding parts of elements of (4.5) at the set of frequencies $\{0, \omega_1, \omega_2, \dots, \omega_K\}$ leads to the following linear systems of equations

$$\left(\mathbf{A} = \begin{bmatrix} 1 & 1 & \dots & 1 \\ 1 & \frac{1}{1 + \omega_1^2 / \omega_{c1}^2} & \dots & \frac{1}{1 + \omega_1^2 / \omega_{cM}^2} \\ & \vdots & & \vdots \\ 1 & \frac{1}{1 + \omega_K^2 / \omega_{c1}^2} & \dots & \frac{1}{1 + \omega_K^2 / \omega_{cM}^2} \\ 0 & \frac{-\omega_1 / \omega_{c1}}{1 + \omega_1^2 / \omega_{c1}^2} & \dots & \frac{-\omega_1 / \omega_{cM}}{1 + \omega_1^2 / \omega_{cM}^2} \\ & \vdots & & \vdots \\ 0 & \frac{-\omega_K / \omega_{c1}}{1 + \omega_K^2 / \omega_{c1}^2} & \dots & \frac{-\omega_K / \omega_{cM}}{1 + \omega_K^2 / \omega_{c1}^2} \end{bmatrix} \right) \mathbf{x} = \begin{bmatrix} [\mathbf{H}_\infty]_{ij} \\ [\mathbf{A}_1]_{ij} \\ [\mathbf{A}_2]_{ij} \\ \vdots \\ [\mathbf{A}_M]_{ij} \end{bmatrix} = \mathbf{b} = \begin{bmatrix} [\mathbf{H}(0)]_{ij} \\ Re([\mathbf{H}(\omega_1)]_{ij}) \\ \vdots \\ Re([\mathbf{H}(\omega_K)]_{ij}) \\ Im([\mathbf{H}(\omega_1)]_{ij}) \\ \vdots \\ Im([\mathbf{H}(\omega_K)]_{ij}) \end{bmatrix}. \quad (4.8)$$

For interpolation $M = 2K$, and both real and imaginary parts of the original transfer function are matched exactly at all of the K frequency points and dc. For an arbitrarily larger number of points, the least square solution of the linear system (4.8) is obtained.

The total computational complexity of the approximation method is that of $N^2 + 1$ real linear solutions and one polynomial factoring. The orders of the polynomial and linear systems depend only on the order of the approximation and not on the number of the original function samples. Because no iterative or relaxation techniques are involved, the method is free from convergence problems.

4.4.2.3. Indirect numerical integration

Once the approximation has been performed, indirect numerical integration formulas (discrete-time difference equations) are readily given in terms of the approximation parameters. For the step invariance the formulas are

$$\begin{cases} \mathbf{y}(t_n) = \tilde{\mathbf{H}}_\infty \mathbf{x}(t_n) + \sum_{m=1}^M \mathbf{z}_m(t_n) \\ \mathbf{z}_m(t_n) = (1 - e^{-\omega_{cm} T_n}) \mathbf{A}_m \mathbf{x}(t_{n-1}) + e^{-\omega_{cm} T_n} \mathbf{z}_m(t_{n-1}), \end{cases} \quad (4.9)$$

where \mathbf{x} , \mathbf{y} and \mathbf{z}_m stand for the excitation, response and state variables, respectively, and $T_n = t_n - t_{n-1}$ is the time step at the n th transient iteration.

For the ramp invariance

$$\begin{cases} \mathbf{y}(t_n) = \tilde{\mathbf{H}}_0 \mathbf{x}(t_n) - \sum_{m=1}^M \mathbf{z}_m(t_n) \\ \mathbf{z}_m(t_n) = \mathbf{D}_m(T_n)(\mathbf{x}(t_n) - \mathbf{x}(t_{n-1})) + e^{-\omega_{cm} T_n} \mathbf{z}_m(t_{n-1}), \end{cases} \quad (4.10)$$

where

$$\mathbf{D}_m(T_n) = \frac{1 - e^{-\omega_{cm} T_n}}{\omega_{cm} T_n} \mathbf{A}_m.$$

An alternative form of the ramp-invariant indirect numerical integration formula has the coefficients of the present-time sample of the excitation lumped together

$$\begin{cases} \mathbf{y}(t_n) = \left(\tilde{\mathbf{H}}_0 - \sum_{m=1}^M \mathbf{D}_m(T_n) \right) \mathbf{x}(t_n) - \sum_{m=1}^M \mathbf{z}_m(t_n) \\ \mathbf{z}_m(t_n) = \left(\mathbf{D}_m(T_{n-1}) e^{-\omega_{cm} T_n} - \mathbf{D}_m(T_n) \right) \mathbf{x}(t_{n-1}) + e^{-\omega_{cm} T_n} \mathbf{z}_m(t_{n-1}). \end{cases} \quad (4.11)$$

This form is especially suitable for the discretization of the characteristic admittance, because, for admittances, the present- and past-time terms in the numerical integration formulas have different physical meanings.

The difference approximation is applied to the delayless propagation function and characteristic admittance. For the characteristic admittance \mathbf{Y}_1 in (4.1), the excitation \mathbf{x} is the terminal voltage \mathbf{v}_1 , and for \mathbf{Y}_2 the excitation is \mathbf{v}_2 . For the propagation function \mathbf{W}_{fr} in (4.4), the excitation \mathbf{x} is the forward current wave \mathbf{i}_{f1} , and response \mathbf{y} is \mathbf{i}_{f2} . For \mathbf{W}_{fb} , the excitation is the backward current wave \mathbf{i}_{b2} , and the response is \mathbf{i}_{b1} .

4.4.3. Companion model

By applying the difference approximation to the propagation function and characteristic admittance, the frequency-domain element characteristic (4.1) is transformed into the following discrete-time element characteristic, or companion model,

$$\begin{cases} \mathbf{i}_1(t_n) = \hat{\mathbf{Y}}_1(t_n) \mathbf{v}_1(t_n) - \hat{\mathbf{j}}_1(t_n) \\ \mathbf{i}_2(t_n) = \hat{\mathbf{Y}}_2(t_n) \mathbf{v}_2(t_n) - \hat{\mathbf{j}}_2(t_n). \end{cases} \quad (4.12)$$

The circuit-diagram interpretation of the companion model is shown in Fig. 4.7.

The admittances $\hat{\mathbf{Y}}_1$ and $\hat{\mathbf{Y}}_2$ represent present-time coefficients in the indirect numerical integration formulas for the admittances \mathbf{Y}_1 and \mathbf{Y}_2 . The current sources $\hat{\mathbf{j}}_1$ and $\hat{\mathbf{j}}_2$ combine the

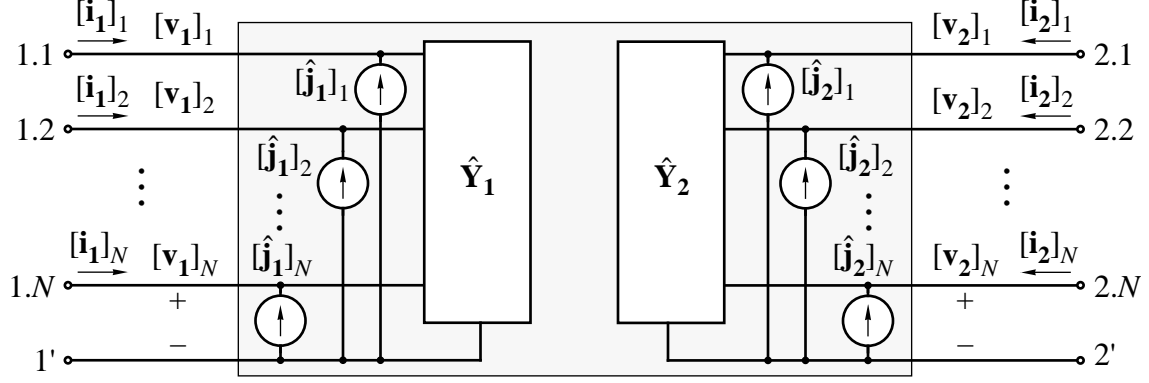


Fig. 4.7. Companion model for a transmission line.

currents \mathbf{j}_{Y_1} and \mathbf{j}_{Y_2} corresponding to the remaining parts of the numerical integration formulas for the admittances, and \mathbf{j}_1 and \mathbf{j}_2 are given by the discretized Eqs. (4.3) and (4.4)

$$\begin{cases} \hat{\mathbf{j}}_1(t_n) = -\mathbf{j}_{Y_1}(t_n) + \mathbf{j}_1(t_n) \\ \hat{\mathbf{j}}_2(t_n) = -\mathbf{j}_{Y_2}(t_n) + \mathbf{j}_2(t_n). \end{cases} \quad (4.13)$$

Equations (4.3) and (4.4) do not contribute to the admittance part of the companion model because the propagation functions contain a delay.

The Modified Nodal Approach (MNA) stamp corresponding to the companion model (4.12) is

KCL at node:	$V_{1,1}$...	$V_{1,N}$	$V_{1'}$	$V_{2,1}$...	$V_{2,N}$	$V_{2'}$				
1.1	$\hat{\mathbf{Y}}_1$			$-\sum_{j=1}^N [\hat{\mathbf{Y}}_1]_{1j}$					$V_{1,1}$	$[\hat{\mathbf{j}}_1]_1$		
...										\vdots	\vdots	
1.N				$-\sum_{j=1}^N [\hat{\mathbf{Y}}_1]_{Nj}$						$V_{1,N}$	$[\hat{\mathbf{j}}_1]_N$	
1'	$-\sum_{i=1}^N [\hat{\mathbf{Y}}_1]_{i1}$...	$-\sum_{i=1}^N [\hat{\mathbf{Y}}_1]_{iN}$	$\sum_{i=1}^N \sum_{j=1}^N [\hat{\mathbf{Y}}_1]_{ij}$				$V_{1'}$	$= -\sum_{i=1}^N [\hat{\mathbf{j}}_1]_i$			
2.1				$\hat{\mathbf{Y}}_2$			$-\sum_{j=1}^N [\hat{\mathbf{Y}}_2]_{j1}$		$V_{2,1}$	$[\hat{\mathbf{j}}_2]_1$		
...											\vdots	\vdots
2.N							$-\sum_{j=1}^N [\hat{\mathbf{Y}}_2]_{jN}$				$V_{2,N}$	$[\hat{\mathbf{j}}_2]_N$
2'				$-\sum_{i=1}^N [\hat{\mathbf{Y}}_2]_{i1}$...	$-\sum_{i=1}^N [\hat{\mathbf{Y}}_2]_{iN}$	$\sum_{i=1}^N \sum_{j=1}^N [\hat{\mathbf{Y}}_2]_{ij}$	$V_{2'}$	$= -\sum_{i=1}^N [\hat{\mathbf{j}}_2]_i$			

(4.14)

In the circuit simulator during the transient analysis, the lines are represented by the tables of numbers (4.14), which are recursively updated at each time iteration using numerical integration. The left-hand side of the stamp (4.14) has to be updated only when the time step changes. If the step-invariant indirect numerical integration formulas (4.6) are used, the left-hand side of the stamp becomes independent of the time step, and only the right-hand side vector has to be updated.

Because the terminal currents are not introduced as variables, the values of \mathbf{i}_1 and \mathbf{i}_2 in (4) are computed from (4.12).

4.4.4. Line model for ac and dc analyses

For ac and dc analyses, the complexity of the transfer functions is not significant, and the element characteristic which does not require the introduction of current variables and is suitable for the ac/dc modeling of transmission lines is the Y -parameter characteristic

$$\begin{cases} \mathbf{i}_1(\omega) = \mathbf{Y}_{11}(\omega) \mathbf{v}_1(\omega) + \mathbf{Y}_{12}(\omega) \mathbf{v}_2(\omega) \\ \mathbf{i}_2(\omega) = \mathbf{Y}_{21}(\omega) \mathbf{v}_1(\omega) + \mathbf{Y}_{22}(\omega) \mathbf{v}_2(\omega). \end{cases} \quad (4.15)$$

The expressions for the Y -parameters are related to the open-loop functions as follows:

$$\begin{aligned} \mathbf{Y}_{11}(\omega) = \mathbf{Y}_{22}(\omega) &= \mathbf{Y}_c(\omega) + 2[\mathbf{I} - \mathbf{W}_I^2(\omega)]^{-1} \mathbf{W}_I^2(\omega) \mathbf{Y}_c(\omega), \\ \mathbf{Y}_{12}(\omega) = \mathbf{Y}_{21}(\omega) &= -2[\mathbf{I} - \mathbf{W}_I^2(\omega)]^{-1} \mathbf{W}_I(\omega) \mathbf{Y}_c(\omega), \end{aligned}$$

where \mathbf{I} is the identity matrix. The expressions are derived by eliminating \mathbf{j}_1 and \mathbf{j}_2 from Eqs. (4.1)-(4.4), and transforming them to the form of (4.15).

The dc model is merely the ac model at zero frequency. For the limiting case of lines with zero distributed conductance, $\mathbf{G} = \mathbf{0}$, the dc values of the Y -parameters are

$$\mathbf{Y}_{11}(0) = \mathbf{Y}_{22}(0) = -\mathbf{Y}_{12}(0) = -\mathbf{Y}_{21}(0) = \frac{1}{l} \mathbf{R}^{-1}. \quad (4.16)$$

The MNA stamp corresponding to (4.15) is

1. Before the transient analysis:
 - a) For each line in the circuit, perform the difference approximation of the propagation function and characteristic admittance.
 - b) Perform op analysis of the circuit to find the initial conditions for the transient analysis. Use the ac/dc model (4.15)-(4.16).
2. At each time iteration:

Recursively update the line stamps using the indirect numerical integration formulas obtained at step 1(a) and companion model (4.12)-(4.14).

Because the method introduces neither additional nodes nor current variables, the optimal line modeling does not increase at all the circuit solution time compared to the simple replacement of interconnects with lumped resistors. The only additional time is required to perform a low-order interpolation once in the beginning of the simulation, and for a low-order numerical integration. As shown in the next section, this time is negligibly small compared to the circuit solution time.

4.4.7. Numerical results

The optimal method has been adopted in several industrial and commercial circuit simulators, and, in numerous real-life simulation exercises, proved to be reliable, accurate and efficient. Table 4.1 presents relative run-time data for circuits of various types and sizes. Table 4.1 shows that even for the worst case of a small circuit consisting of lines only, the optimal model is virtually as efficient as the simple lumped resistors. The resistive model was chosen for the comparison because it represents the limiting case in the simplicity and computational efficiency of the interconnect modeling.

Figure 4.8 shows verification of the optimal model accuracy with the Spice3e2 lossy multiconductor line model [16]. A simple network was chosen as an example to reduce the influence of factors other than the line model on the simulation accuracy. A variable, third-to-fifth-order frequency-domain difference approximation was applied. As one can observe, the compared waveforms are indistinguishable. In fact, the accuracy of the optimal method depends exclusively on the accuracy of the difference approximation which is very high (see Table 3.1). The runtime for the optimal model was three orders of magnitude shorter than that for the Spice model, which is, in turn, an order of magnitude faster than the segmentation models.

TABLE 4.1
RUNTIME COMPARISONS

Number of Nodes	Circuit Description	Relative Runtime ^a				
		Lines Modeled with Lumped Resistors ^b	Lines Modeled with the Optimal Method			Difference Approximation ^d
			Total Circuit Simulation ^c	Indirect Numerical Integration ^d	Frequency Domain	
10	2 two-conductor lines, 1 four-conductor line (lines and excitation sources only)	0.937	1.00	0.0927	0.0793	0.0550
10	2 two-conductor lines, 12 MOSFETs	1.00	1.00	$9.66 \cdot 10^{-3}$	$9.47 \cdot 10^{-3}$	$6.57 \cdot 10^{-3}$
100	20 two-conductor lines, 10 four-conductor lines (lines and excitation sources only)	0.999	1.00	$2.06 \cdot 10^{-3}$	$1.75 \cdot 10^{-3}$	$1.21 \cdot 10^{-3}$
1000	200 two-conductor lines, 100 four-conductor lines (lines and excitation sources only)	1.00	1.00	$1.64 \cdot 10^{-5}$	$1.39 \cdot 10^{-5}$	$9.64 \cdot 10^{-6}$

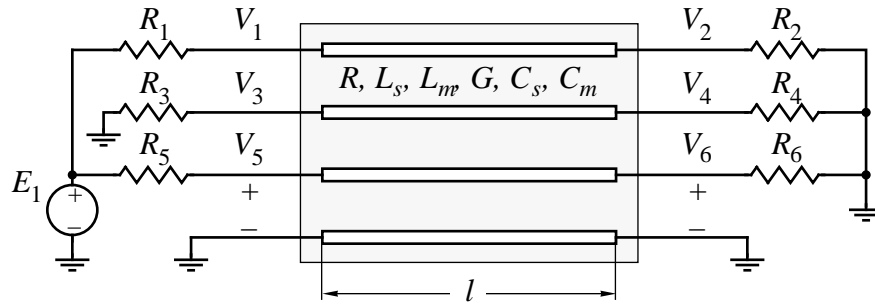
^a For 1000 time points.

^b One resistor per signal conductor.

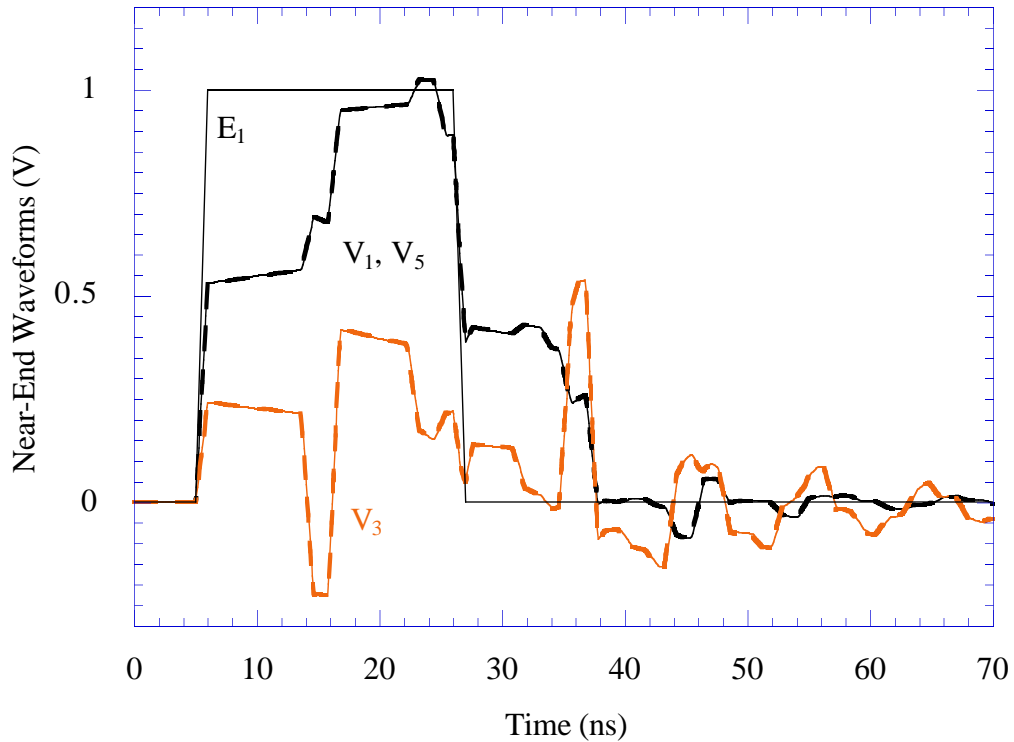
^c Does not include the difference approximation time.

^d Seventh-order.

^e The runtime includes automatic determination of the approximation interval and interpolation points.



(a)



(b)

Fig. 4.8. (a) The network configuration and (b) comparison of the transient waveforms generated using the optimal line model installed in an MNA-based circuit simulator (thick broken curves) and SPICE3e2 (thin continuous curves). $R_1=R_5=50\ \Omega$, $R_2=R_6=1\ \text{k}\Omega$, $R_3=R_4=10\ \text{M}\Omega$; self-inductance $L_s=418\ \text{nH/m}$, self-capacitance $C_s=94\ \text{pF/m}$, mutual inductance $L_m=125\ \text{nH/m}$, mutual capacitance $C_m=22\ \text{pF/m}$, $R=15\ \Omega/\text{m}$, $G=0$, $l=0.677\ \text{m}$ (all signal conductors are the same).

4.5. Simulation of Nonuniform Lines

4.5.1. Open-loop model

A substantial amount of study has been devoted to the transient simulation of nonuniform transmission lines in recent years [9], [20], [37], [43], [46]-[52]. The optimal method introduced in this dissertation handles both uniform and nonuniform lines in exactly the same manner. The open-loop element characteristic (4.1), companion model (4.12), ac/dc element characteristic (4.15), and simulation algorithm remain the same. The uniform line model, and, as a result, the characteristic equations, (4.2)-(4.4), and expressions for the Y -parameters, (4.16), are simply a special case of those for nonuniform lines as described below.

Nonuniform lines can still be represented by the system model shown in Fig. 4.1, with the only difference that the propagation functions in the forward and backward directions are no longer the same, and the characteristic admittances become dependent on the position along the line as well as on the direction of the wave propagation.

Then, the open-loop characteristic equations become

$$\begin{cases} \mathbf{Y}_1(\omega) = \mathbf{Y}_{f1}(\omega) \\ \mathbf{Y}_2(\omega) = \mathbf{Y}_{b2}(\omega), \end{cases} \quad (4.17)$$

$$\begin{cases} \mathbf{j}_1(\omega) = [\mathbf{X}_1(\omega) = \mathbf{I} + \mathbf{Y}_{f1}(\omega)\mathbf{Z}_{b1}(\omega)]\mathbf{i}_{b1}(\omega) \\ \mathbf{j}_2(\omega) = [\mathbf{X}_2(\omega) = \mathbf{I} + \mathbf{Y}_{b2}(\omega)\mathbf{Z}_{f2}(\omega)]\mathbf{i}_{f2}(\omega), \end{cases} \quad (4.18)$$

$$\begin{cases} \mathbf{i}_{b1}(\omega) = \mathbf{W}_{lb}(\omega) [\mathbf{i}_{b2}(\omega) = \mathbf{i}_2(\omega) + \mathbf{i}_{f2}(\omega)] \\ \mathbf{i}_{f2}(\omega) = \mathbf{W}_{lf}(\omega) [\mathbf{i}_{f1}(\omega) = \mathbf{i}_1(\omega) + \mathbf{i}_{b1}(\omega)], \end{cases} \quad (4.19)$$

where \mathbf{Y}_{f1} , \mathbf{Y}_{b2} and \mathbf{Z}_{f2} , \mathbf{Z}_{b1} are forward and backward characteristic admittances and impedances at the near- and far-end terminals. The equations are derived as described for uniform lines in Section 4.4. The propagation functions for voltage and current waves are related as follows: $\mathbf{W}_{lf}(\omega) = \mathbf{Y}_{f2}(\omega)\mathbf{W}_{vf}(\omega)\mathbf{Z}_{f1}(\omega)$ and $\mathbf{W}_{lb}(\omega) = \mathbf{Y}_{b1}(\omega)\mathbf{W}_{vb}(\omega)\mathbf{Z}_{b2}(\omega)$. Equations (4.17)-(4.19) show that for nonuniform lines, the open-loop device model is no longer given by the generalized method of characteristics. However, Eqs. (4.17)-(4.19) cover the generalized method of characteristics as a special case, in which $\mathbf{Y}_{f1} = \mathbf{Y}_{f2} = \mathbf{Y}_{b1} = \mathbf{Y}_{b2} = \mathbf{Y}_c$, $\mathbf{W}_{lf} = \mathbf{W}_{lb}$ and $\mathbf{X}_1 = \mathbf{X}_2 = 2\mathbf{I}$.

The Y -parameters (for the ac/dc model (4.6)) are expressed in terms of the open-loop functions as follows:

$$\begin{aligned}
\mathbf{Y}_{11}(\omega) &= [\mathbf{I} + \mathbf{X}_1(\omega)\mathbf{P}_1^{-1}(\omega)\mathbf{W}_{\text{lb}}(\omega)(\mathbf{X}_2(\omega) - \mathbf{I})\mathbf{W}_{\text{fr}}(\omega)]\mathbf{Y}_{f1}(\omega), \\
\mathbf{Y}_{12}(\omega) &= -\mathbf{X}_1(\omega)\mathbf{P}_1^{-1}(\omega)\mathbf{W}_{\text{lb}}(\omega)\mathbf{Y}_{b2}(\omega), \\
\mathbf{Y}_{21}(\omega) &= -\mathbf{X}_2(\omega)\mathbf{P}_2^{-1}(\omega)\mathbf{W}_{\text{fr}}(\omega)\mathbf{Y}_{f1}(\omega), \\
\mathbf{Y}_{22}(\omega) &= [\mathbf{I} + \mathbf{X}_2(\omega)\mathbf{P}_2^{-1}(\omega)\mathbf{W}_{\text{fr}}(\omega)(\mathbf{X}_1(\omega) - \mathbf{I})\mathbf{W}_{\text{lb}}(\omega)]\mathbf{Y}_{b2}(\omega),
\end{aligned} \tag{4.20}$$

where

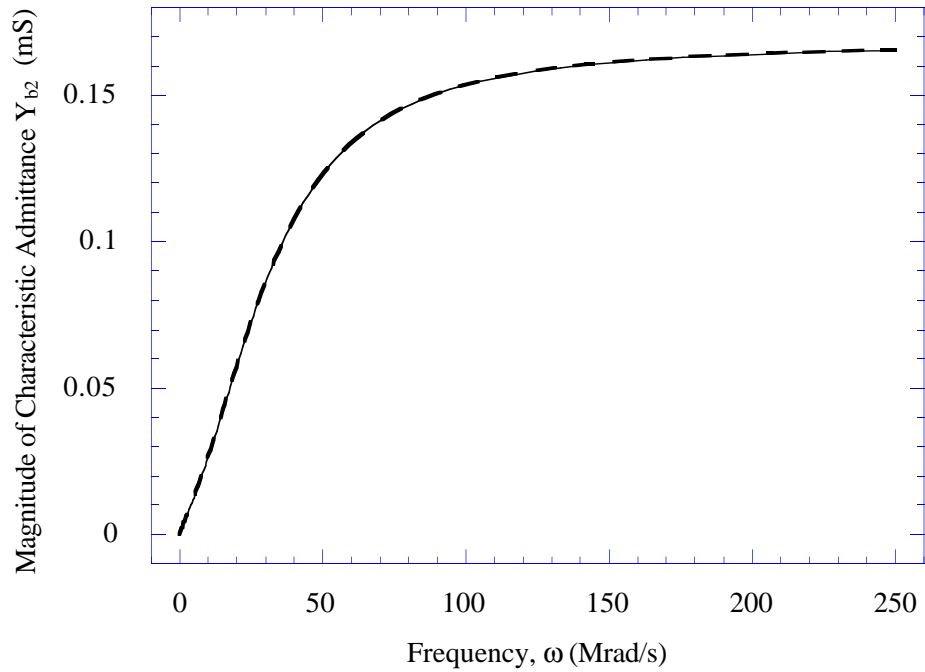
$$\begin{aligned}
\mathbf{P}_1(\omega) &= \mathbf{I} - \mathbf{W}_{\text{lb}}(\omega)(\mathbf{X}_2(\omega) - \mathbf{I})\mathbf{W}_{\text{fr}}(\omega)(\mathbf{X}_1(\omega) - \mathbf{I}), \\
\mathbf{P}_2(\omega) &= \mathbf{I} - \mathbf{W}_{\text{fr}}(\omega)(\mathbf{X}_1(\omega) - \mathbf{I})\mathbf{W}_{\text{lb}}(\omega)(\mathbf{X}_2(\omega) - \mathbf{I}).
\end{aligned}$$

Again, the derivation procedure for these expressions is identical to that for uniform lines, and the corresponding expressions for uniform lines, (4.7), are a special case of (4.20).

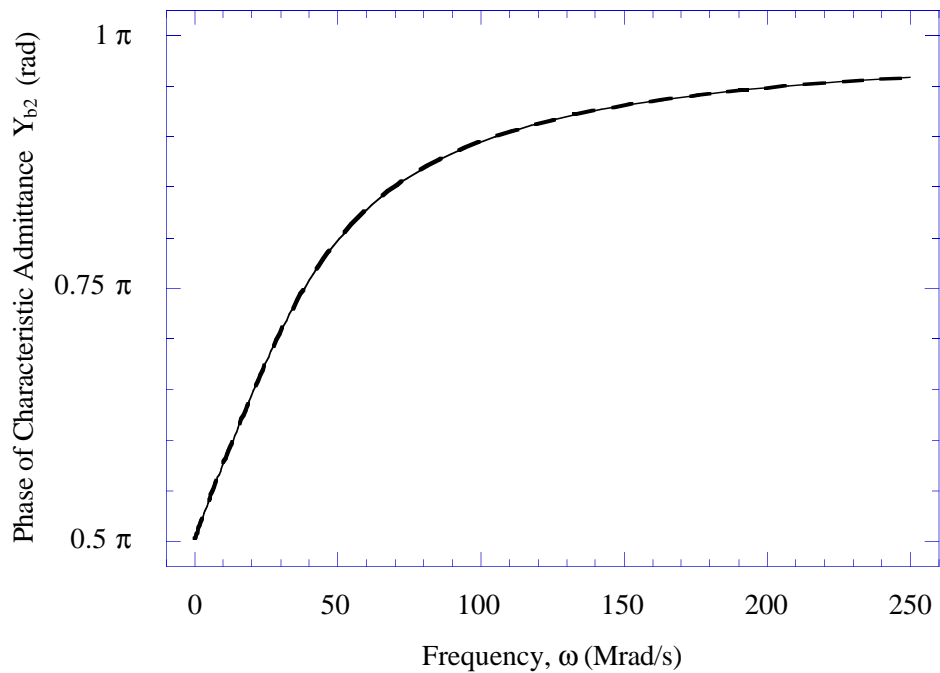
The open-loop propagation functions and characteristic admittances for nonuniform lines can be obtained from the general solution of telegrapher's equations by asymptotically separating the terms corresponding to the forward and backward directions of propagation. The expressions for the open-loop propagation functions and characteristic admittances for parabolically tapered lines are given in Appendix D. Parabolically tapered lines have the simplest analytical solutions, and are convenient to use for testing of nonuniform line models.

As long as a nonuniform line does not have abrupt discontinuities, the open-loop responses are simple, aperiodic functions of frequency and time (as they are for uniform lines), and can be accurately represented by a few samples and simulated using a low-order difference approximation with only real poles. Figure 4.9 shows the typical behavior of an open-loop transfer function and its rational interpolation.

In contrast to uniform lines, the open-loop functions for nonuniform lines, while providing the simplest possible characterization, do not represent distinct physical phenomena which would have to satisfy the energy conservation law. As a result, they can be nonminimum-phase functions with unstable time-domain responses. The reason for this is that in nonuniform lines the forward and backward waves are coupled via the internal distributed reflections, which are not explicitly included in the open-loop model.



(a)



(b)

Fig. 4.9. (a) Magnitude and (b) phase of an open-loop transfer function for a four-conductor parabolically tapered line. Thin continuous curves show the original function, and thick dashed curves show the fifth-order rational interpolation.

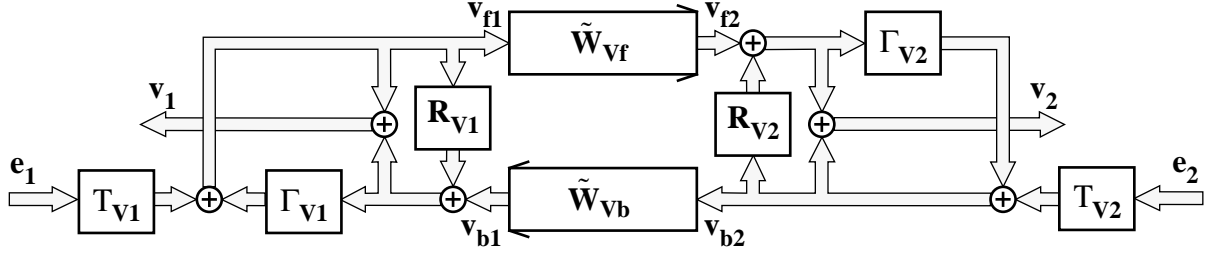


Fig. 4.10. The internal-reflection system model for nonuniform lines.

For instance, for parabolically tapered lines, the far-end backward characteristic admittance \mathbf{Y}_{b2} is a nonminimum-phase function (see Appendix D and Fig. 4.9). Nonminimum-phase functions have to be approximated using positive poles, which, under certain conditions, can lead to unacceptably large transient simulation errors. However, for parabolically tapered lines, \mathbf{Y}_{b2} is the only nonminimum-phase function in the open-loop element characteristic, and a completely stable characterization can be obtained by premultiplying both sides of the second equation in (4.1) by \mathbf{Y}_{b2}^{-1} .

4.5.2. Open-loop internal-reflection model

For a nonuniform-line characterization to be stable in a general case, the line model has to explicitly include the internal distributed reflections. The system-diagram representation of a nonuniform transmission line taking into account the internal reflections is shown in Fig. 4.10.

The near- and far-end internal-reflection coefficients \mathbf{R}_{V1} and \mathbf{R}_{V2} combine the total effect of the internal distributed reflections produced by the forward wave on its way from the near- to the far-end terminal, and by the backward wave on its way from the far- to the near-end terminal, respectively.

The internal-reflection propagation functions, $\tilde{\mathbf{W}}_{Vf}$ and $\tilde{\mathbf{W}}_{Vb}$, and reflection coefficients, \mathbf{R}_{V1} and \mathbf{R}_{V2} , are identical to the scattering parameters with the matched (at both ends) reference system (as are the propagation functions for uniform lines) and can be directly measured: $\tilde{\mathbf{W}}_{Vf} = \mathbf{S}_{21}$, $\tilde{\mathbf{W}}_{Vb} = \mathbf{S}_{12}$, $\mathbf{R}_{V1} = \mathbf{S}_{11}$ and $\mathbf{R}_{V2} = \mathbf{S}_{22}$. Formulas relating the open-loop internal-reflection functions to the open-loop functions are given in Appendix E.

Because of their distinct physical meaning, the open-loop internal-reflection functions have to satisfy the energy conservation law, and are guaranteed to be stable. The internal-reflection system model presented in Fig. 4.10 covers the system model for uniform lines (see Fig. 4.1) as a special case in which no internal reflections are present, i.e., $\mathbf{R}_{V1} = \mathbf{R}_{V2} = \mathbf{0}$. By taking into account internal distributed reflections and eliminating reflections from the

terminations, *the open-loop internal-reflection functions provide the simplest possible stable characterization for nonuniform lines.*

From the internal-reflection system model, one can derive the following open-loop internal-reflection characteristic equations

$$\begin{cases} \mathbf{Y}_1(\omega) = (\mathbf{X}_1(\omega) - \mathbf{I}) \mathbf{Y}_{c1}(\omega) \\ \mathbf{Y}_2(\omega) = (\mathbf{X}_2(\omega) - \mathbf{I}) \mathbf{Y}_{c2}(\omega), \end{cases} \quad (4.21)$$

$$\begin{cases} \mathbf{j}_1(\omega) = \left[\mathbf{X}_1(\omega) = \mathbf{I} + (\mathbf{I} - \mathbf{R}_{11}(\omega))(\mathbf{I} + \mathbf{R}_{11}(\omega))^{-1} \right] \mathbf{i}_{b1}(\omega) \\ \mathbf{j}_2(\omega) = \left[\mathbf{X}_2(\omega) = \mathbf{I} + (\mathbf{I} - \mathbf{R}_{12}(\omega))(\mathbf{I} + \mathbf{R}_{12}(\omega))^{-1} \right] \mathbf{i}_{f2}(\omega), \end{cases} \quad (4.22)$$

$$\begin{cases} \mathbf{i}_{b1}(\omega) = \tilde{\mathbf{W}}_{1b}(\omega) \left[\mathbf{i}_{b2}(\omega) = (\mathbf{I} - \mathbf{R}_{12}(\omega))^{-1} (\mathbf{i}_2(\omega) + \mathbf{i}_{f2}(\omega)) \right] \\ \mathbf{i}_{f2}(\omega) = \tilde{\mathbf{W}}_{1f}(\omega) \left[\mathbf{i}_{f1}(\omega) = (\mathbf{I} - \mathbf{R}_{11}(\omega))^{-1} (\mathbf{i}_1(\omega) + \mathbf{i}_{b1}(\omega)) \right]. \end{cases} \quad (4.23)$$

The derivation proceeds in the manner described in Section 4.4. The near- and far-end characteristic admittances, \mathbf{Y}_{c1} and \mathbf{Y}_{c2} , are equal to the characteristic admittances of uniform lines with the same values of distributed parameters as those of the nonuniform line at the ends, and do not depend on the direction of propagation. The propagation functions and internal reflection coefficients for voltage and current waves are related as follows: $\tilde{\mathbf{W}}_{1f}(\omega) = \mathbf{Y}_{c2}(\omega) \tilde{\mathbf{W}}_{vf}(\omega) \mathbf{Z}_{c1}(\omega)$, $\tilde{\mathbf{W}}_{1b}(\omega) = \mathbf{Y}_{c1}(\omega) \tilde{\mathbf{W}}_{vb}(\omega) \mathbf{Z}_{c2}(\omega)$, $\mathbf{R}_{11}(\omega) = \mathbf{Y}_{c1}(\omega) \mathbf{R}_{v1}(\omega) \mathbf{Z}_{c1}(\omega)$ and $\mathbf{R}_{12}(\omega) = \mathbf{Y}_{c2}(\omega) \mathbf{R}_{v2}(\omega) \mathbf{Z}_{c2}(\omega)$. Equations (4.21)-(4.23) cover the generalized method of characteristics as a special case in which $\mathbf{Y}_{c1} = \mathbf{Y}_{c2} = \mathbf{Y}_c$, $\mathbf{W}_{1f} = \mathbf{W}_{1b}$, $\mathbf{R}_{v1} = \mathbf{R}_{v2} = \mathbf{0}$ and $\mathbf{X}_1 = \mathbf{X}_2 = 2\mathbf{I}$.

For practical application, it is advantageous to combine Eqs. (4.22) and (4.23) and to express them in terms of the termination voltages instead of the currents.

$$\begin{cases} \mathbf{j}_1(\omega) = \left[\mathbf{H}_{1b}(\omega) = \mathbf{X}_1(\omega) \tilde{\mathbf{W}}_{1b}(\omega) (\mathbf{I} + \mathbf{R}_{12}(\omega))^{-1} \mathbf{X}_2^{-1}(\omega) \right] \left[\mathbf{X}_2(\omega) \mathbf{Y}_{c2}(\omega) \mathbf{v}_2(\omega) - \mathbf{j}_2(\omega) \right] \\ \mathbf{j}_2(\omega) = \left[\mathbf{H}_{1f}(\omega) = \mathbf{X}_2(\omega) \tilde{\mathbf{W}}_{1f}(\omega) (\mathbf{I} + \mathbf{R}_{11}(\omega))^{-1} \mathbf{X}_1^{-1}(\omega) \right] \left[\mathbf{X}_1(\omega) \mathbf{Y}_{c1}(\omega) \mathbf{v}_1(\omega) - \mathbf{j}_1(\omega) \right]. \end{cases}$$

In this way, the terminal currents do not have to be recovered.

The transfer functions \mathbf{H}_{1f} and \mathbf{H}_{1b} contain delays which originate from the propagation functions $\tilde{\mathbf{W}}_{1f}$ and $\tilde{\mathbf{W}}_{1b}$. Before the difference approximation is applied, the delays are separated via the matrix delay separation technique, which represents the matrix transfer functions in the following form

$$\mathbf{H}_{\text{If}}(\omega) = \hat{\mathbf{H}}_{\text{If}}(\omega) \mathbf{M}_{\text{If}} \mathbf{e}^{-j\omega \mathbf{T}_{\text{Im}}} \mathbf{M}_{\text{If}}^{-1},$$

$$\mathbf{H}_{\text{Ib}}(\omega) = \hat{\mathbf{H}}_{\text{Ib}}(\omega) \mathbf{M}_{\text{Ib}} \mathbf{e}^{-j\omega \mathbf{T}_{\text{Im}}} \mathbf{M}_{\text{Ib}}^{-1},$$

where the delayless transfer functions, $\hat{\mathbf{H}}_{\text{If}}$ and $\hat{\mathbf{H}}_{\text{Ib}}$, are found as

$$\hat{\mathbf{H}}_{\text{If}}(\omega) = \mathbf{H}_{\text{If}}(\omega) \mathbf{e}^{j\omega \mathbf{T}_{\text{If}}},$$

$$\hat{\mathbf{H}}_{\text{Ib}}(\omega) = \mathbf{H}_{\text{Ib}}(\omega) \mathbf{e}^{j\omega \mathbf{T}_{\text{Ib}}}.$$

The matrix propagation delays, \mathbf{T}_{If} and \mathbf{T}_{Ib} , are the same in the forward and backward directions: $\mathbf{T}_{\text{If}} = \mathbf{T}_{\text{Ib}} = \mathbf{T}_{\text{I}}$, and are equal for all of \mathbf{W}_{If} , \mathbf{W}_{Ib} , $\tilde{\mathbf{W}}_{\text{If}}$, $\tilde{\mathbf{W}}_{\text{Ib}}$, \mathbf{H}_{If} and \mathbf{H}_{Ib} . \mathbf{T}_{Im} and \mathbf{T}_{Ibm} and \mathbf{M}_{If} and \mathbf{M}_{Ib} are diagonal eigenvalue and constant eigenvector matrices of \mathbf{T}_{If} and \mathbf{T}_{Ib} , respectively.

The Y -parameters in the ac/dc model are expressed in terms of the internal-reflection functions as follows:

$$\mathbf{Y}_{11}(\omega) = \left\{ \mathbf{X}_1(\omega) \left[\mathbf{I} + \mathbf{P}_1^{-1}(\omega) \tilde{\mathbf{W}}_{\text{Ib}}(\omega) (\mathbf{I} + \mathbf{R}_{\text{I2}}(\omega)) \tilde{\mathbf{W}}_{\text{If}}(\omega) \right] - \mathbf{I} \right\} \mathbf{Y}_{\text{c1}}(\omega),$$

$$\mathbf{Y}_{12}(\omega) = -\mathbf{X}_1(\omega) \mathbf{P}_1^{-1}(\omega) \tilde{\mathbf{W}}_{\text{Ib}}(\omega) \mathbf{Y}_{\text{c2}}(\omega),$$

$$\mathbf{Y}_{21}(\omega) = -\mathbf{X}_2(\omega) \mathbf{P}_2^{-1}(\omega) \tilde{\mathbf{W}}_{\text{If}}(\omega) \mathbf{Y}_{\text{c1}}(\omega),$$

$$\mathbf{Y}_{22}(\omega) = \left\{ \mathbf{X}_2(\omega) \left[\mathbf{I} + \mathbf{P}_2^{-1}(\omega) \tilde{\mathbf{W}}_{\text{If}}(\omega) (\mathbf{I} + \mathbf{R}_{\text{I1}}(\omega)) \tilde{\mathbf{W}}_{\text{Ib}}(\omega) \right] - \mathbf{I} \right\} \mathbf{Y}_{\text{c2}}(\omega),$$

where

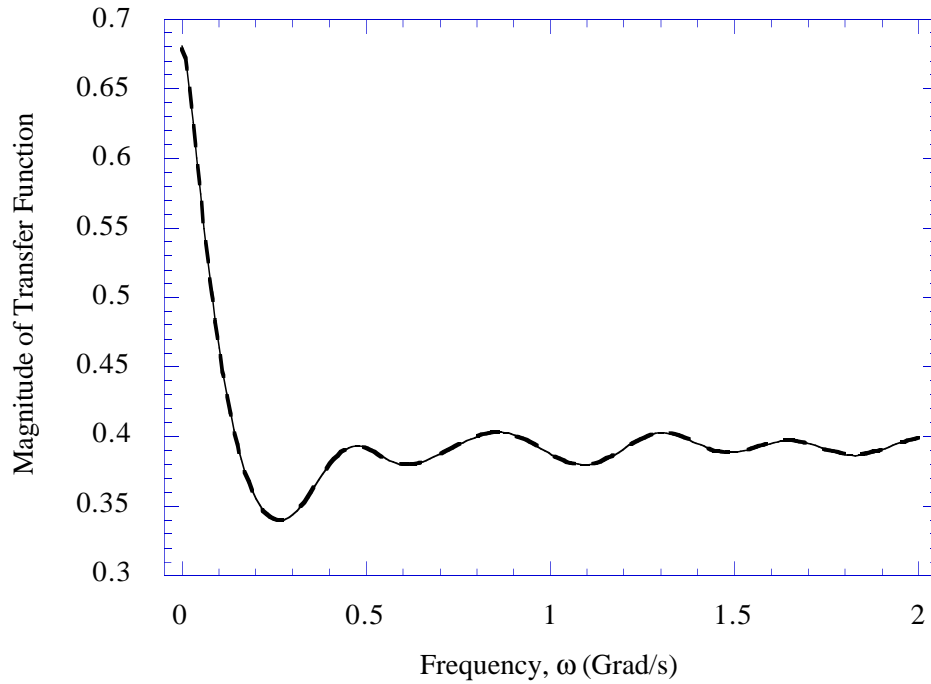
$$\mathbf{P}_1(\omega) = \mathbf{I} - \tilde{\mathbf{W}}_{\text{Ib}}(\omega) (\mathbf{I} + \mathbf{R}_{\text{I2}}(\omega)) \tilde{\mathbf{W}}_{\text{If}}(\omega) (\mathbf{I} + \mathbf{R}_{\text{I1}}(\omega)),$$

$$\mathbf{P}_2(\omega) = \mathbf{I} - \tilde{\mathbf{W}}_{\text{If}}(\omega) (\mathbf{I} + \mathbf{R}_{\text{I1}}(\omega)) \tilde{\mathbf{W}}_{\text{Ib}}(\omega) (\mathbf{I} + \mathbf{R}_{\text{I2}}(\omega)).$$

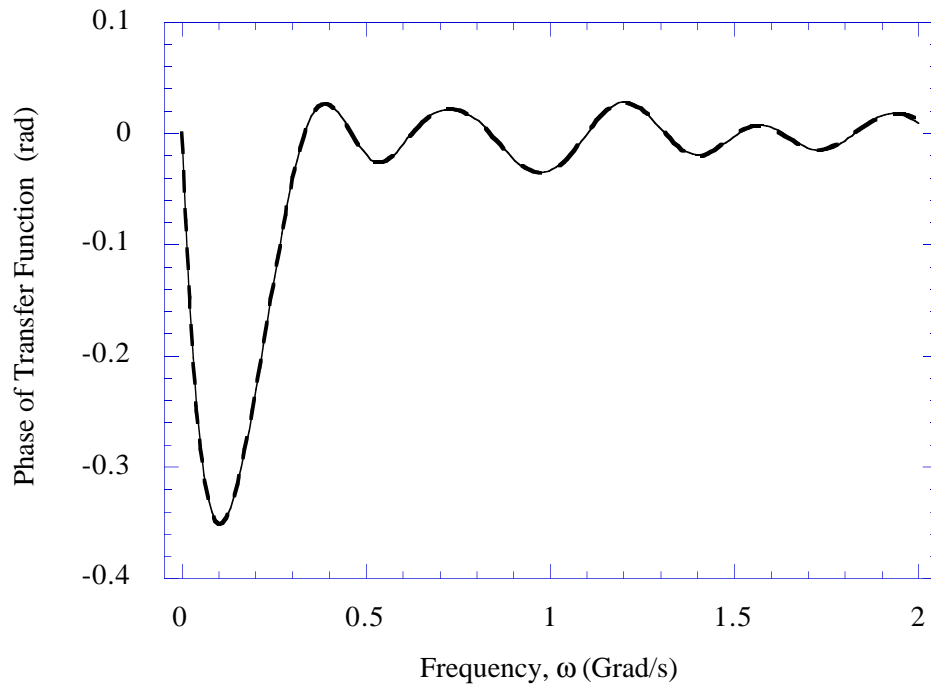
Again, these expressions cover the corresponding expressions for uniform lines as a special case, and are derived in the same manner.

Because they include the distributed feedback resulting from the internal reflections, the open-loop internal-reflection functions are more complicated than the open-loop functions. Consequently, they require a higher-order approximation and have to be approximated using both real and complex poles. However, because the reflections from the terminations are eliminated, the open-loop internal-reflection transfer functions do not contain nondecaying oscillations (provided that the nonuniform line does not contain abrupt discontinuities inside), and still can be approximated in the full range from zero to infinity.

Figure 4.11 shows the typical behavior of an internal-reflection transfer function and its approximation. Note that the delay component is completely removed by the matrix delay separation technique.



(a)



(b)

Fig. 4.11. (a) Magnitude and (b) phase of the delayless transfer function $\hat{\mathbf{H}}_{1b}$ for a four-conductor parabolically tapered line. Thin continuous curves show the original function, and thick dashed curves show the 21st-order rational approximation.

The required order of approximation can be estimated by multiplying the number of peaks falling into the approximation interval by a factor of 3-5, which typically leads to a 15-to-30-order approximation for the full frequency/time range (in contrast to the 3-to-10-order approximation for the open-loop functions). This is the price to be paid to insure stability of the line characterization. However, the open-loop internal-reflection characterization is still simpler than any other stable characterization, such as S -, Y -, Z - or H -parameter, because it is the only characterization that opens the feedback loop formed by reflections from the terminations.

4.5.3. Numerical results

The accuracy and reliability of the method have been tested in numerous simulation exercises. Figure 4.12 shows transient waveforms for the four-conductor parabolically tapered frequency-dependent line of [20] simulated with the open-loop and open-loop internal-reflection models installed in an MNA-based circuit simulator. The results are in excellent agreement with the analytical solutions in [20], p. 12, Fig. 4(a) and (b).

Figure 4.13 presents the transient simulation results for a completely asymmetric parabolically tapered nine-conductor line. A simple circuit was used to reduce the influence of factors other than the line model on the simulation accuracy. The line parameters are: $l = 0.97$ m, $a = 1.03$ m⁻¹,

$$\mathbf{L} = \begin{bmatrix} 2.311 & 0.414 & 0.0842 & 0.01693 & 3.91 \cdot 10^{-3} & 7.58 \cdot 10^{-4} & 1.250 \cdot 10^{-4} & 2.656 \cdot 10^{-5} \\ 0.414 & 2.988 & 0.527 & 0.1045 & 0.02307 & 4.21 \cdot 10^{-3} & 6.28 \cdot 10^{-4} & 1.805 \cdot 10^{-4} \\ 0.0842 & 0.527 & 2.813 & 0.480 & 0.0743 & 0.01915 & 3.95 \cdot 10^{-3} & 7.69 \cdot 10^{-4} \\ 0.01693 & 0.1045 & 0.480 & 2.592 & 0.385 & 0.0984 & 0.01525 & 3.74 \cdot 10^{-3} \\ 3.91 \cdot 10^{-3} & 0.02307 & 0.0743 & 0.385 & 2.845 & 0.432 & 0.0995 & 0.02395 \\ 7.58 \cdot 10^{-4} & 4.21 \cdot 10^{-3} & 0.01915 & 0.0984 & 0.432 & 2.708 & 0.380 & 0.1010 \\ 1.250 \cdot 10^{-4} & 6.28 \cdot 10^{-4} & 3.95 \cdot 10^{-3} & 0.01525 & 0.0995 & 0.380 & 2.172 & 0.382 \\ 2.656 \cdot 10^{-5} & 1.805 \cdot 10^{-4} & 7.69 \cdot 10^{-4} & 3.74 \cdot 10^{-3} & 0.02395 & 0.1010 & 0.382 & 2.040 \end{bmatrix} \frac{\mu\text{H}}{\text{m}},$$

$$\mathbf{C} = \begin{bmatrix} 23.92 & -5.41 & -1.080 & -0.3092 & -0.0567 & -0.01563 & -0.00360 & -0.000634 \\ -5.41 & 21.23 & -5.72 & -1.111 & -0.3081 & -0.0498 & -0.01588 & -0.00337 \\ -1.080 & -5.72 & 24.47 & -3.95 & -1.200 & -0.2201 & -0.0469 & -0.01435 \\ -0.3092 & -1.111 & -3.95 & 21.08 & -4.01 & -1.368 & -0.2995 & -0.0666 \\ -0.0567 & -0.3081 & -1.200 & -4.01 & 23.26 & -3.72 & -1.064 & -0.3136 \\ -0.01563 & -0.0498 & -0.2201 & -1.368 & -3.72 & 25.18 & -5.48 & -1.330 \\ -0.00360 & -0.01588 & -0.0469 & -0.2995 & -1.064 & -5.48 & 16.63 & -4.58 \\ -0.000634 & -0.00337 & -0.01435 & -0.0666 & -0.3136 & -1.330 & -4.58 & 24.74 \end{bmatrix} \frac{\text{pF}}{\text{m}},$$

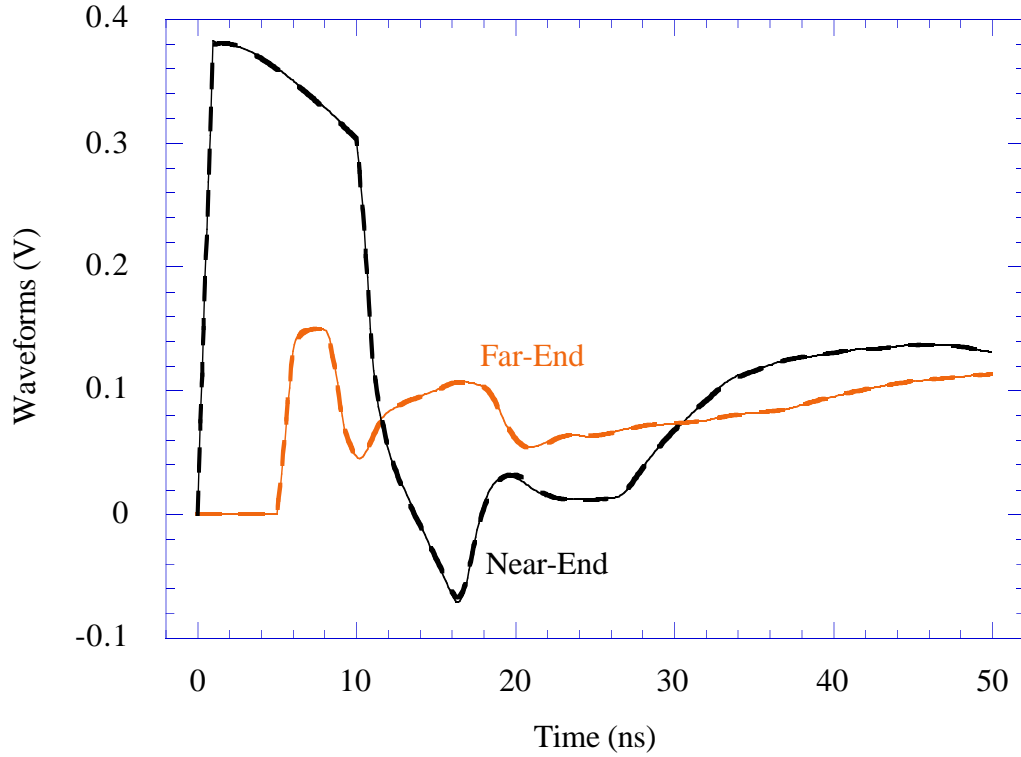
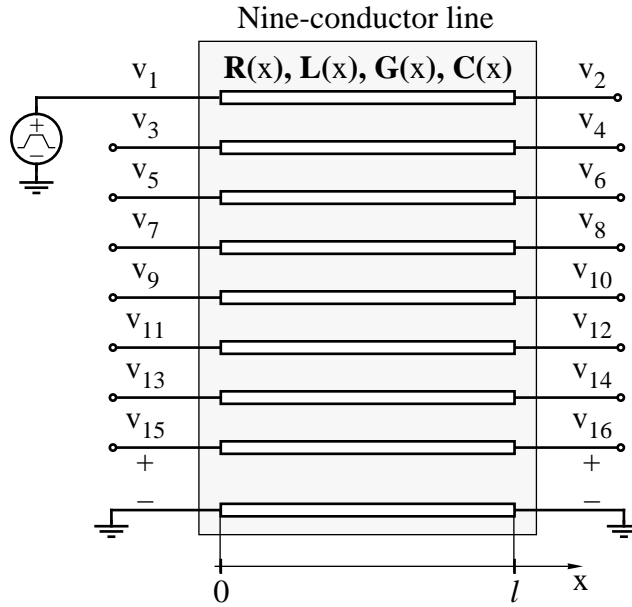


Fig. 4.12. Transient waveforms at conductor #3 of the four-conductor frequency-dependent parabolically tapered line of [20]. Thin continuous curves show the results obtained with the open-loop model and thick dashed curves show those for the open-loop internal-reflection model.

$$\mathbf{R} = \begin{bmatrix} 42.5 & 0 & 0 & 0 & 0 & 0 & 0 & 0 \\ 0 & 41 & 0 & 0 & 0 & 0 & 0 & 0 \\ 0 & 0 & 33.5 & 0 & 0 & 0 & 0 & 0 \\ 0 & 0 & 0 & 38.8 & 0 & 0 & 0 & 0 \\ 0 & 0 & 0 & 0 & 43.7 & 0 & 0 & 0 \\ 0 & 0 & 0 & 0 & 0 & 39.6 & 0 & 0 \\ 0 & 0 & 0 & 0 & 0 & 0 & 47.1 & 0 \\ 0 & 0 & 0 & 0 & 0 & 0 & 0 & 39.5 \end{bmatrix} \frac{\Omega}{\text{m}},$$

and



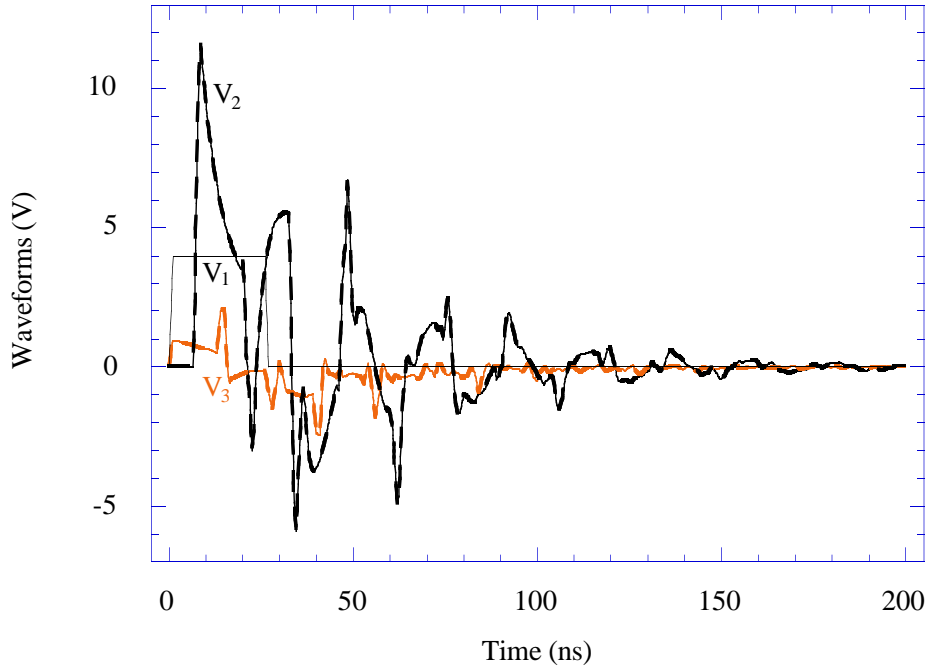
(a)

Fig. 4.13. (a) The circuit diagram, and (b) and (c) transient simulation results for a nine-conductor parabolically tapered line. Thin continuous curves show the results obtained with the open-loop model and thick dashed curves show those for the open-loop internal-reflection model.

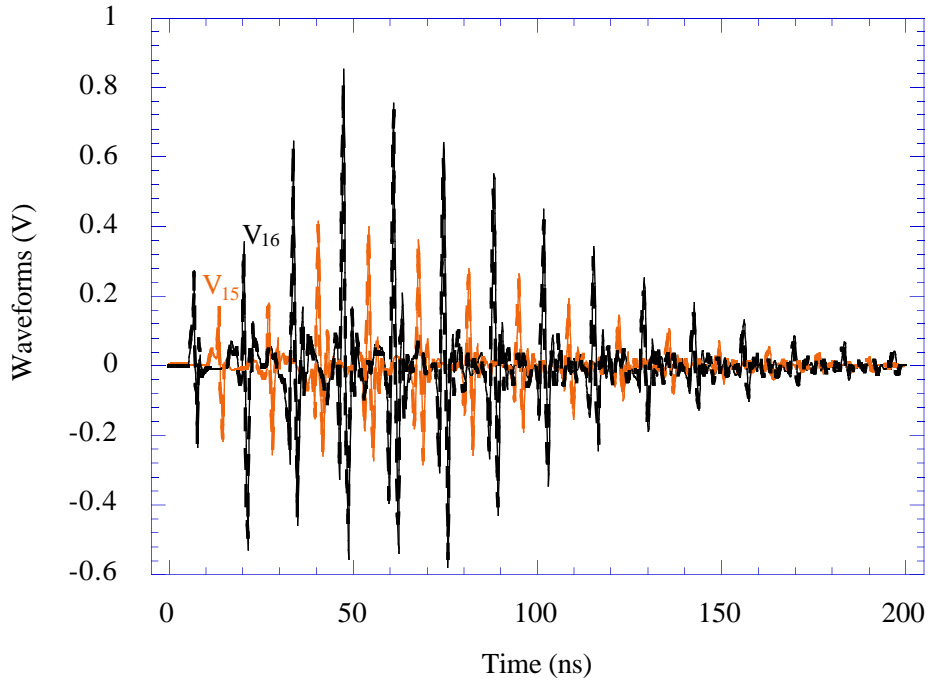
$$\mathbf{G} = \begin{bmatrix} 609 & 141.9 & 23.23 & 4.17 & 0.829 & 0.2186 & 0.0355 & 0.00693 \\ 141.9 & 600 & 90 & 22.04 & 4.92 & 1.047 & 0.1793 & 0.0397 \\ 23.23 & 90 & 502 & 108.4 & 28.47 & 4.99 & 1.006 & 0.2256 \\ 4.17 & 22.04 & 108.4 & 715 & 106.5 & 21.83 & 4.28 & 0.713 \\ 0.829 & 4.92 & 28.47 & 106.5 & 684 & 92.7 & 18.27 & 3.96 \\ 0.2186 & 1.047 & 4.99 & 21.83 & 92.7 & 569 & 130.9 & 23.59 \\ 0.0355 & 0.1793 & 1.006 & 4.28 & 18.27 & 130.9 & 485 & 91.6 \\ 0.00693 & 0.0397 & 0.2256 & 0.713 & 3.96 & 23.59 & 91.6 & 479 \end{bmatrix} \frac{\mu\text{S}}{\text{m}}$$

In both examples, a 7th-order real-pole approximation was used for the open-loop model, and a 17th-order complex-pole approximation was used for the open-loop internal-reflection model.

Because of the higher-order approximation and a larger number of dynamic modules, the difference approximation and numerical integration execution times for nonuniform lines are larger than those for uniform lines. The total simulation time, however, is dominated by the circuit solution time, and remains virtually the same. The runtime comparisons for circuits of various sizes and types can be found in [14]. The runtime data in [14] were obtained with the open-loop nonuniform line model.



(b)



(c)

Fig. 4.13 continued.

4.6. Conclusions

From a novel analysis, based on identification of the most significant aspects of the problem and comparison of alternative approaches in each of the aspects, it was shown that to achieve maximum efficiency, accuracy, and practical applicability the line simulation should be based on time-only formulation, open-loop characterization, a device model that does not require the introduction of current variables, indirect numerical integration, and frequency-domain difference approximation based on interpolation and matrix delay separation.

The practical implementation of the optimal method for uniform and nonuniform multiconductor lossy frequency-dependent lines characterized by discrete samples of their responses was outlined, including extraction of initial conditions from op analysis and the line model for ac/dc analysis. The complete set of expressions for the open-loop transmission line functions was given, including new formulas for the matrix delay separation from the propagation functions, which avoid the use of frequency-dependent modal transformation matrices. The complete set of analytical expressions for the fundamental open-loop time-domain responses of two-conductor uniform lines was presented, including a new simple and accurate asymptotic approximation for the responses of propagation function. The novel interpolation-based complex rational approximation method was extended to the matrix form, and suitable ramp- and step-invariant indirect numerical formulas were reviewed.

It was shown on an extensive set of run-time data that, based on the optimal approach, accurate line modeling in a circuit simulator is as efficient as simple replacement of interconnects with lumped resistors. The method is compatible with recursive time-domain solvers employed by circuit simulators and supports variable time-stepping. The method has been adopted in several industrial and commercial circuit simulators and in numerous real-life simulation exercises proved to be reliable and accurate.

The novel open-loop and open-loop internal-reflection models for nonuniform lines were presented. The open-loop model for nonuniform lines results in the simplest aperiodic responses (similar to those for uniform lines), which can be accurately represented by a few samples and a low-order interpolation with only real poles. The model, however, does not guarantee stability of the line characterization. The open-loop internal-reflection model provides the simplest stable characterization, which is, however, more complex than the open-loop characterization and requires a higher-order approximation with complex poles.

5. CONCLUSIONS

This dissertation discussed indirect numerical integration, difference approximation, and circuit simulation of transmission lines.

Indirect numerical integration is a new class of numerical integration methods based on the novel time-response invariant discrete synthesis. While offering the ideal accuracy, convergence and stability properties, the discrete-time difference equations obtained via indirect numerical integration differ from those obtained via the conventional numerical integration methods only in the values of the coefficients, and, in many cases, can replace the latter to efficiently perform transient simulation of dynamic circuits and systems in exactly the same manner.

The foundations of indirect numerical integration and its general principles were discussed in detail. The complete set of the step- and ramp-invariant indirect numerical integration formulas is presented in Appendix A.

The difference approximation is a general method for applying numerical integration to systems whose differential equations are not known. The general principles of time- and frequency-domain difference approximation were analyzed, including the fundamental possibility of the approximation, three canonic forms of the state-variable representation, complex-to-real mapping, magnitude, real- and imaginary-part approximations, and approximation of multiport systems. A novel matrix delay separation technique was introduced, which avoids the use of frequency-dependent eigenvector matrices. The complete set of indirect numerical integration formulas for time- and frequency-domain difference approximation was given in matrix form for multiport systems with an arbitrary number of inputs and outputs, and in the three canonic forms of the state variable representation.

Various approximation methods were compared, and novel interpolation-based methods were introduced. The relaxation interpolation method is applicable for low-order time- and frequency-domain real-pole approximation of aperiodic systems. The direct interpolation-based method performs frequency-domain complex-pole approximation of an arbitrary number of

arbitrarily spaced complex samples. The method averages out the noise in measured data and fits both real and imaginary parts of the original function at once. The method proceeds in two steps. First, the poles of the system are extracted with the method of averages, and then the partial expansion coefficients are adjusted via least-square approximation. The complexity of the method is that of two linear solutions and one polynomial factoring. The order of the linear systems and polynomial depend only on the order of the approximation and not on the number of samples. Both approximation methods can fit the initial and final values of the original response exactly, impose constraints on the poles, and, in numerous real-life simulation exercises, proved to be reliable, accurate and efficient.

Finally, the indirect numerical integration and difference approximation were applied to the circuit simulation of transmission lines. From a novel analysis, based on identification of the most significant aspects of the problem and comparison of alternative approaches in each of the aspects, it was shown that to achieve maximum efficiency, accuracy and practical applicability the line simulation should be based on time-only formulation, open-loop characterization, a device model that does not require the introduction of current variables, indirect numerical integration, and frequency-domain difference approximation based on interpolation and matrix delay separation.

The practical implementation of the optimal method for multiconductor lossy frequency-dependent lines characterized by discrete samples of their responses was outlined, including extraction of initial conditions from op analysis and the line model for ac/dc analysis. The complete set of expressions for the open-loop transmission line functions was given, including new formulas for the matrix delay separation from the propagation functions, which avoid the use of frequency-dependent modal transformation matrices. The complete set of analytical expressions for the fundamental open-loop time-domain responses of two-conductor lines was presented, including a new simple and accurate asymptotic approximation for the responses of the propagation function.

It was shown on an extensive set of run-time data that, based on the optimal approach, accurate line modeling in a circuit simulator is as efficient as simple replacement of interconnects with lumped resistors. The method is compatible with recursive time-domain solvers employed by circuit simulators and supports variable time-stepping. The method has been adopted in several industrial and commercial circuit simulators, and, in numerous real-life simulation exercises, proved to be reliable and accurate.

The novel open-loop and open-loop internal-reflection models for nonuniform lines were presented. The open-loop model for nonuniform lines results in the simplest, aperiodic responses (similar to those for uniform lines), which can be accurately represented by a few samples and a low-order interpolation with only real poles. The model, however, does not guarantee stability of

the line characterization. The open-loop internal-reflection model provides the simplest stable characterization, which is, however, more complex than the open-loop characterization and requires a higher-order approximation with complex poles.

APPENDIX A. INDIRECT NUMERICAL INTEGRATION FORMULAS

A.1. Canonic and Parallel Canonic Forms

Table A.1 presents the set of step- and ramp-invariant indirect numerical integration formulas in the canonic and parallel canonic forms. The formulas are in matrix form for arbitrary-order multiport systems with arbitrarily numbers of inputs and outputs. The ramp-invariant formulas are given in two forms: with equalized present- and past-time coefficients of the excitation, and with zero present-time coefficient. The latter form is more suitable for modeling of immittances.

TABLE A.1
CANONIC AND PARALLEL CANONIC FORMS OF INDIRECT NUMERICAL INTEGRATION
FORMULAS

	Canonic Form ^a	Parallel Canonic Form ^b
Transfer function, $\mathbf{H}(s)$	$\mathbf{U}^T (s\mathbf{I} - \Omega)^{-1} \mathbf{C} + \mathbf{H}_\infty$	$\mathbf{H}_\infty + \sum_{m=1}^M \frac{1}{1 + s/\omega_{cm}} \mathbf{A}_m$
State equations	$\begin{cases} \mathbf{y}(t) = \mathbf{U}^T \mathbf{z}(t) + \mathbf{H}_\infty \mathbf{x}(t) \\ \dot{\mathbf{z}}(t) = \Omega \mathbf{z}(t) + \mathbf{C} \mathbf{x}(t) \end{cases}$	$\begin{cases} \mathbf{y}(t) = \mathbf{H}_\infty \mathbf{x}(t) + \sum_{m=1}^M \mathbf{z}_m(t) \\ \frac{1}{\omega_{cm}} \dot{\mathbf{z}}_m(t) + \mathbf{z}_m(t) = \mathbf{A}_m \mathbf{x}(t), \quad m = 1, 2, \dots, M \end{cases}$
Impulse characteristic ^c , $\mathbf{g}(t)$	$\mathbf{H}_\infty \delta(t) + \mathbf{U}^T \mathbf{F}(t) \mathbf{C} \, 1(t)$, where $\mathbf{F}(t) = \mathbf{e}^{\Omega t}$	$\mathbf{H}_\infty \delta(t) + \sum_{m=1}^M \omega_{cm} e^{-\omega_{cm} t} \mathbf{A}_m \, 1(t)$
Transient characteristic ^d , $\mathbf{h}(t)$	$(\mathbf{H}_\infty + \mathbf{U}^T \Omega^{-1} (\mathbf{F}(t) - \mathbf{I}) \mathbf{C}) \, 1(t)$	$\left(\mathbf{H}_0 - \sum_{m=1}^M e^{-\omega_{cm} t} \mathbf{A}_m \right) \, 1(t)$, where $\mathbf{H}_0 = \mathbf{H}_\infty + \sum_{m=1}^M \mathbf{A}_m$
Ramp response, $\mathbf{r}(t)$	$(\mathbf{H}_\infty t + \mathbf{U}^T \Omega^{-2} (\mathbf{F}(t) - \Omega t - \mathbf{I}) \mathbf{C}) \, 1(t)$	$\left(\mathbf{H}_0 t - \sum_{m=1}^M \frac{1 - e^{-\omega_{cm} t}}{\omega_{cm}} \mathbf{A}_m \right) \, 1(t)$
Step-invariant difference model	$\begin{cases} \mathbf{z}_n = \mathbf{F}(T_n) \mathbf{z}_{n-1} + \Omega^{-1} (\mathbf{F}(T_n) - \mathbf{I}) \mathbf{C} \mathbf{x}_{n-1} \\ \mathbf{y}_n = \mathbf{U}^T \mathbf{z}_n + \mathbf{H}_\infty \mathbf{x}_n \end{cases}$	$\begin{cases} \mathbf{z}_{m,n} = (1 - e^{-\omega_{cm} T_n}) \mathbf{A}_m \mathbf{x}_{n-1} + e^{-\omega_{cm} T_n} \mathbf{z}_{m,n-1}, \quad m = 1, 2, \dots, M \\ \mathbf{y}_n = \mathbf{H}_\infty \mathbf{x}_n + \sum_{m=1}^M \mathbf{z}_{m,n} \end{cases}$
Ramp-invariant difference model with equalized coefficients	$\begin{cases} \hat{\mathbf{z}}_n = \mathbf{F}(T_n) \hat{\mathbf{z}}_{n-1} + \mathbf{D}(T_n) (\mathbf{x}_n - \mathbf{x}_{n-1}) \\ \mathbf{y}_n = \mathbf{U}^T \hat{\mathbf{z}}_n + \mathbf{H}_0 \mathbf{x}_n \end{cases}$ where $\mathbf{H}_0 = \mathbf{H}_\infty - \mathbf{U}^T \Omega^{-1} \mathbf{C}$, $\mathbf{D}(T_n) = \frac{1}{T_n} \Omega^{-2} (\mathbf{F}(T_n) - \mathbf{I}) \mathbf{C}$	$\begin{cases} \hat{\mathbf{z}}_{m,n} = \mathbf{D}_m(T_n) (\mathbf{x}_n - \mathbf{x}_{n-1}) + e^{-\omega_{cm} T_n} \hat{\mathbf{z}}_{m,n-1}, \quad m = 1, 2, \dots, M \\ \mathbf{y}_n = \mathbf{H}_0 \mathbf{x}_n - \sum_{m=1}^M \hat{\mathbf{z}}_{m,n} \end{cases}$ where $\mathbf{D}_m(T_n) = \frac{1 - e^{-\omega_{cm} T_n}}{\omega_{cm} T_n} \mathbf{A}_m$
Ramp-invariant difference model with zero present-time coefficients	$\begin{cases} \tilde{\mathbf{z}}_n = \mathbf{F}(T_n) \tilde{\mathbf{z}}_{n-1} + (\mathbf{F}(T_n) \mathbf{D}(T_{n-1}) - \mathbf{D}(T_n)) \mathbf{x}_{n-1} \\ \mathbf{y}_n = \mathbf{U}^T \tilde{\mathbf{z}}_n + (\mathbf{H}_0 + \mathbf{U}^T \mathbf{D}(T_n)) \mathbf{x}_n \end{cases}$	$\begin{cases} \tilde{\mathbf{z}}_{m,n} = (e^{-\omega_{cm} T_n} \mathbf{D}_m(T_{n-1}) - \mathbf{D}_m(T_n)) \mathbf{x}_{n-1} + e^{-\omega_{cm} T_n} \tilde{\mathbf{z}}_{m,n-1}, \quad m = 1, 2, \dots, M \\ \mathbf{y}_n = \left(\mathbf{H}_0 - \sum_{m=1}^M \mathbf{D}_m(T_n) \right) \mathbf{x}_n - \sum_{m=1}^M \tilde{\mathbf{z}}_{m,n} \end{cases}$

Note : $\mathbf{x}(t)$ is the excitation, $\mathbf{y}(t)$ is the response, $\mathbf{z}(t)$ is the system state vector, $\dot{\mathbf{z}}(t) = d\mathbf{z}(t)/dt$, M is the order of the system, \mathbf{H}_0 and \mathbf{H}_∞ are the initial and final values of the transfer function, $T_n = t_n - t_{n-1}$ is the time step, and $1(t)$ is the unit-step function.

^a Ω is the system matrix, \mathbf{C} is the control matrix, \mathbf{U} is the observation matrix, and $\mathbf{F}(t)$ is the fundamental matrix [3]. The boldface $\mathbf{e}^{\Omega t}$ stands for the matrix exponential.

^b The system poles, $-\omega_{cm}$, and partial expansion coefficients, \mathbf{A}_m , can be either real or occur in complex-conjugate pairs.

^c The δ -impulse response.

^d The unit-step response.

A.2. Cascade Canonic Form

The transfer function

$$H(s) = H_0 \prod_{m=1}^M \frac{1 + s/\omega_{pm}}{1 + s/\omega_{cm}},$$

where the system poles, $-\omega_{cm}$, and zeros, $-\omega_{pm}$, can either be real or occur in complex-conjugate pairs.

The state equations are

$$\begin{cases} y(t) = H_0 z_M(t) \\ \frac{1}{\omega_{cm}} \dot{z}_m(t) + z_m(t) = \frac{1}{\omega_{pm}} \dot{z}_{m-1}(t) + z_{m-1}(t), \quad m = 1, 2, \dots, M \\ z_0(t) = x(t). \end{cases}$$

The difference model is

$$\begin{cases} z_{0,n} = x_n \\ z_{m,n} = a_m(T_n) z_{m-1,n} + b_m(T_n) z_{m-1,n-1} + e^{-\omega_{cm} T_n} z_{m,n-1}, \quad m = 1, 2, \dots, M \\ y_n = H_0 z_{M,n}, \end{cases}$$

where for the step invariance

$$a_m(T_n) = \frac{\omega_{cm}}{\omega_{pm}},$$

$$b_m(T_n) = 1 - \frac{\omega_{cm}}{\omega_{pm}} - e^{-\omega_{cm} T_n},$$

and for the ramp invariance

$$a_m(T_n) = 1 + \frac{1}{T_n} \left(\frac{1}{\omega_{pm}} - \frac{1}{\omega_{cm}} \right) (1 - e^{-\omega_{cm} T_n}),$$

$$b_m(T_n) = -e^{-\omega_{cm} T_n} - \frac{1}{T_n} \left(\frac{1}{\omega_{pm}} - \frac{1}{\omega_{cm}} \right) (1 - e^{-\omega_{cm} T_n}).$$

APPENDIX B. OPEN-LOOP TRANSMISSION-LINE TRANSFER FUNCTIONS

Table B.1 presents a set of frequency-domain expressions for the open-loop transmission-line functions for voltage and current waves in terms of the $\mathbf{R}(\omega)$, $\mathbf{L}(\omega)$, $\mathbf{G}(\omega)$ and $\mathbf{C}(\omega)$ distributed-parameter matrices. The expressions are given in both standard and modal bases. The table also contains the matrix delay separation formulas.

TABLE B.1
OPEN-LOOP TRANSMISSION-LINE TRANSFER FUNCTIONS

Name of Function	Function for Current Waves ^a		Function for Voltage Waves ^a	
	In Standard Basis	In Modal Basis	In Standard Basis	In Modal Basis
Admittance and impedance per unit length	$\mathbf{Y}(\omega) = \mathbf{G}(\omega) + j\omega\mathbf{C}(\omega)$ $= \mathbf{M}_I(\omega) \mathbf{Y}_m(\omega) \mathbf{M}_V^{-1}(\omega)$	$\mathbf{Y}_m(\omega)$ $= \mathbf{M}_I^{-1}(\omega) \mathbf{Y}(\omega) \mathbf{M}_V(\omega)$	$\mathbf{Z}(\omega) = \mathbf{R}(\omega) + j\omega\mathbf{L}(\omega)$ $= \mathbf{M}_V(\omega) \mathbf{Z}_m(\omega) \mathbf{M}_I^{-1}(\omega)$	$\mathbf{Z}_m(\omega)$ $= \mathbf{M}_V^{-1}(\omega) \mathbf{Z}(\omega) \mathbf{M}_I(\omega)$
Modal transformation matrices	$\mathbf{M}_I(\omega)$ $= \text{Eigenvectors}(\mathbf{Y}(\omega) \mathbf{Z}(\omega))$ $\hat{\mathbf{M}}_I = \mathbf{M}_I(\infty)$ $= \text{Eigenvectors}(\mathbf{C}(\infty) \mathbf{L}(\infty))$	$\mathbf{M}_I^{-1}(\omega) = \mathbf{M}_V^T(\omega)$, $\hat{\mathbf{M}}_I^{-1} = \hat{\mathbf{M}}_V^T$	$\mathbf{M}_V(\omega)$ $= \text{Eigenvectors}(\mathbf{Z}(\omega) \mathbf{Y}(\omega))$ $\hat{\mathbf{M}}_V = \mathbf{M}_V(\infty)$ $= \text{Eigenvectors}(\mathbf{L}(\infty) \mathbf{C}(\infty))$	$\mathbf{M}_V^{-1}(\omega) = \mathbf{M}_I^T(\omega)$, $\hat{\mathbf{M}}_V^{-1} = \hat{\mathbf{M}}_I^T$
Characteristic admittance and impedance	$\mathbf{Y}_c(\omega) = \mathbf{K}_I(\omega) \mathbf{Z}^{-1}(\omega)$ $= \mathbf{K}_I^{-1}(\omega) \mathbf{Y}(\omega) = \mathbf{Z}_c^{-1}(\omega)$ $= \mathbf{M}_I(\omega) \mathbf{Y}_{cm}(\omega) \mathbf{M}_V^{-1}(\omega)$	$\mathbf{Y}_{cm}(\omega) = (\mathbf{Z}_m^{-1}(\omega) \mathbf{Y}_m(\omega))^{\frac{1}{2}}$ $= \mathbf{K}_{Im}^{-1}(\omega) \mathbf{Y}_m(\omega) = \mathbf{Z}_{cm}^{-1}(\omega)$ $= \mathbf{M}_I^{-1}(\omega) \mathbf{Y}_c(\omega) \mathbf{M}_V(\omega)$	$\mathbf{Z}_c(\omega) = \mathbf{K}_V(\omega) \mathbf{Y}^{-1}(\omega)$ $= \mathbf{K}_V^{-1}(\omega) \mathbf{Z}(\omega) = \mathbf{Y}_c^{-1}(\omega)$ $= \mathbf{M}_V(\omega) \mathbf{Z}_{cm}(\omega) \mathbf{M}_I^{-1}(\omega)$	$\mathbf{Z}_{cm}(\omega) = (\mathbf{Y}_m^{-1}(\omega) \mathbf{Z}_m(\omega))^{\frac{1}{2}}$ $= \mathbf{K}_{Vm}^{-1}(\omega) \mathbf{Z}_m(\omega) = \mathbf{Y}_{cm}^{-1}(\omega)$ $= \mathbf{M}_V^{-1}(\omega) \mathbf{Z}_c(\omega) \mathbf{M}_I(\omega)$
Propagation constant ^b	$\mathbf{K}_I(\omega) = (\mathbf{Y}(\omega) \mathbf{Z}(\omega))^{\frac{1}{2}}$ $= \mathbf{Y}(\omega) \mathbf{Y}_c^{-1}(\omega)$ $= \mathbf{M}_I(\omega) \mathbf{K}_{Im}(\omega) \mathbf{M}_I^{-1}(\omega)$	$\mathbf{K}_{Im}(\omega) = (\mathbf{Y}_m(\omega) \mathbf{Z}_m(\omega))^{\frac{1}{2}}$ $= \mathbf{Y}_m(\omega) \mathbf{Y}_{cm}^{-1}(\omega)$ $= \text{Eigenvalues}(\mathbf{K}_I(\omega))$ $= \mathbf{M}_I^{-1}(\omega) \mathbf{K}_I(\omega) \mathbf{M}_I(\omega)$ $= \mathbf{K}_{Vm}(\omega)$	$\mathbf{K}_V(\omega) = (\mathbf{Z}(\omega) \mathbf{Y}(\omega))^{\frac{1}{2}}$ $= \mathbf{Z}(\omega) \mathbf{Z}_c^{-1}(\omega)$ $= \mathbf{M}_V(\omega) \mathbf{K}_m(\omega) \mathbf{M}_V^{-1}(\omega)$	$\mathbf{K}_{Vm}(\omega) = (\mathbf{Z}_m(\omega) \mathbf{Y}_m(\omega))^{\frac{1}{2}}$ $= \mathbf{Z}_m(\omega) \mathbf{Z}_{cm}^{-1}(\omega)$ $= \text{Eigenvalues}(\mathbf{K}_V(\omega))$ $= \mathbf{M}_V^{-1}(\omega) \mathbf{K}_V(\omega) \mathbf{M}_V(\omega) =$ $= \mathbf{K}_{Im}(\omega)$
Propagation delay ^b	$T_I = (\mathbf{C}(\infty) \mathbf{L}(\infty))^{\frac{1}{2}} l$ $= \mathbf{K}_I(\infty) l = \hat{\mathbf{M}}_I T_{Im} \hat{\mathbf{M}}_I^{-1}$	$T_{Im} = \mathbf{K}_{Im}(\infty) l$ $= \text{Eigenvalues}(T_I)$ $= \hat{\mathbf{M}}_I^{-1} T_I \hat{\mathbf{M}}_I = T_{Vm}$	$T_V = (\mathbf{L}(\infty) \mathbf{C}(\infty))^{\frac{1}{2}} l$ $= \mathbf{K}_V(\infty) l = \hat{\mathbf{M}}_V T_{Vm} \hat{\mathbf{M}}_V^{-1}$	$T_{Vm} = \mathbf{K}_{Vm}(\infty) l$ $= \text{Eigenvalues}(T_V)$ $= \hat{\mathbf{M}}_V^{-1} T_V \hat{\mathbf{M}}_V = T_{Im}$
Propagation function ^b	$\mathbf{W}_I(\omega) = e^{-\mathbf{K}_I(\omega) l}$ $= \mathbf{M}_I(\omega) \mathbf{W}_{Im}(\omega) \mathbf{M}_I^{-1}(\omega)$ $= \mathbf{Y}_c(\omega) \mathbf{W}_V(\omega) \mathbf{Z}_c(\omega)$ $= \hat{\mathbf{W}}_I(\omega) e^{-j\omega T_I}$ $= \hat{\mathbf{W}}_I(\omega) \hat{\mathbf{M}}_I e^{-j\omega T_{Im}} \hat{\mathbf{M}}_I^{-1}$	$\mathbf{W}_{Im}(\omega) = e^{-\mathbf{K}_{Im}(\omega) l}$ $= \mathbf{M}_I^{-1}(\omega) \mathbf{W}_I(\omega) \mathbf{M}_I(\omega)$ $= \mathbf{W}_{Vm}(\omega)$	$\mathbf{W}_V(\omega) = e^{-\mathbf{K}_V(\omega) l}$ $= \mathbf{M}_V(\omega) \mathbf{W}_{Vm}(\omega) \mathbf{M}_V^{-1}(\omega)$ $= \mathbf{Z}_c(\omega) \mathbf{W}_I(\omega) \mathbf{Y}_c(\omega)$ $= \hat{\mathbf{W}}_V(\omega) e^{-j\omega T_V}$ $= \hat{\mathbf{W}}_V(\omega) \hat{\mathbf{M}}_V e^{-j\omega T_{Vm}} \hat{\mathbf{M}}_V^{-1}$	$\mathbf{W}_{Vm}(\omega) = e^{-\mathbf{K}_{Vm}(\omega) l}$ $= \mathbf{M}_V^{-1}(\omega) \mathbf{W}_V(\omega) \mathbf{M}_V(\omega)$ $= \mathbf{W}_{Im}(\omega)$
Delayless propagation function ^b	$\hat{\mathbf{W}}_I(\omega) = \mathbf{W}_I(\omega) e^{j\omega T_I}$		$\hat{\mathbf{W}}_V(\omega) = \mathbf{W}_V(\omega) e^{j\omega T_V}$	
Transmission coefficient ^c	$\mathbf{T}_I(\omega) = (\mathbf{I} + \mathbf{Y}_t(\omega) \mathbf{Z}_c(\omega))^{-1}$ $= \mathbf{Y}_c(\omega) \mathbf{T}_V(\omega) \mathbf{Z}_t(\omega)$		$\mathbf{T}_V(\omega) = (\mathbf{I} + \mathbf{Z}_t(\omega) \mathbf{Y}_c(\omega))^{-1}$ $= \mathbf{Z}_c(\omega) \mathbf{T}_I(\omega) \mathbf{Y}_t(\omega)$	
Reflection coefficient ^c	$\Gamma_I(\omega) = (\mathbf{I} + \mathbf{Y}_t(\omega) \mathbf{Z}_c(\omega))^{-1}$ $\cdot (\mathbf{I} - \mathbf{Y}_t(\omega) \mathbf{Z}_c(\omega))$ $= \mathbf{Y}_c(\omega) \Gamma_V(\omega) \mathbf{Z}_c(\omega)$		$\Gamma_V(\omega) = (\mathbf{Z}_t(\omega) \mathbf{Y}_c(\omega) + \mathbf{I})^{-1}$ $\cdot (\mathbf{Z}_t(\omega) \mathbf{Y}_c(\omega) - \mathbf{I})$ $= \mathbf{Z}_c(\omega) \Gamma_I(\omega) \mathbf{Y}_c(\omega)$	

^a Voltage and current functions are related via the following duality replacement rules: $\mathbf{V} \leftrightarrow \mathbf{I}$, $\mathbf{Z} \leftrightarrow \mathbf{Y}$, $\mathbf{R} \leftrightarrow \mathbf{G}$, $\mathbf{L} \leftrightarrow \mathbf{C}$.

^b Boldface $(\cdot)^{\frac{1}{2}}$ and $e^{(\cdot)}$ denote matrix square root and matrix exponential, respectively.

^c For a Thevenin's termination $\mathbf{Z}_t(\omega)$.

APPENDIX C. FUNDAMENTAL TIME-DOMAIN OPEN-LOOP RESPONSES OF TWO-CONDUCTOR LINES

Table C.1 presents a set of expressions for the transient characteristics (unit-step responses) and impulse characteristics (δ -impulse responses) corresponding to the open-loop transmission-line transfer functions. The expressions are for two-conductor constant-parameter lossy lines. The table also gives simple and accurate approximate expressions for the responses of propagation functions with $G=0$. The expressions are based on the asymptotic approximation of the modified Bessel function, and are within 1% accurate within the full time range from zero to infinity.

TABLE C.1
FUNDAMENTAL TIME-DOMAIN OPEN-LOOP RESPONSES OF TWO-CONDUCTOR LINES

Name of Function	G	Transient Characteristic, $h(t)$	Impulse Characteristic, $g(t)$
Propagation function, $W(\omega)^a$	Arbitrary G	$h_w(t) = \left(e^{-\alpha} + a \int_{\tau}^t e^{-\beta t} \frac{I_1(b \sqrt{t^2 - \tau^2})}{\sqrt{t^2 - \tau^2}} dt \right) u(t - \tau)$	$g_w(t) = e^{-\alpha} \delta(t) + a e^{-\beta t} \frac{I_1(b \sqrt{t^2 - \tau^2})}{\sqrt{t^2 - \tau^2}} u(t - \tau)$
	$G = 0$	$h_w(t) \approx \left(1 - \frac{2a}{\sqrt{2\pi b(t+d)}} \right) u(t - \tau)^b$	$g_w(t) \approx e^{-\alpha} \delta(t) + \frac{a}{(2\pi b(t+d))^{3/2}} u(t - \tau)^b$
Characteristic admittance, $Y_c(\omega)^c$	Arbitrary G	$h_y(t) = Y_0 \left(e^{-\beta t} I_0(bt) + \frac{G}{C} \int_0^t e^{\beta \tau} I_0(b\tau) d\tau \right)$	$g_y(t) = Y_0 \left\{ \delta(t) + e^{-\beta t} \left[\left(\frac{G}{C} - \beta \right) I_0(bt) + b I_1(bt) \right] \right\}$
	$G = 0$	$h_y(t) = Y_0 e^{-\beta t} I_0(\beta t)$	$g_y(t) = Y_0 \left\{ \delta(t) + \beta e^{-\beta t} [I_1(\beta t) - I_0(\beta t)] \right\}$
Transmission coefficient for voltage waves, $T_v(\omega)^c, d$	Arbitrary G	$h_r(t) = \frac{Z_0}{R_t - Z_0} \left\{ -Z_0 \left[\frac{R}{cL} + \left(1 - \frac{R}{cL} \right) e^{-ct} \right] + R_t \left[e^{-\beta t} I_0(bt) + (2\beta - c) e^{-ct} \int_0^t e^{-\beta - c\tau} I_0(b\tau) d\tau + \frac{RG}{LC} \int_{\tau=0}^t e^{-c\tau} \int_{\tau=0}^{\tau} e^{-\beta - c\tau'} I_0(b\tau) d\tau d\tau' \right] \right\}$	$g_r(t) = \frac{Z_0}{R_t + Z_0} \delta(t) + \frac{Z_0}{R_t - Z_0} \left\{ Z_0 \left(c - \frac{R}{L} \right) e^{-ct} + R_t \left[e^{-\beta t} [(\beta - c) I_0(bt) + b I_1(bt)] + \left(c(c - 2\beta) + \frac{RG}{LC} \right) e^{-ct} \int_0^t e^{-\beta - c\tau} I_0(b\tau) d\tau \right] \right\}$
	$G = 0$	$h_r(t) = \frac{Z_0}{R_t - Z_0} \left\{ -Z_0 \left[\frac{R}{cL} + \left(1 - \frac{R}{cL} \right) e^{-ct} \right] + R_t \left[e^{-\beta t} I_0(bt) + (2\beta - c) e^{-ct} \int_0^t e^{-\beta - c\tau} I_0(b\tau) d\tau \right] \right\}$	$g_r(t) = \frac{Z_0}{R_t + Z_0} \delta(t) + \frac{Z_0}{R_t - Z_0} \left\{ Z_0 \left(c - \frac{R}{L} \right) e^{-ct} + R_t \left[e^{-\beta t} [(\beta - c) I_0(bt) + b I_1(bt)] + c(c - 2\beta) e^{-ct} \int_0^t e^{-\beta - c\tau} I_0(b\tau) d\tau \right] \right\}$
Reflection coefficient, $\Gamma(\omega)^d$		$h_r(t) = 1 - 2h_f(t)$	$g_r(t) = \delta(t) - 2g_f(t)$

Note: $u(t)$ is the unit-step function, $\alpha = \frac{1}{2} \left(GZ_0 + \frac{R}{Z_0} \right) l$, $a = \frac{1}{2} \left| GZ_0 - \frac{R}{Z_0} \right| l$, $\beta = \frac{1}{2} \left(\frac{G}{C} + \frac{R}{L} \right)$, $b = \frac{1}{2} \left| \frac{G}{C} - \frac{R}{L} \right|$, $c = -\frac{R}{L} \frac{Z_0^2}{R_t - Z_0}$, $d = \frac{4a^2}{2\pi b(1 - e^{-a})^2}$, $\tau = \sqrt{CL} l$, $Y_0 = \sqrt{\frac{C}{L}}$, and $Z_0 = \sqrt{\frac{L}{C}}$. For $G = 0$: $\alpha = a = \frac{Rl}{2Z_0}$ and $\beta = b = \frac{R}{2L}$.

^a In the case of two-conductor lines, these functions are the same for both voltage and current waves.

^b Approximation based on the asymptotic expansion of the modified Bessel function $I_1(x)$. The accuracy is within 1% in the full time range.

^c Expressions for the corresponding dual (voltage/current) functions can be obtained via the duality replacement rules (see Appendix B).

^d For a Thevenin's termination R_t .

APPENDIX D. OPEN-LOOP TRANSFER FUNCTIONS OF PARABOLICALLY TAPERED LINES

Table D.1 gives frequency-domain expressions for the open-loop functions of Parabolically tapered multiconductor lines: $\mathbf{Z}(x, \omega) = (1 + ax)^2 \mathbf{Z}(\omega)$, $\mathbf{Y}(x, \omega) = (1 + ax)^{-2} \mathbf{Y}(\omega)$. The expressions are given the open-loop functions for both voltage and current waves. The table also contains the matrix delay separation formulas.

TABLE D.1
OPEN-LOOP TRANSFER FUNCTIONS OF PARABOLICALLY TAPERED LINES

Name of Function	Function for Current Waves	Function for Voltage Waves
Immittance per unit length	$\mathbf{Y}(\omega) = \mathbf{G}(\omega) + j\omega \mathbf{C}(\omega)$	$\mathbf{Z}(\omega) = \mathbf{R}(\omega) + j\omega \mathbf{L}(\omega)$
Propagation constant	$\mathbf{K}_1(\omega) = \mathbf{Y}(\omega)\mathbf{K}_V(\omega)\mathbf{Y}^{-1}(\omega) = [\mathbf{Y}(\omega) \mathbf{Z}(\omega)]^{\frac{1}{2}}$	$\mathbf{K}_V(\omega) = \mathbf{Z}(\omega)\mathbf{K}_1(\omega)\mathbf{Z}^{-1}(\omega) = [\mathbf{Z}(\omega) \mathbf{Y}(\omega)]^{\frac{1}{2}}$
Propagation delay	$T_1 = [\mathbf{C}(\infty) \mathbf{L}(\infty)]^{\frac{1}{2}} l$	$T_V = [\mathbf{L}(\infty) \mathbf{C}(\infty)]^{\frac{1}{2}} l$
Propagation function	$\mathbf{W}_{f1}(\omega) = \mathbf{Y}_{r2}(\omega) \mathbf{W}_{v1}(\omega) \mathbf{Z}_{r1}(\omega) = \hat{\mathbf{W}}_{f1}(\omega) e^{-j\omega T_1}$ $= \frac{1}{1+al} e^{-\mathbf{K}_1(\omega) l},$ $\mathbf{W}_{b1}(\omega) = \mathbf{Y}_{b1}(\omega) \mathbf{W}_{v2}(\omega) \mathbf{Z}_{b2}(\omega) = \hat{\mathbf{W}}_{b1}(\omega) e^{-j\omega T_1}$ $= (1+al) e^{-\mathbf{K}_1(\omega) l}$	$\mathbf{W}_{v1}(\omega) = \mathbf{Z}_{r2}(\omega) \mathbf{W}_{f1}(\omega) \mathbf{Y}_{r1}(\omega) = \hat{\mathbf{W}}_{v1}(\omega) e^{-j\omega T_V}$ $= \left[\mathbf{I} + \frac{1+al}{a} \mathbf{K}_V(\omega) \right] \left\{ \left[\mathbf{I} + \frac{1}{a} \mathbf{K}_V(\omega) \right] e^{\mathbf{K}_V(\omega) l} \right\}^{-1},$ $\mathbf{W}_{v2}(\omega) = \mathbf{Z}_{b1}(\omega) \mathbf{W}_{f2}(\omega) \mathbf{Y}_{b2}(\omega) = \hat{\mathbf{W}}_{v2}(\omega) e^{-j\omega T_V}$ $= \left[\mathbf{I} - \frac{1}{a} \mathbf{K}_V(\omega) \right] \left\{ \left[\mathbf{I} - \frac{1+al}{a} \mathbf{K}_V(\omega) \right] e^{\mathbf{K}_V(\omega) l} \right\}^{-1}$
Delayless propagation function	$\hat{\mathbf{W}}_{f1}(\omega) = \mathbf{W}_{f1}(\omega) e^{j\omega T_1}, \quad \hat{\mathbf{W}}_{b1}(\omega) = \mathbf{W}_{b1}(\omega) e^{j\omega T_1}$	$\hat{\mathbf{W}}_{v1}(\omega) = \mathbf{W}_{v1}(\omega) e^{j\omega T_V}, \quad \hat{\mathbf{W}}_{v2}(\omega) = \mathbf{W}_{v2}(\omega) e^{j\omega T_V}$
Characteristic immittance	$\mathbf{Y}_{r1}(\omega) = \mathbf{Z}_{r1}^{-1}(\omega) = (\mathbf{K}_1(\omega) + a\mathbf{I})^{-1} \mathbf{Y}(\omega),$ $\mathbf{Y}_{b1}(\omega) = \mathbf{Z}_{b1}^{-1}(\omega) = (\mathbf{K}_1(\omega) - a\mathbf{I})^{-1} \mathbf{Y}(\omega),$ $\mathbf{Y}_{r2}(\omega) = \mathbf{Z}_{r2}^{-1}(\omega) = \frac{1}{1+al} [(1+al)\mathbf{K}_1(\omega) + a\mathbf{I}]^{-1} \mathbf{Y}(\omega),$ $\mathbf{Y}_{b2}(\omega) = \mathbf{Z}_{b2}^{-1}(\omega) = \frac{1}{1+al} [(1+al)\mathbf{K}_1(\omega) - a\mathbf{I}]^{-1} \mathbf{Y}(\omega)$	$\mathbf{Z}_{r1}(\omega) = \mathbf{Y}_{r1}^{-1}(\omega) = (\mathbf{K}_V(\omega) + a\mathbf{I}) \mathbf{Y}^{-1}(\omega),$ $\mathbf{Z}_{b1}(\omega) = \mathbf{Y}_{b1}^{-1}(\omega) = (\mathbf{K}_V(\omega) - a\mathbf{I}) \mathbf{Y}^{-1}(\omega),$ $\mathbf{Z}_{r2}(\omega) = \mathbf{Y}_{r2}^{-1}(\omega) = (1+al) [(1+al)\mathbf{K}_V(\omega) + a\mathbf{I}] \mathbf{Y}^{-1}(\omega),$ $\mathbf{Z}_{b2}(\omega) = \mathbf{Y}_{b2}^{-1}(\omega) = (1+al) [(1+al)\mathbf{K}_V(\omega) - a\mathbf{I}] \mathbf{Y}^{-1}(\omega)$

Note: The subscripts “f”, “b”, “V”, “I”, “1” and “2” refer to the forward and backward voltage and current waves at the near and far-end terminals, respectively.

APPENDIX E. EXPRESSIONS FOR OPEN-LOOP INTERNAL-REFLECTION FUNCTIONS IN TERMS OF OPEN-LOOP FUNCTIONS

Table E.1 gives frequency-domain expressions for open-loop internal-reflection transmission-line functions in terms of the open-loop functions. The expressions are for arbitrary nonuniform multiconductor lossy lines. The table gives expressions for the functions for both voltage and current waves.

TABLE E.1
EXPRESSIONS FOR OPEN-LOOP INTERNAL-REFLECTION FUNCTIONS IN TERMS OF OPEN-LOOP
FUNCTIONS

Name of Function	Function for Current Waves	Function for Voltage Waves
Propagation function	$\tilde{\mathbf{W}}_{\text{fr}}(\omega) = \mathbf{Y}_{\text{c}2}(\omega) \tilde{\mathbf{W}}_{\text{vr}}(\omega) \mathbf{Z}_{\text{c}1}(\omega) = \mathbf{T}_{122}(\omega) \mathbf{W}_{\text{fr}}(\omega) \cdot [\mathbf{I} - \Gamma_{112}(\omega) \mathbf{W}_{\text{lb}}(\omega) \Gamma_{122}(\omega) \mathbf{W}_{\text{fr}}(\omega)]^{-1} \mathbf{T}_{111}(\omega),$ $\tilde{\mathbf{W}}_{\text{lb}}(\omega) = \mathbf{Y}_{\text{c}1}(\omega) \tilde{\mathbf{W}}_{\text{vb}}(\omega) \mathbf{Z}_{\text{c}2}(\omega) = \mathbf{T}_{112}(\omega) \mathbf{W}_{\text{lb}}(\omega) \cdot [\mathbf{I} - \Gamma_{122}(\omega) \mathbf{W}_{\text{fr}}(\omega) \Gamma_{112}(\omega) \mathbf{W}_{\text{lb}}(\omega)]^{-1} \mathbf{T}_{121}(\omega)$	$\tilde{\mathbf{W}}_{\text{vr}}(\omega) = \mathbf{Z}_{\text{c}2}(\omega) \tilde{\mathbf{W}}_{\text{fr}}(\omega) \mathbf{Y}_{\text{c}1}(\omega) = \mathbf{T}_{\text{v}22}(\omega) \mathbf{W}_{\text{vr}}(\omega) \cdot [\mathbf{I} - \Gamma_{\text{v}12}(\omega) \mathbf{W}_{\text{vb}}(\omega) \Gamma_{\text{v}22}(\omega) \mathbf{W}_{\text{vr}}(\omega)]^{-1} \mathbf{T}_{\text{v}11}(\omega),$ $\tilde{\mathbf{W}}_{\text{vb}}(\omega) = \mathbf{Z}_{\text{c}1}(\omega) \tilde{\mathbf{W}}_{\text{lb}}(\omega) \mathbf{Y}_{\text{c}2}(\omega) = \mathbf{T}_{\text{v}12}(\omega) \mathbf{W}_{\text{vb}}(\omega) \cdot [\mathbf{I} - \Gamma_{\text{v}22}(\omega) \mathbf{W}_{\text{vr}}(\omega) \Gamma_{\text{v}12}(\omega) \mathbf{W}_{\text{vb}}(\omega)]^{-1} \mathbf{T}_{\text{v}21}(\omega)$
Internal reflection coefficient	$\mathbf{R}_{11}(\omega) = \mathbf{Y}_{\text{c}1}(\omega) \mathbf{R}_{\text{v}1}(\omega) \mathbf{Z}_{\text{c}1}(\omega) = \Gamma_{111}(\omega) + \mathbf{T}_{112}(\omega) \mathbf{W}_{\text{lb}}(\omega) \Gamma_{122}(\omega) \mathbf{W}_{\text{fr}}(\omega) \cdot [\mathbf{I} - \Gamma_{112}(\omega) \mathbf{W}_{\text{lb}}(\omega) \Gamma_{122}(\omega) \mathbf{W}_{\text{fr}}(\omega)]^{-1} \mathbf{T}_{111}(\omega),$ $\mathbf{R}_{12}(\omega) = \mathbf{Y}_{\text{c}2}(\omega) \mathbf{R}_{\text{v}2}(\omega) \mathbf{Z}_{\text{c}2}(\omega) = \Gamma_{121}(\omega) + \mathbf{T}_{122}(\omega) \mathbf{W}_{\text{fr}}(\omega) \Gamma_{112}(\omega) \mathbf{W}_{\text{lb}}(\omega) \cdot [\mathbf{I} - \Gamma_{122}(\omega) \mathbf{W}_{\text{fr}}(\omega) \Gamma_{112}(\omega) \mathbf{W}_{\text{lb}}(\omega)]^{-1} \mathbf{T}_{121}(\omega)$	$\mathbf{R}_{\text{v}1}(\omega) = \mathbf{Z}_{\text{c}1}(\omega) \mathbf{R}_{11}(\omega) \mathbf{Y}_{\text{c}1}(\omega) = \Gamma_{\text{v}11}(\omega) + \mathbf{T}_{\text{v}12}(\omega) \mathbf{W}_{\text{vb}}(\omega) \Gamma_{\text{v}22}(\omega) \mathbf{W}_{\text{vr}}(\omega) \cdot [\mathbf{I} - \Gamma_{\text{v}12}(\omega) \mathbf{W}_{\text{vb}}(\omega) \Gamma_{\text{v}22}(\omega) \mathbf{W}_{\text{vr}}(\omega)]^{-1} \mathbf{T}_{\text{v}11}(\omega),$ $\mathbf{R}_{\text{v}2}(\omega) = \mathbf{Z}_{\text{c}2}(\omega) \mathbf{R}_{12}(\omega) \mathbf{Y}_{\text{c}2}(\omega) = \Gamma_{\text{v}21}(\omega) + \mathbf{T}_{\text{v}22}(\omega) \mathbf{W}_{\text{vr}}(\omega) \Gamma_{\text{v}12}(\omega) \mathbf{W}_{\text{vb}}(\omega) \cdot [\mathbf{I} - \Gamma_{\text{v}22}(\omega) \mathbf{W}_{\text{vr}}(\omega) \Gamma_{\text{v}12}(\omega) \mathbf{W}_{\text{vb}}(\omega)]^{-1} \mathbf{T}_{\text{v}21}(\omega)$
Characteristic immittance	$\mathbf{Y}_{\text{c}1}(\omega) = \mathbf{Z}_{\text{c}1}^{-1}(\omega) = [\mathbf{Y}(0, \omega) \mathbf{Z}(0, \omega)]^{\frac{1}{2}} \mathbf{Z}^{-1}(0, \omega),$ $\mathbf{Y}_{\text{c}2}(\omega) = \mathbf{Z}_{\text{c}2}^{-1}(\omega) = [\mathbf{Y}(l, \omega) \mathbf{Z}(l, \omega)]^{\frac{1}{2}} \mathbf{Z}^{-1}(l, \omega)$	$\mathbf{Z}_{\text{c}1}(\omega) = \mathbf{Y}_{\text{c}1}^{-1}(\omega) = [\mathbf{Z}(0, \omega) \mathbf{Y}(0, \omega)]^{\frac{1}{2}} \mathbf{Y}^{-1}(0, \omega),$ $\mathbf{Z}_{\text{c}2}(\omega) = \mathbf{Y}_{\text{c}2}^{-1}(\omega) = [\mathbf{Z}(l, \omega) \mathbf{Y}(l, \omega)]^{\frac{1}{2}} \mathbf{Y}^{-1}(l, \omega)$
Transmission coefficient	$\mathbf{T}_{111}(\omega) = 2[\mathbf{I} + \mathbf{Y}_{\text{c}1}(\omega) \mathbf{Z}_{\text{r}1}(\omega)]^{-1},$ $\mathbf{T}_{112}(\omega) = [\mathbf{I} + \mathbf{Y}_{\text{r}1}(\omega) \mathbf{Z}_{\text{c}1}(\omega)]^{-1} [\mathbf{I} + \mathbf{Y}_{\text{r}1}(\omega) \mathbf{Z}_{\text{b}1}(\omega)],$ $\mathbf{T}_{121}(\omega) = 2[\mathbf{I} + \mathbf{Y}_{\text{c}2}(\omega) \mathbf{Z}_{\text{b}2}(\omega)]^{-1},$ $\mathbf{T}_{122}(\omega) = [\mathbf{I} + \mathbf{Y}_{\text{b}2}(\omega) \mathbf{Z}_{\text{c}2}(\omega)]^{-1} [\mathbf{I} + \mathbf{Y}_{\text{b}2}(\omega) \mathbf{Z}_{\text{r}2}(\omega)]$	$\mathbf{T}_{\text{v}11}(\omega) = 2[\mathbf{I} + \mathbf{Z}_{\text{c}1}(\omega) \mathbf{Y}_{\text{r}1}(\omega)]^{-1},$ $\mathbf{T}_{\text{v}12}(\omega) = [\mathbf{I} + \mathbf{Z}_{\text{r}1}(\omega) \mathbf{Y}_{\text{c}1}(\omega)]^{-1} [\mathbf{I} + \mathbf{Z}_{\text{r}1}(\omega) \mathbf{Y}_{\text{b}1}(\omega)],$ $\mathbf{T}_{\text{v}21}(\omega) = 2[\mathbf{I} + \mathbf{Z}_{\text{c}2}(\omega) \mathbf{Y}_{\text{b}2}(\omega)]^{-1},$ $\mathbf{T}_{\text{v}22}(\omega) = [\mathbf{I} + \mathbf{Z}_{\text{b}2}(\omega) \mathbf{Y}_{\text{c}2}(\omega)]^{-1} [\mathbf{I} + \mathbf{Z}_{\text{b}2}(\omega) \mathbf{Y}_{\text{r}2}(\omega)]$
Reflection coefficient	$\Gamma_{111}(\omega) = [\mathbf{I} + \mathbf{Y}_{\text{r}1}(\omega) \mathbf{Z}_{\text{c}1}(\omega)]^{-1} [\mathbf{I} - \mathbf{Y}_{\text{r}1}(\omega) \mathbf{Z}_{\text{c}1}(\omega)],$ $\Gamma_{112}(\omega) = [\mathbf{I} + \mathbf{Y}_{\text{c}1}(\omega) \mathbf{Z}_{\text{r}1}(\omega)]^{-1} [\mathbf{I} - \mathbf{Y}_{\text{c}1}(\omega) \mathbf{Z}_{\text{b}1}(\omega)],$ $\Gamma_{121}(\omega) = [\mathbf{I} + \mathbf{Y}_{\text{b}2}(\omega) \mathbf{Z}_{\text{c}2}(\omega)]^{-1} [\mathbf{I} - \mathbf{Y}_{\text{b}2}(\omega) \mathbf{Z}_{\text{c}2}(\omega)],$ $\Gamma_{122}(\omega) = [\mathbf{I} + \mathbf{Y}_{\text{c}2}(\omega) \mathbf{Z}_{\text{b}2}(\omega)]^{-1} [\mathbf{I} - \mathbf{Y}_{\text{c}2}(\omega) \mathbf{Z}_{\text{r}2}(\omega)]$	$\Gamma_{\text{v}11}(\omega) = [\mathbf{I} + \mathbf{Z}_{\text{r}1}(\omega) \mathbf{Y}_{\text{c}1}(\omega)]^{-1} [\mathbf{Z}_{\text{r}1}(\omega) \mathbf{Y}_{\text{c}1}(\omega) - \mathbf{I}],$ $\Gamma_{\text{v}12}(\omega) = [\mathbf{I} + \mathbf{Z}_{\text{c}1}(\omega) \mathbf{Y}_{\text{r}1}(\omega)]^{-1} [\mathbf{Z}_{\text{c}1}(\omega) \mathbf{Y}_{\text{b}1}(\omega) - \mathbf{I}],$ $\Gamma_{\text{v}21}(\omega) = [\mathbf{I} + \mathbf{Z}_{\text{b}2}(\omega) \mathbf{Y}_{\text{c}2}(\omega)]^{-1} [\mathbf{Z}_{\text{b}2}(\omega) \mathbf{Y}_{\text{c}2}(\omega) - \mathbf{I}],$ $\Gamma_{\text{v}22}(\omega) = [\mathbf{I} + \mathbf{Z}_{\text{c}2}(\omega) \mathbf{Y}_{\text{b}2}(\omega)]^{-1} [\mathbf{Z}_{\text{c}2}(\omega) \mathbf{Y}_{\text{r}2}(\omega) - \mathbf{I}]$

LIST OF REFERENCES

- [1] D. B. Kuznetsov and J. E. Schutt-Ainé, "Difference Approximation," submitted for publication in *IEEE Trans. Circuits Syst. I Fundam. Theory Appl.*
- [2] D. B. Kuznetsov, "Transmission Line Modeling and Transient Simulation", M.S. thesis, University of Illinois at Urbana-Champaign, 1993.
- [3] Г. Ф. Коновалов, *Радиоавтоматика*. Москва: Высшая школа, 1990. In Russian.
- [4] J. M. Ortega and W. C. Rheinboldt, *Interactive Solution of Nonlinear Equations in Several Variables*. New York: Academic Press, 1970.
- [5] *Fundamentals Handbook of Electrical and Computer Engineering*, vol. 3, S. S. L. Chang, Ed. New York: John Wiley & Sons, 1983, pp. 374-377, 381-399.
- [6] J. D. Lambert, *Computational Methods in Ordinary Differential Equations*. New York: John Wiley & Sons, 1973.
- [7] W. D. Stanley, G. R. Dougherty and R. Dougherty, *Digital Signal Processing*. Reston, VA: Reston Publishing Company, 1984.
- [8] A. Semlyen and A. Dabuleanu, "Fast and accurate switching transient calculations on transmission lines with ground return using recursive convolutions," *IEEE Trans. Power Appar. Syst.*, vol. PAS-94, pp. 561-569, Mar./Apr. 1975.
- [9] F.-Y. Chang, "Transient simulation of nonuniform coupled lossy transmission lines characterized by frequency-dependent parameters, Part II: Discrete-time analysis," *IEEE Trans. Circuits Syst.*, vol. 39, pp. 907-927, Nov. 1992.
- [10] K. S. Oh and J. E. Schutt-Ainé, "An efficient implementation of surface impedance boundary conditions for the finite-difference time-domain method," *IEEE Trans. Antennas Propag.*, vol. 43, pp. 660-666, Jul. 1995.
- [11] M. La Scala, G. Sblendorio and R. Sbrizzai, "Parallel-in-time implementation of transient stability simulations on a transputer network," *IEEE Trans. Power Syst.*, vol. 9, pp. 1117-1125, May 1994.
- [12] T. K. Tang, M. S. Nakhla and R. Griffith, "Analysis of lossy multiconductor transmission lines using the Asymptotic Waveform Evaluation technique," *IEEE Trans. Microw. Theory Tech.*, vol. 39, pp. 2107-2116, Dec. 1991.

- [13] J. E. Bracken, V. Raghavan and R. A. Rohrer, "Interconnect simulation with asymptotic waveform evaluation (AWE)," *IEEE Trans. Circuits Syst.*, vol. 39, pp. 869-878, Nov. 1992.
- [14] D. B. Kuznetsov and J. E. Schutt-Ainé, "Optimal transient simulation of distributed lines," *IEEE Trans. Circuits Syst. I Fundam. Theory Appl.*, vol. 43, Feb. 1996, pp. 111-121.
- [15] D. B. Kuznetsov and J. E. Schutt-Ainé, "Efficient circuit simulation of nonuniform transmission lines," submitted for publication in *IEEE Trans. Microw. Theory Tech.*
- [16] J. S. Roychowdhury and D. O. Pederson, "Efficient transient simulation of lossy interconnect," in *Proc. 28th ACM/IEEE Design Automation Conf.*, 1991, pp. 740-745.
- [17] W. T. Beyene and J. E. Schutt-Ainé, "Accurate diode forward recovery reverse model using asymptotic waveform evaluation techniques," to be published in *Proc. ICSAD*, 1996.
- [18] K. S. Kunz and R. J. Raymond, *The Finite Difference Time Domain Method for Electromagnetics*. Boca Raton, FL: CRC Press, 1993, pp. 123-183.
- [19] A. J. Gruodis and C. S. Chang, "Coupled lossy transmission line characterization and simulation," *IBM J. Res. Dev.*, vol. 25, pp. 25-41, Jan. 1981.
- [20] F.-Y. Chang, "Transient simulation of frequency-dependent nonuniform coupled lossy transmission lines," *IEEE Trans. Compon. Packaging Hybrids Manuf. Technol.*, vol. 17, pp. 3-14, Feb. 1994.
- [21] D. B. Kuznetsov and J. E. Schutt-Ainé, "Indirect numerical integration," submitted for publication in *IEEE Trans. Circuits Syst. I Fundam. Theory Appl.*
- [22] И. Н. Бронштейн и К. А. Семендяев, *Справочник по математике*. Москва: Наука, 1967, стр. 130, 505, 578. In Russian.
- [23] W. Caplan, *Advanced Calculus*. Reading, MA: Addison-Wesley, 1956, pp. 545-549, 562-570.
- [24] C.-E. Froberg, *Numerical Mathematics: Theory and Computer Applications*. Menlo Park, CA: Benjamin/Cummings, 1985.
- [25] A. Ralston and P. Rabinowitz, *A First Course in Numerical Analysis*, 2nd ed. New York: McGraw-Hill, 1978.
- [26] S. L. Marple, Jr., *Digital Spectral Analysis*. Englewood Cliffs, NJ: Prentice-Hall, 1987, pp. 303-349.
- [27] Y. Hua and T. K. Sarkar, "Generalized pencil-of-function method for extracting poles of an EM system from its transient response," *IEEE Trans. Antennas Propag.*, vol. 37, pp. 229-234, Feb. 1989.
- [28] L. T. Pillage and R. A. Rohrer, "Asymptotic waveform evaluation for timing analysis," *IEEE Trans. Comput.-Aided Des. Integr. Circuits Syst.*, vol. 9, pp. 352-366, Apr. 1990.

- [29] E. Chiprout and M. S. Nakhla, "Transient waveform estimation of high-speed MCM networks using complex frequency hopping," in *Proc. 1993 IEEE Multi-Chip Module Conf.*, 1993, pp. 134-139.
- [30] R. Sanaie, E. Chiprout, M. S. Nakhla and Q. Zhang, "A fast method for frequency and time domain simulation of high-speed VLSI interconnects," *IEEE Trans. Microw. Theory Tech.*, vol. 42, pp. 2562-2571, Dec. 1994.
- [31] K. S. Oh, D. B. Kuznetsov and J. E. Schutt-Ainé, "Capacitance computations in a multilayered dielectric medium using closed-form spatial Green's functions," *IEEE Trans. Microw. Theory Tech.*, vol. 42, pp. 1443-1453, Aug. 1994.
- [32] S. J. Leon, *Linear Algebra with Applications*, 3rd ed. New York, NY: Macmillan Publishing Company, 1990, pp. 208-216, 403-405.
- [33] J. E. Bracken, V. Raghavan and R. A. Rohrer, "Extension of the asymptotic waveform evaluation technique with the method of characteristics," in *Tech. Dig. IEEE Int. Conf. Computer-Aided Design*, pp. 71-75, Nov. 1992.
- [34] G. Doetsch, *Guide to the Applications of the Laplace and Z-Transforms*. London: Van Nostrand Reinhold Company, 1971, pp. 110-113.
- [35] T. Dhaene, L. Martens and D. De Zutter, "Transient simulation of arbitrary nonuniform interconnection structures characterized by scattering parameters," *IEEE Trans. Circuits Syst.*, vol. 39, pp. 928-937, Nov. 1992.
- [36] T. Dhaene and D. De Zutter, "Selection of lumped element models for coupled lossy transmission lines," *IEEE Trans. Comput.-Aided Des. Integr. Circuits Syst.*, vol. 11, pp. 805-815, Jul. 1992.
- [37] K. S. Oh and J. E. Schutt-Ainé, "Transient analysis of coupled, tapered transmission lines with arbitrary nonlinear terminations," *IEEE Trans. Microw. Theory Tech.*, vol. 41, pp. 268-273, Feb. 1993.
- [38] J. E. Schutt-Ainé and R. Mittra, "Nonlinear transient analysis of coupled transmission lines," *IEEE Trans. Circuits Syst.*, vol. 36, pp. 959-967, Jul. 1989.
- [39] I. Maio, S. Pignari and F. Canavero, "Influence of the line characterization on the transient analysis of nonlinearly loaded lossy transmission lines," *IEEE Trans. Circuits Syst.*, vol. 41, pp. 197-209, Mar. 1994.
- [40] F. Romeo and M. Santomauro, "Time-domain simulation of n coupled transmission lines," *IEEE Trans. Microw. Theory Tech.*, vol. MTT-35, pp. 131-137, Feb. 1987.
- [41] F.-Y. Chang, "Transient analysis of lossy transmission lines with arbitrary initial potential and current distributions," *IEEE Trans. Circuits Syst.*, vol. 39, pp. 180-198, Mar. 1992.
- [42] F. H. Branin, Jr., "Transient analysis of lossless transmission lines," *Proc. IEEE*, vol. 55, pp. 2012-2013, Nov. 1967.
- [43] F.-Y. Chang, "Transient simulation of nonuniform coupled lossy transmission lines characterized by frequency-dependent parameters, Part I: Waveform relaxation analysis," *IEEE Trans. Circuits Syst.*, vol. 39, pp. 585-603, Aug. 1992.

- [44] C. R. Paul, "On uniform multimode transmission lines," *IEEE Trans. Microw. Theory Tech.*, pp. 556-558, Aug. 1973.
- [45] J. E. Schutt-Ainé, "Modeling and simulation of high-speed digital circuit interconnections," Ph.D. dissertation, University of Illinois at Urbana, 1988.
- [46] J. E. Schutt-Ainé, "Transient analysis of nonuniform transmission lines," *IEEE Trans. Circuits Syst. I Fundam. Theory Appl.*, vol. 39, pp. 268-273, May 1992.
- [47] A. S. AlFuhaid, "s-domain analysis of electromagnetic transients on nonuniform lines," *IEEE Trans. Power Deliv.*, vol. 5, pp. 2072-2083, Nov. 1990.
- [48] M. A. Mehalic and R. Mittra, "Investigation of tapered multiple microstrip lines for VLSI circuits," *IEEE Trans. Microw. Theory Tech.*, vol. 38, pp. 1559-1567, Nov. 1990.
- [49] C. Hsue and C. C. Hechtman, "Transient analysis of nonuniform, high-pass transmission lines," *IEEE Trans. Microw. Theory Tech.*, vol. 38, pp. 1023-1030, Aug. 1990.
- [50] O. A. Palusinski and A. Lee, "Analysis of transients in nonuniform and uniform multiconductor transmission lines," *IEEE Trans. Microw. Theory Tech.*, vol. 37, pp. 127-138, Jan. 1989.
- [51] Y.-C. Yang, J. A. Kong and Q. Gu, "Time-domain perturbation analysis of nonuniformly coupled transmission lines," *IEEE Trans. Microw. Theory Tech.*, vol. 33, pp. 1120-1130, Nov. 1985.
- [52] J. L. Hill and D. Mathews, "Transient analysis of systems with exponential transmission lines," *IEEE Trans. Microw. Theory Tech.*, vol. 25, pp. 777-783, Sept. 1977.

VITA

Dmitri Boris Kuznetsov was born June 26, 1966, in Moscow, U.S.S.R. He received, Summa Cum Laude, the Dipl. Ing. degree in electronics engineering with a specialization in space electronics from the Moscow Electrotechnical Institute of Telecommunication, Department of Automatics, Telemechanics and Electronics, in 1988.

From 1987 to 1991 he worked as an electronics engineer at the Space Research Institute, Academy of Sciences of the U.S.S.R., Moscow, on the design, manufacturing, testing, maintenance and repair of computer graphics systems. From 1988 to 1991 he attended the post-graduate school of the Space Research Institute, specializing in information and measuring systems in space research.

Because 1991 he has conducted research in computational electronics, transient simulation, and transmission line modeling at the University of Illinois at Urbana, Department of Electrical and Computer Engineering, where he received the M.S. degree in 1993 and is currently completing the Ph.D. degree.

He is a coauthor of the following publications.

1. D. B. Kuznetsov and J. E. Schutt-Ainé, "Transmission line modeling and transient simulation," EMC Lab., Dept. of ECE, Univ. of Illinois at Urbana, Tech. Rep. 92-4, Dec. 1992.
2. D. B. Kuznetsov and J. E. Schutt-Ainé, "Difference model approach for the transient simulation of transmission lines," in *Proc. ISCAS'93*, 1993, pp. 1547-1550.
3. J. E. Schutt-Ainé and D. B. Kuznetsov, "Efficient transient simulation of distributed interconnects," presented at 10th Int. Conf. Num. Analysis Semicond. Dev. Integr. Circuits (NASECODE X), Dublin, Ireland, Jun. 1994.
4. K. S. Oh, D. B. Kuznetsov and J. E. Schutt-Ainé, "Capacitance computations in a multilayered dielectric medium using closed-form spatial Green's functions," *IEEE Trans. Microw. Theory Tech.*, vol. 42, pp. 1443-1453, Aug. 1994.

5. J. E. Schutt-Ainé and D. B. Kuznetsov, "Efficient transient simulation of distributed interconnects," *Int. Journ. Computation Math. Electr. Eng. (COMPEL)*, vol. 13, no. 4, Dec. 1994, pp. 795-806.
6. D. B. Kuznetsov, J. E. Schutt-Ainé and R. Mittra, "Optimal transient simulation of distributed lines," in *Proc. MCMC'95*, 1995, pp. 164-169.
7. D. B. Kuznetsov and J. E. Schutt-Ainé, "Optimal transient simulation of transmission lines," *IEEE Trans. Circuits Syst. I Fundam. Theory Appl.*, vol. 43, Feb. 1996, pp. 111-121.
8. D. B. Kuznetsov and J. E. Schutt-Ainé, "Indirect numerical integration," submitted for publication in *IEEE Trans. Circuits Syst. I Fundam. Theory Appl.*
9. D. B. Kuznetsov and J. E. Schutt-Ainé, "Efficient circuit simulation of nonuniform transmission lines," submitted for publication in *IEEE Trans. Microw. Theory Tech.*
10. D. B. Kuznetsov and J. E. Schutt-Ainé, "Difference approximation," submitted for publication in *IEEE Trans. Circuits Syst. I Fundam. Theory Appl.*
11. D. B. Kuznetsov, K. S. Oh and J. E. Schutt-Ainé, "Equivalent circuit modeling of EM systems," submitted for publication in *IEEE Trans. Circuits Syst. I Fundam. Theory Appl.*
12. D. B. Kuznetsov and J. E. Schutt-Ainé, "Efficient circuit simulation of transmission lines," in preparation.
13. D. B. Kuznetsov, C. Kumar and J. E. Schutt-Ainé, "Efficient circuit simulation of lossy coupled transmission lines with frequency-dependent parameters," submitted for publication in *IEEE Trans. VLSI Syst.*